PACIFIC EARTHQUAKE ENGINEERING RESEARCH CENTER

Evaluation and Calibration of an OpenSees Layered Shell Element Model for Simulating the Earthquake Response of Flexure-Controlled Reinforced Concrete Walls

Joshua Stokley

Boeing Corporation

Laura N Lowes

Department of Civil and Environmental Engineering

University of Washington, Seattle, WA

PEER Report No. 2024/11
Pacific Earthquake Engineering Research Center
Headquarters at the University of California, Berkeley
November 2024

PEER 2024/11
November 2024

Evaluation and Calibration of an OpenSees Layered Shell Element Model for Simulating the Earthquake Response of Flexure-Controlled Reinforced Concrete Walls

Joshua Stokley

Boeing Corporation

Laura N Lowes

Department of Civil and Environmental Engineering
University of Washington, Seattle, WA

PEER Report 2024/11
Pacific Earthquake Engineering Research Center
Headquarters at the University of California, Berkeley

November 2024

ABSTRACT

Reinforced concrete walls are used commonly to resist lateral loads; often, concrete walls have three-dimensional configurations to maximize stiffness and strength. Seismic design, evaluation, and retrofit of concrete wall structures often require nonlinear analysis to predict performance; assessment of earthquake risk for regions and for individual structures often require nonlinear analysis to predict damage, loss of functionality, and repair time and cost. This report presents the results of a research study in which high-performance cloud-computing resources were used to calibrate an OpenSees Version 3.3.0 model for simulating the earthquake response of planar walls. Jupyter notebooks were used to create OpenSees models of individual walls included in an experimental dataset published in the NHERI DesignSafe-CI DataDepot, and Jupyter notebooks were used to visualize results and define error functions for the model calibration effort. Creation of an efficient research workflow was enabled by use of the NHERI SimCenter quoFEM software. Computational time was reduced by using cloud computing resources provided by the NHERI DesignSafe-CI facility. Results of the effort include recommendations for modeling walls to provide accurate simulation of response and a series of Jupyter notebooks that can support future projects.

Keywords: OpenSees, reinforced concrete, walls, earthquake engineering, finite element analysis, nonlinear analysis.

ACKNOWLEDGMENTS AND DISCLAIMER

This work was supported by the State of California through the Transportation System Research Program of the Pacific Earthquake Engineering Research Center (PEER) and by the National Science Foundation under grant CMMI-2022469, which funds the NHERI DesignSafe Cyberinfrastructure facility. Any opinions, findings, and conclusions or recommendations expressed in this material are those of the author(s) and do not necessarily reflect those of the funding agencies.

CONTENTS

LIST OF TABLES

LIST OF FIGURES

1 INTRODUCTION

Reinforced concrete walls are used commonly in buildings to resist lateral forces resulting from wind and earthquakes; walls can easily and efficiently be designed to provide high lateral strength and stiffness. In regions of high seismicity, walls are designed to exhibit flexure-controlled response under earthquake loading. Under service-level lateral loading, flexure-controlled walls are expected to exhibit modest cracking in the regions of high flexural demand; under design-level loading, walls are expected to exhibit significant damage, including concrete cracking and spalling as well as yielding and buckling of reinforcing steel. The *American Concrete Institute (ACI) Concrete Design Code 318-25* (ACI 318 2025) provides requirements for detailing concrete walls so that damaged walls maintain lateral and axial load-carrying capacity at large deformation demand, and *Minimum Design Loads and Associated Criteria for Buildings and Other Structures, ASCE/SEI 7-22* (ASCE/SEI 2022) specifies wind, earthquake and other demands to be used in wall design. Both ACI 318-25 and ASCE/SEI 7-22 provide requirements for analysis to determine demands used in design of individual walls; though, local jurisdictions often supplemented these requirements. For example, in regions of high seismicity on the West Coast, the design of walls in tall buildings requires nonlinear analysis using suites of site-specific ground motion records to demonstrate acceptable performance under service- and design-level lateral loading.

Current design requirements and standards of practice for design and construction of walls were developed primarily using data from laboratory tests of wall specimens with relatively simple configurations, very simple load patterns, and quasi-static loading. Expanding the existing experimental data to include data for walls with distributed earthquake loading and a variety of complex configurations that are representative of current design practice is not viable, given that there are few testing facilities that have the physical size, equipment capacity, and control software to support representative loading scenarios and instrumentation to accomplish high-resolution monitoring of specimen deformation. However, numerical modeling, using models that have been validated using experimental data, can be used to generate data to support advancement of design procedures and requirements for walls with nonplanar and complex configurations subjected to complex load patterns.

The research presented here seeks to advance numerical modeling of reinforced concrete walls for use in i) performance-based design of tall walled buildings, which requires nonlinear dynamic analyses to demonstrate that a proposed design will exhibit acceptable performance under wind as well as service-level and design-level earthquake loading, ii) research to advance understanding of the earthquake behavior and performance of walls with complex configurations, and iii) research to advance design requirements and performance-based design processes for concrete wall buildings. Specifically, the research presented here employs data for planar reinforced concrete wall specimens tested previously by others in the laboratory and subjected to quasi-static cyclic lateral loading and constant gravity loading. The research i) develops a series of Jupyter notebooks (Kluyver et al. 2016) that create OpenSees (McKenna 1997, McKenna et al. 2010) shell-element models (Lu et al., 2015) of planar concrete wall test specimens for which specimen design and response data were assembled and archived in a published database (Shegay et al., 2021) and post processes OpenSees simulation data to visualize simulated results and provide error functions to determine the accuracy of simulations, ii) calibrates key model parameters using simulated and measured response history data, the SimCenter quoFEM software tool (McKenna et al. 2025, Deierlein et al. 2020), and high-performance computing resources provided by the Texas Advanced Computing Center and accessed via DesignSafe (Rathje et al. 2017), and iii) provides recommendations for using the OpenSees shell element model to simulate the response of concrete walls with planar and nonplanar configurations.

1.1 RESEARCH OBJECTIVES

The primary objectives of the research presented in this report are to 1) provide recommendations for modeling reinforced concrete walls using the layered shell elements and material models, developed by Lu et al. (2015), which are included in the OpenSees Version 3.3.0 software platform and 2) quantify the accuracy and precision of the models. Specific research objectives included the following:

1. Create a series of Jupyter notebooks to support the research workflow.
2. Investigate the two layered shell element formulations available within OpenSees Version 3.3.0 and provide recommendations for their use in simulating concrete wall response.
3. Conduct sensitivity studies and employ optimization algorithms to calibrate model parameters that are not directly defined by wall geometry or by measured concrete and reinforcing steel material properties. Model parameters that are calibrated as part of this study include concrete shear retention factor (*stc*), confined concrete crushing energy (*rev*), and the tensile strain capacity reduction factor (*srs*) for reinforcing steel subjected to large cyclic strain demands.

1.2 REPORT ORGANIZATION

These research activities and results are presented in this report as follows:

- Chapter 2 introduces the experimental data set used in the study as well as the three subsets of this dataset that are used to support i) preliminary evaluation and calibration of the model, ii) calibration of the model, and iii) validation of the calibrated model. A series of error functions are defined to support model calibration.

- Chapter 3 reviews nonlinear response models that have been used previously by practicing engineers and university researchers as well as presents the layered shell element and associated material models used in the current study. The results of a series of preliminary analyses, using the layered shell element, that investigate model configuration (e.g., preferred element size, smeared versus discrete reinforcing steel, and mesh sensitivity) are presented, and a preferred modeling approach is established.

- Chapter 4 introduces computational tools and resources used in this study. The Jupyter notebooks created for this study are presented, and use of the SimCenter quoFEM software is discussed.
- Chapter 5 presents the results of multiple simulations and recommendations for modeling wall response using the material models and layered shell element formulations available in OpenSees Version 3.3.0. Results are presented for i) initial simulations of four wall test specimens to validate the Jupyter notebook workflow and investigate the impact on wall response of the model parameters of interest to the current study, ii) a calibration study employing a larger "calibration" data set comprising data from 16 laboratory tests of walls to determine the best values to use for the model parameters of interest to the current study, and iii) the results of a validation study, in which wall modeling recommendations are used to simulate the response of a "validation" data set comprising 17 laboratory test specimens.

2 EXPERIMENTAL DATA

2.1 INTRODUCTION

This chapter presents the experimental data used for model evaluation, calibration, and validation. Experimental data were sought that characterize the behavior of planar walls, exhibiting flexure-controlled response when subjected to quasi-static cyclic lateral loading and constant axial loading. The data set compiled by Shegay et al. (2021) and published in the NHERI DesignSafe Data Depot (Rathje et al. 2017) was found to provide comprehensive design and performance data for 33 planar walls meeting these criteria. In this Chapter, Section 2.1 presents the Shegay et al. dataset, Section 2.2 describes the behavior of the slender planar wall test specimens used in this study, and Section 2.3 presents the MATLAB (The MathWorks Inc. 2023) data structure created by Shegay et al. as well as discusses how this data structure was ported to Python (Van Rossum and Drake 2009) for use in the current study.

2.2 EXPERIMENTAL DATA

Previous research by Pugh et al. (2015) and Marafi et al. (2019) shows that code-compliant slender walls typically exhibit flexure-controlled response when subjected to cyclic lateral loading and modest axial load. Previous research shows also that walls with high shear demand, high axial load, or non-planar configurations that results in high localized compression demands may exhibit flexure-controlled response or flexure-shear-controlled response with low ductility (Ahmed et al. 2023, Lowes et al. 2019). While the layered shell element considered in the current study is appropriate for modeling the response and failure of planar and non-planar concrete walls exhibiting the full range of ductile and non-ductile response modes, this preliminary study focusses on the simplest wall configuration and wall response modes: planar walls exhibiting tension- and compression-controlled flexural failure.

A first step in the research process was to assemble an experimental data set comprising planar wall test specimens, with a breadth of design characteristics, exhibiting flexure-controlled response in the laboratory. The wall data set published by Shegay et al. the NHERI DesignSafe Data Depot was found to meet the needs of the project. The Shegay et al. data set provides design details and measured response data for 142 walls with a wide range of configurations and design details. For the current study, only planar walls exhibiting flexure-controlled response, with a thickness greater than 4 inches, without spliced reinforcing steel, and with a shear span ratio (height from foundation to the point of applied shear divided by the length of the wall) of approximately 2 or greater were used. Planar walls not meeting these criteria were considered to have a high likelihood of exhibiting reduced strength or deformation capacity due to out-of-plane deformation (often observed in thin walls), splice failure, relocation of the zone of flexural yielding away from the plane of maximum moment demand due to the presence of a splice, and/or the interaction of flexure and shear load-transfer and damage mechanisms. Figure 2.1 shows the distribution of nine design parameters considered to be particularly influential in determining wall behavior and performance, for the 33 walls planar walls from 11 experimental test programs that met the requirements for inclusion in the current study. Appendix A provides the data presented in Figure 2.1 and Appendix B provides additional relevant computed and measured response quantities.

As shown in Figure 2.1, the walls are divided into two data sets: a calibration data set comprising 16 specimens and a validation data set comprising 17 specimens. Both data sets have walls with a range of axial load ratios, shear spans, and cross-sectional aspect ratios. Specimens from test programs comprising one or two walls were grouped together in the calibration or the validation data set; specimens from test programs with three or more walls were split between the calibration and validation data sets.

The design parameters presented in Figure 2.1 are defined as follows.

- Shear Span Ratio: Effective height divided by length of wall. The effective height is defined as the base moment of the wall divided by the base shear of the wall. For wall RW1 shown in Figures 2.2, 2.3 and 2.4, the effective height of the wall is 150 inches and the length of the wall is 48 inches.
- Cross Section Aspect Ratio (CSAR): Length of the wall divided by the thickness of the wall. For wall RW1 shown in Figure 2.2, CSAR equals 12.
- Axial Load Ratio (ALR): The vertical load applied at the top of the wall (see Figure 2.4 where this load is applied by hydraulic jacks) divided by the product of the concrete compressive strength and the wall area, with wall area computed as the thickness of the wall multiplied by the length of the wall.
- Shear Stress Demand: Maximum shear force attained in the test divided by the multiplication of thickness of the wall, length of the wall, and the square root of the compressive strength of the concrete. Note that ACI 318 (2025) defines the concrete contribution to shear strength to be a function of the square root of the concrete compressive strength.
- Horizontal Reinforcement Volumetric Ratio in the Boundary Element (BE): Volume of one layer of hoops/ties in the BE divided by the product of the length of the BE, spacing of the hoops, and thickness of the wall. For wall RW1 shown in Figure 2.2, the length of the boundary region is 7.5 inches, the spacing of the hoops is 3 inches, the thickness of the wall is 4 inches, and the BE horizontal reinforcement volumetric ratio is 0.46%.
- Horizontal Reinforcement ratio: Area of horizontal reinforcement in the direction of the wall length divided by spacing of the horizontal reinforcement layers and thickness of the wall. For wall RW1 shown in Figure 2.2, the horizontal reinforcement comprises two #2 bars spaced at 7.5 in. and the horizontal reinforcement ratio is 0.33%.

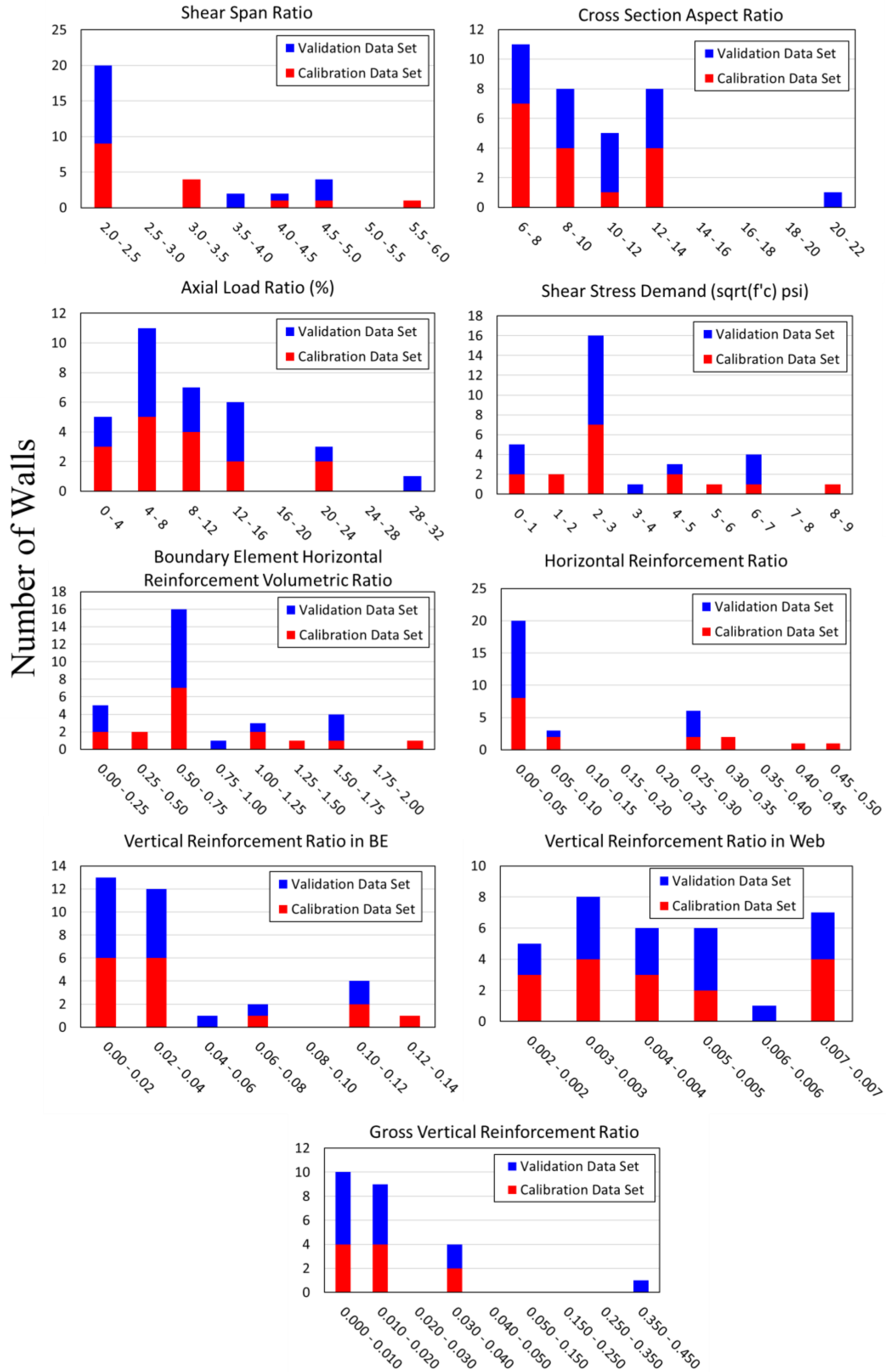

Figure 2.1 Wall design parameters for calibration (red) and validation (blue) data sets

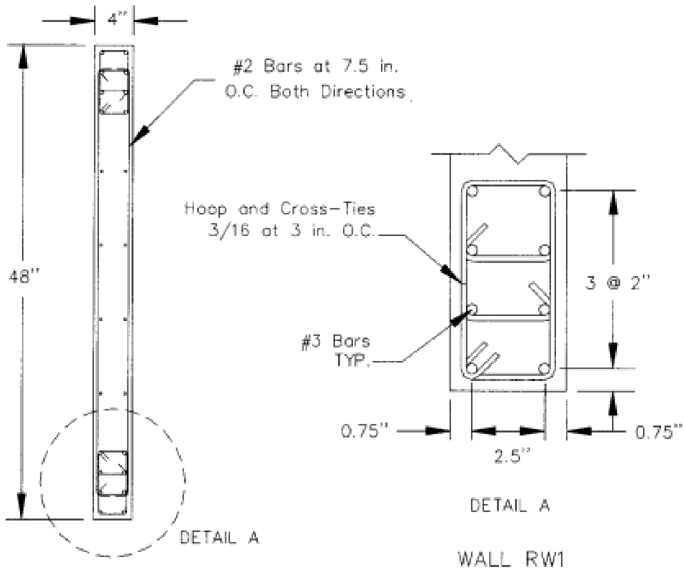

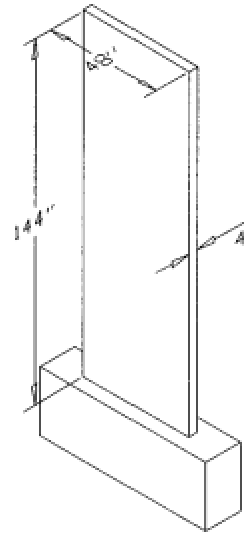

Figure 2.2 **Boundary reinforcement detail** **Figure 2.3** **Three-dimensional view**

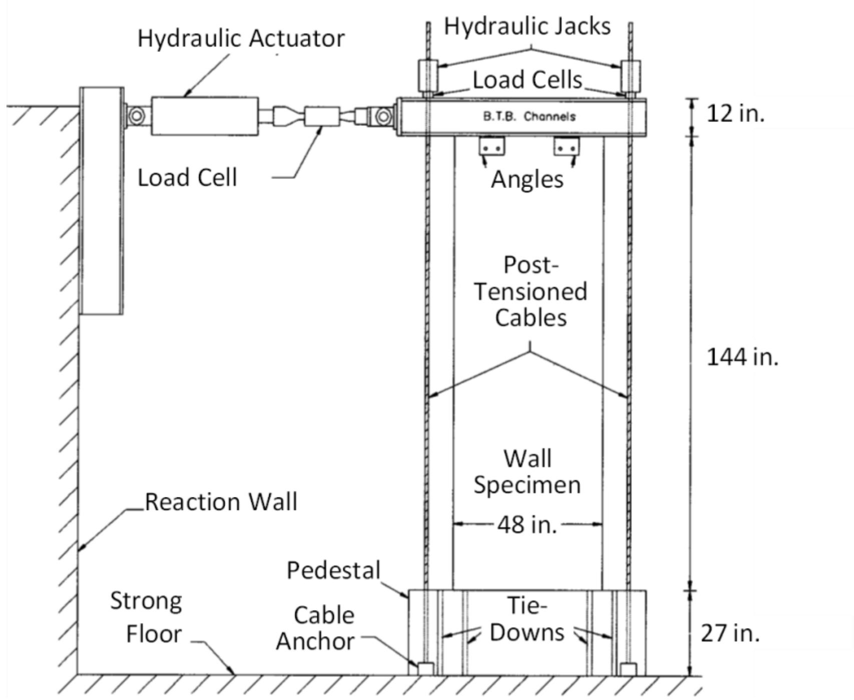

Figure 2.4 **Specimen test set up**

- Vertical Reinforcement Ratio in the BE: Area of longitudinal reinforcement in the BE divided by the length of the BE and thickness of the wall. For wall RW1 shown in Figure 2.2, the area of the BE is 30 in^2, vertical reinforcement area is 0.88 in^2 and the vertical reinforcement ratio in the BE is 2.9%.
- Vertical Reinforcement Ratio in Web: Area of longitudinal reinforcement in the web divided by the web area, where the web area is the wall area less the boundary

element area. For wall RW1 (Figure 2.2), the vertical reinforcement ratio in the web is 0.33%.

- Gross Vertical Reinforcement Ratio: Area of all longitudinal reinforcement divided by the wall area (i.e., length of wall multiplied by the thickness of wall). For wall RW1 shown in Figure 2.2, gross vertical reinforcement ratio is 1.15%.

2.3 SUMMARY OF EXPERIMENTAL TESTS

Following is a brief summary of the test programs from which data were used for the current study:

- Wallace and Thomsen (1995): The research assesses the performance of walls designed using a displacement-based design approach. Four walls were designed: two with T-shaped cross sections and two with rectangular cross sections. Walls were subjected to constant axial load and reverse cyclic lateral loading applied under displacement control. Walls were designed using ACI 318-89, and test variables comprised wall shape, transverse steel configuration, and the distribution of web steel. Test results indicated that displacement-based design procedures resulted in acceptable performance and enabled the use of reduced transverse reinforcement
- Zhang and Wang (2000): At the time of this experimental investigation, little research had been done investigating the behavior of RC walls under high axial load. Three laboratory test specimens were designed using ACI 318-95 and JGJ 3-91 (Ministry of Housing, PRC 1991) standards; walls were subjected to ALRs of 25% and 35%. Test data showed that walls subjected to an ALR of 25% exhibited flexural strength that was approximately equal to that predicted using the Chinese code; flexural strength for the wall subjected to an ALR of 35% strength exceeded that predicted using the Chinese code by 6%. For both axial load levels, strengths predicted using the ACI 318-95 Code were slightly conservative. In the laboratory, the wall with an ALR of 0.35 exhibited out of plane buckling at a low ductility level, while the walls with an ALR of 0.25 exhibited crushing in the boundary elements.
- Oh et al. (2002): Three planar reinforced concrete wall specimens were tested under constant axial load and quasi-static cyclic lateral loading to investigate the impact of boundary element detailing on deformation capacity. Walls were representative of construction in Korea and Chile and had a vertical height to length ratio of 2.0; walls differed on the basis of boundary element transverse reinforcement detailing.
- Liu (2004): The experimental program was designed to investigate the impact of concrete compressive strength on wall performance for specimens subjected to cyclic lateral load protocols. Two walls were tested; the walls were identical in design with the exception that they were constructed using concrete with different compressive strengths.
- Dazio et al. (2009): Six reinforced concrete walls were tested to investigate the impact on deformation capacity of vertical reinforcement ratio and strain capacity. Wall designs were consistent with existing construction in Europe, and walls were representative of mid-rise construction with relatively low axial load ratio. Results of laboratory testing show that

deformation and ductility capacity is reduced with low reinforcement ratios and use of low ductility reinforcing steel.

- Lowes et al. (2012): The experimental program investigated the earthquake response of mid-rise slender walls designed using ACI 318-14. Four planar wall specimens were tested; test specimens differed with respect to a splice at the base of the wall, shear stress demand, and use of uniformly distributed reinforcement versus a reinforcement layout with heavily reinforced boundary elements and a lightly reinforced web region. Walls without splices sustained damage at the base of the wall; walls with splices sustained damage at both the top of the splice and the base of the wall, with the critical region depending on the shear demand. Shear demand also affected response; a moderate increase in shear demand resulted in the failure mechanism changing from bar fracture to flexure–compression failure of the boundary elements. Only the wall without splices was used in the current study.
- Tran (2012): The experimental program was designed to evaluate the impact of shear span, axial load ratio, and peak shear stress on wall response for specimens with a relatively low cross-sectional aspect ratio (CSAR = 8.0). Test specimen design parameters varied as follows: shear spans ranged from 1.5 to 2.0, ALRs ranged from 2.5% to 7.5%, and peak shear stresses ranged from $4\sqrt{f'c}$ to $8\sqrt{f'c}$ psi.
- Lu et al. (2017): The research investigated the performance of lightly reinforced concrete walls subjected to constant axial and reverse-cyclic lateral loading. Six specimens were tested. Specimens had vertical reinforcement ratios of 0.53%, ALRs ranging 0 to 6.6%, and shear demand-capacity ratios ranging from 14% to 53% of capacity per NZS 3101:2006 and ACI 318-14 (requirements were identical for both standards). Two specimens included boundary element confining reinforcement; four did not. Results supported revision of minimum reinforcement limits in the NZ 3101.
- Segura (2017) and Segura and Wallace (2018): The experimental program investigated the theory that thin, code-compliant walls may be susceptible to compression failure prior to achieving expected lateral deformation capacity. Seven walls were subjected to reversed cyclic lateral loading under displacement control with constant axial load. The specimens represented approximately the bottom 1.5 stories of an eight-story cantilever wall. The first phase of testing (WP1-WP4) was conducted to identify potential deficiencies in the ACI 318-14 provisions. Test variables for the phase 1 specimens included the configuration of boundary longitudinal reinforcement, quantity and arrangement of boundary transverse reinforcement, and compression depth (influence by axial load, quantity of longitudinal reinforcement, and wall cross-section). For the second phase of testing (WP5-WP7), walls were designed either with thicker cross-sections or improved boundary transverse reinforcement details.
- Shegay et al. (2018): Experimental testing was done to understand the impact of axial load ratio on flexure-controlled walls with rectangular cross sections. Variables that were changed are the use of crossties, the length of the boundary element, and using full hoops versus crossties in the boundary element. The reference wall designed to the standard of

NZS 3101:2006-A2 and A3. In all walls, the full axial load was sustained following lateral load failure. However, once lateral load capacity was lost, walls sustained axial load for at most one additional drift cycle. Data from this test program was combined with data from previous tests conducted by others and published in the DesignSafe Data Depot as the "UoA-UW Reinforced Concrete Wall Database" (Shegay et al. 2021).

2.4 DATA STRUCTURES USED FOR THE WALL DATA SET

The Shegay et al. (2021) dataset was found to be particularly valuable to the current study because, in addition to providing a comprehensive data set, the Shegay et al. dataset presents the data in a structured format that greatly facilitates scripted data extraction. Specifically, data are provided as a structured MATLAB file. The top level of the data structure contains the main branches that stem all the variables needed to create a model of a wall. Below is a summarized version of each top-level branch. Figures 2.5 and 2.6 visualize the data structure in a tree format. Additional information about variables included in the dataset are provided in Appendix C.

- 'Authors': Representative author of the study
- 'SpecimenID': Specimen ID as classified by author
- 'UniqueID': Unique specimen ID - amalgamation of Author and SpecimenID
- 'WallType': Shape and steel layout of wall
- 'Geometry': Wall geometric details
- 'Reinf': Wall reinforcement detailing
- 'Material': Material information for the steel and concrete
- 'Loading': Information about the loading conditions for the test
- 'ExperimentalData': Summary of experimental data
- 'SectionAnalysis': Data used to create a fiber-section of the wall for use in performing section analysis, including moment-curvature analysis

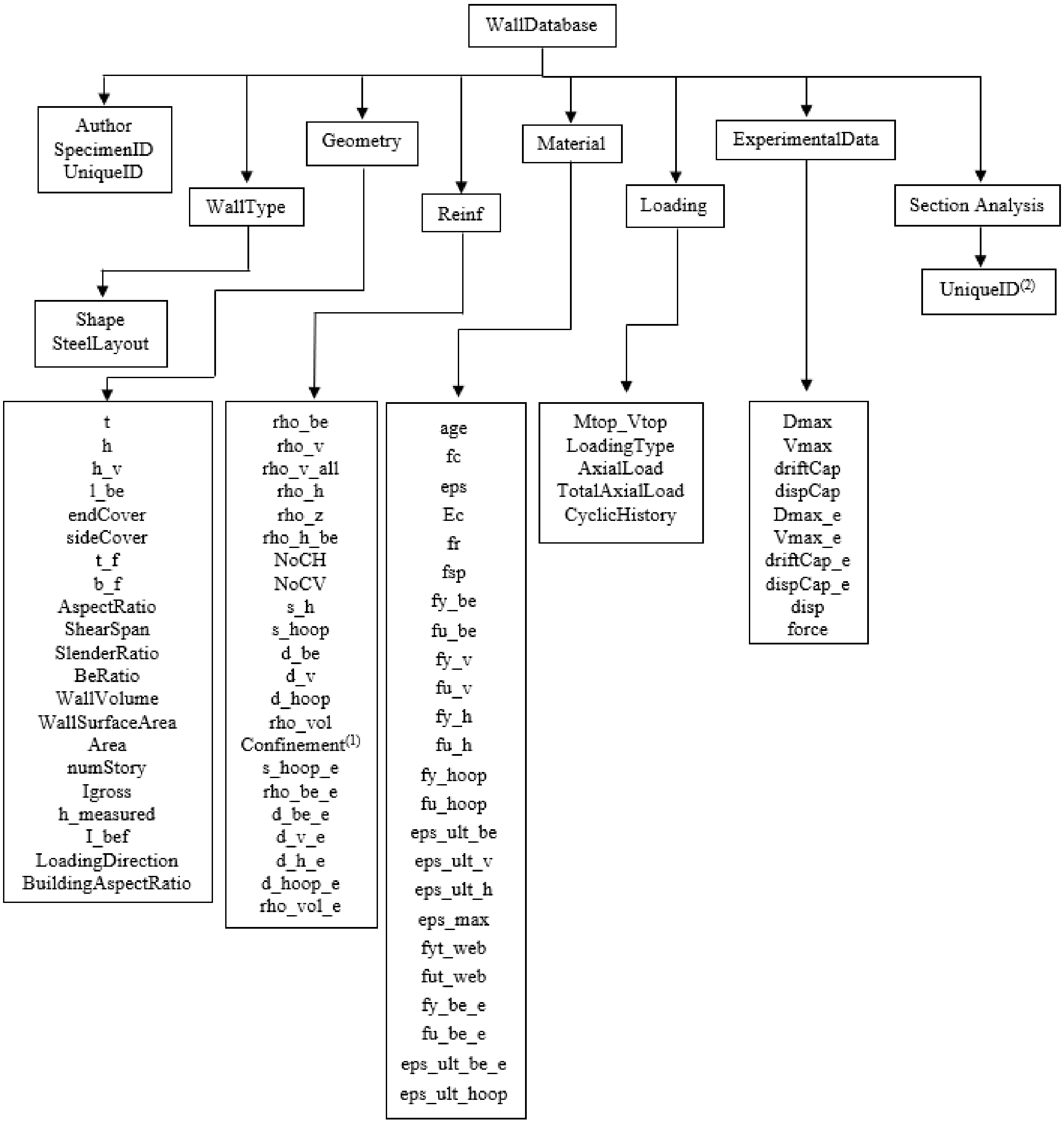

Figure 2.5 MATLAB structure for Shegay et al. (2021) database.

Notes: (1), (2) extended trees shown in Figure 2.6. Additional information in Appendix C.

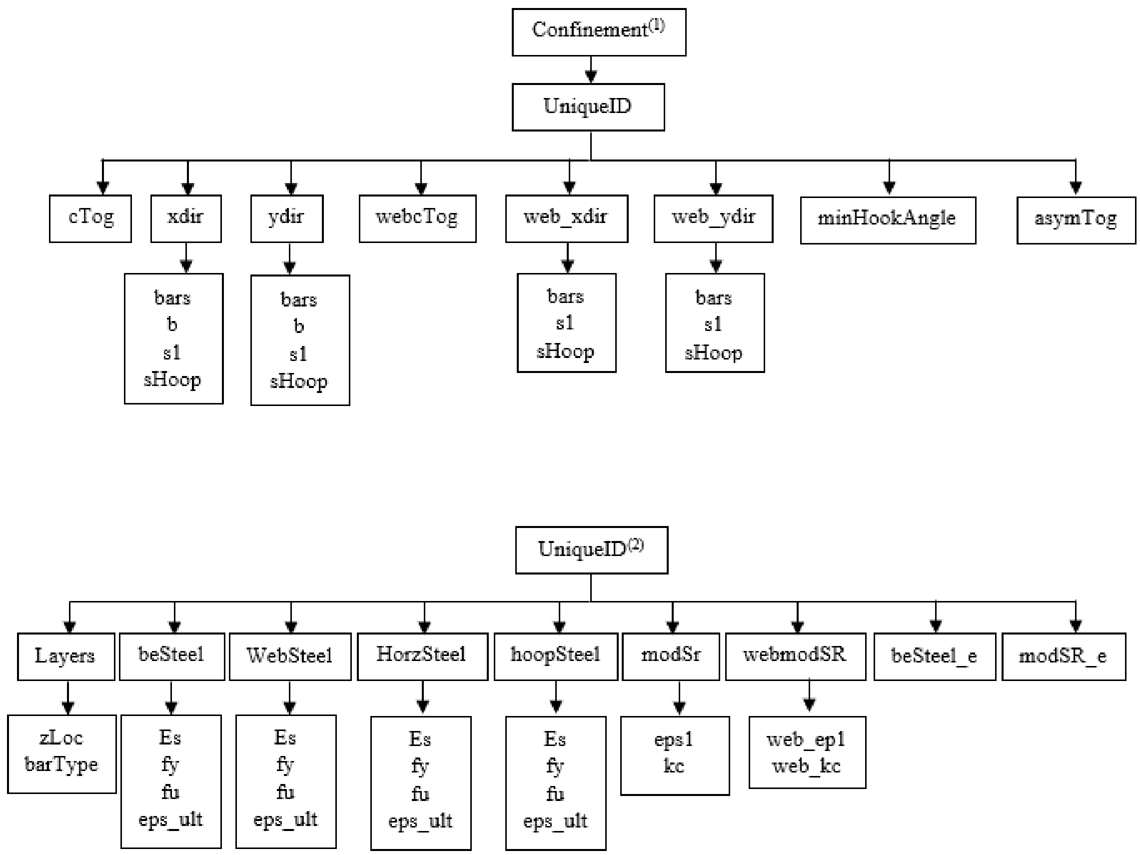

Figure 2.6 Extended MATLAB structure of Shegay et al. (2021) database.

Notes: (1), (2) are extended trees referenced in Figure 2.5. Additional information in Appendix C.

2.5 SUMMARY

The reinforced concrete wall experimental data set assembled and published by Shegay et al. was used to support the current research effort. This data set provides comprehensive data (e.g., specimen design, material properties, loading, and response) for a large number of reinforced concrete wall tests conducted around the world during the last 30 years. These data are presented in a structured format, specifically a hierarchical MATLAB data structure, which facilitates their reuse for the current research project. Data for 33 planar wall tests, from 11 experimental test programs, that met the specific needs of the current study were extracted from the Shegay et al. data set for use in the current project. These wall tests were split into a calibration data set comprising 16 walls and a validation data set comprising 17 walls.

3 WALL MODELING

This chapter reviews commonly used approaches for modeling the nonlinear response of flexure-controlled concrete walls, presents the layered shell element models and associated material models that are available in OpenSees Version 3.3.0 (McKenna 1997, McKenna et al. 2010) and that were used in the current study, and presents the results of a preliminary investigation to establish a preferred modeling approach for using the layered shell element to achieve accurate results and minimize computational demand for the current study. Section 3.1 reviews element formulations and material models used in past research studies by others to simulate the response of reinforced concrete walls exhibiting flexure-controlled response. Sections 3.2 and 3.3 presents the layered shell elements and associated two-dimensional material models, developed and implemented in OpenSees by Lu et al. (2015). Section 3.4 presents the Jupyter notebooks (Kluyver et al., 2016) developed to support this research project. Section 3.5 presents the results of preliminary OpenSees simulations to investigate the impact on simulated response of multiple modeling decisions, including shell element formulation, the level of mesh refinement, the use of discrete versus smeared vertical reinforcing steel, and the lack of inclusion of cover concrete at the ends of the wall. The chapter concludes with identification of a preferred approach for using OpenSees to model flexure-controlled walls; this approach is used for the remainder of the project.

3.1 ELEMENT FORMULATIONS USED PREVIOUSLY BY OTHERS TO SIMULATE SLENDEAR WALL RESPONSE

Previous research has developed, calibrated, and applied a variety of modeling approaches to simulate the response of reinforced concrete walls exhibiting flexure-controlled response when subjected to constant axial and quasi-static cyclic and lateral loading. Table 3.1 lists modeling approaches used commonly to simulate wall response, the strengths and weaknesses of these approaches, and representative research studies in which these models were calibrated, evaluated, and applied.

3.2 OPENSEES LAYERED SHELL ELEMENT

The information presented in Table 3.1 suggests the potential for layered shell elements to be an ideal modeling approach for planar and non-planar reinforced concrete walls. These models offer the potential for accurate simulation of response for walls with two- and three-dimensional geometries and multi-dimensional stress and strain fields as well as substantially reduced computational demand in comparison with solid element models. However, given the assumptions embedded in this model, additional research is required to develop recommendations for using the model and to validate the model for simulation of walls with a range of design parameters.

Table 3.1 Previous wall modeling approaches

Model Type	Strengths	Weaknesses	Example Applications
Either Fiber-Hinge Model or Lumped-Plasticity Fiber-Type Beam-Column Element	• Computationally efficient • Provides accurate prediction of strength for planar and nonplanar walls • Can be calibrated to accurate simulation of deformation capacity, regardless of assumed hinge length	• Assumption that plane sections remain plane • Requires use of unconfined and confined concrete material models • Does not account for flexure-shear interaction • Cannot simulate distributed inelasticity • Location of yielding defined a priori based on location of plastic hinge • Elastic elements must be calibrated to provide accurate simulation of stiffness	**Berry et al., 2008**
Regularized Distributed-Plasticity Beam-Column Element w/ Fiber Section	• Computationally efficient • Provides accurate prediction of strength, and stiffness. • Can be calibrated and regularized to enable accurate simulation of deformation capacity • Provides accurate simulation of distributed yielding	• Assumption that plane sections remain plane • Requires use of unconfined and confined concrete material models • Uses two-node line elements to model 3D geometry • Cannot simulate flexure-shear interaction	**Pugh 2012, Marafi et al. 2019, Lowes et al. 2020**
Multi-Vertical Line Element	• Computationally efficient • Provides accurate prediction of strength and stiffness • Can be calibrated and regularized to enable accurate, mesh-independent simulation of deformation capacity	• Assumption that plane sections remain plane • Requires use of unconfined and confined concrete material models. • Uses two-node line elements to model 3D geometry • Has not been calibrated to provide accurate simulation of deformation capacity. • Does not provide simulation of flexure-shear interaction	**Orakcal and Wallace 2006**
Perform3D Fiber Shell Element	• Computationally efficient • Can be calibrated to provide accurate prediction of stiffness, strength and deformation capacity • 2D shell elements can be used to model 3D geometry	• Does not simulate the impact of out-of-plane confinement on concrete response; this can be simulated using unconfined and confined concrete material models • Flexure and shear responses are decoupled	**NIST 2013**
Layered Shell	• Does not require many of the assumptions about stress and strain fields that are used in the above models. • Previous research demonstrates potential for accurate prediction of strength, stiffness, deformation capacity, and failure mode • Can be used with truss elements and beam-column elements • Can be used to represent two- and three-dimensional geometries • Can simulate distributed yielding	• Does not simulate the impact of out-of-plane confinement on concrete response; this can be simulated using unconfined and confined concrete material models. • Moderately computationally expensive	**Lu et al., 2015**
2D Continuum Model using VecTor2	• Does not assume that plane sections remain plane • Flexure-shear interaction is simulated • Provides accurate prediction of strength • Can be used to represent two- and three-dimensional geometries • Can simulate distributed yielding	• Does not simulate the impact of out-of-plane confinement on concrete response; this can be simulated using unconfined and confined concrete material models • Moderately computationally expensive • Does not provide an accurate prediction of stiffness • Difficult to calibrate material models to achieve accurate, mesh independent, simulation of deformation capacity	**Palermo and Vecchio 2007, Pugh 2012, Wond et al. 2013**
3D Continuum Analysis	• Does not require the assumptions about stress and strain fields that are used in the above models. • Previous research demonstrates potential for accurate prediction of strength, stiffness, deformation capacity, and failure mode • Uses 3D elements to model 3D geometry • Can simulate distributed inelastic action and localization of failure	• Computationally expensive	**Lowes, Lehman, Whitman, 2019**

The current study employs the OpenSees software platform and the two-dimensional layered shell elements and concrete and steel constitutive models developed by Lu et al. (2015), which are available for use in OpenSees Version 3.3.0. OpenSees was chosen for use because it is widely used by the earthquake engineering research community to simulate the response of structural and geotechnical systems subjected to quasi-static cyclic and dynamic earthquake loading. OpenSees Version 3.3.0 includes three shell element formulations (MITC4, DKGQ, and NLDKGQ), tools for creating layered shell materials appropriate for use with these shell element formulations, two-dimensional plane stress concrete constitutive models developed by Lu et al. (2015), and one-dimensional steel material models (e.g., Steel02). The following paragraphs discuss these.

All three of the four-node, multi-layer shell elements available in OpenSees 3.3.0 were considered in this study: MITC4 (Dvorkin and Bathe 1984, Love 1996) and DKGQ and NLDKGQ (Lu et al. 2015). These layered shell elements can be used to provide a simplified representation of the 3D nonlinear behavior of thin reinforced concrete elements, such as walls, by neglecting stress-strain response in the through-thickness direction and representing the in-plane response of different through-thickness layers (e.g., cover concrete, confining steel, confined core concrete) by discretizing the component into multiple bonded layers in the through-thickness direction. Figure 3.1 shows an idealization of a layered shell element.

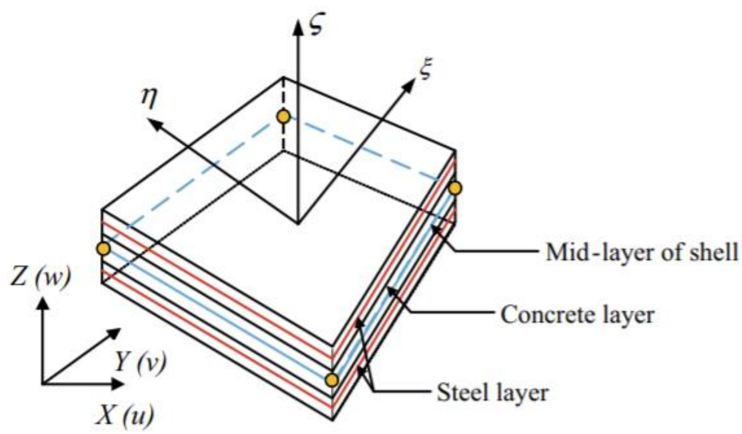

Figure 3.1 Multi-layer shell element (from Dvorkin and Bathe 1984)

In a layered shell element, the axial strains and curvature of the middle layer (mid-layer) are calculated at the quadrature points using the nodal rotations and displacements. For each layer, strains are computed at the layer quadrature points using mid-layer strains, curvatures and the assumption that through-thickness plane sections remain plane. Stresses are computed for each layer, at each quadrature point, using quadrature point strains and specified material model parameters and history variable values (Lu et al. 2015). Figure 3.2 shows the assumed stress field for the layered shell element.

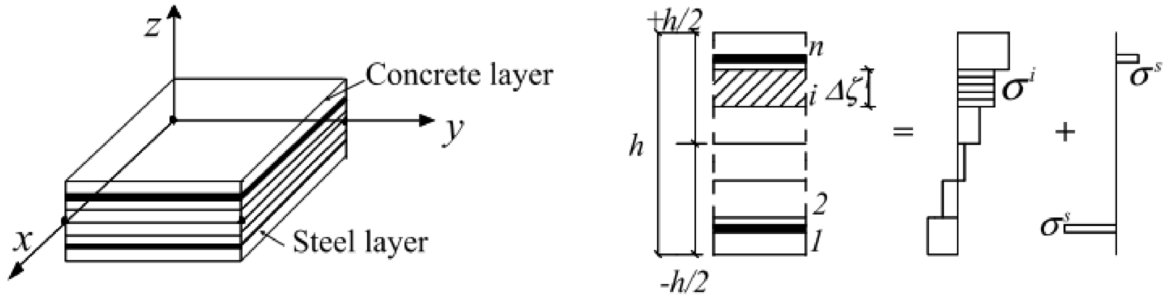

Figure 3.2 Steel and concrete layers and shell element stress and strain profiles

This study investigates two shell element formulations that are available in the OpenSees 3.3.0 platform, DKGQ and MITC4, for use in simulating the response of reinforced concrete walls. Lu et al. (2015) investigated application of the MITC4 element and concluded that the element formulation posed too many computational issues; specifically, they found that the element exhibited shear locking and artificial stiffness. As a result, they formulated two new shell elements, DKGQ and NLDKGQ. Figure 3.3 (from Lu et al. 2015) compares simulation results for an analysis of a column generated using the MITC4 and the NLDKGQ element formulations. The NLDKGQ element formulation, which extends the DKGQ formulation by introducing a Lagrangian formulation to provide more accurate results for simulations with large deformations and rotations, is *not* considered in the current study because the wall test specimens used in this study do not exhibit large deformations and rotations.

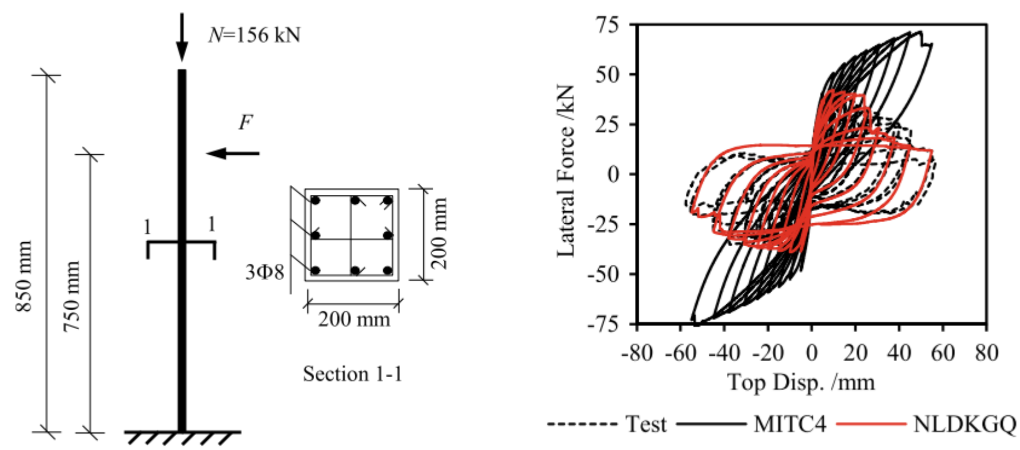

Figure 3.3 RC column collapse simulation setup and results

The MITC4 element is a 4-node flat shell element that employs mixed interpolation for deformation modes. It employs a bilinear isoparametric formulation for bending and axial deformations in combination with modified shear interpolation; specifically, the MITC4 formulation assumes a linear distribution for in-plane strain components and a constant shear strain distribution in the transverse direction. The MITC4 element includes only five (5) DOFs per node, with the out-of-plane "drilling" DOF ignored. This can cause inaccuracy in simulated results for nonplanar systems; this is not an issue for the current study which considering only planar walls.

The DKGQ element is a 4-node flat shell element that combines a planar membrane element formulation (GQ12) with a plate bending element (DKQ), as seen in Figure 3.4. It includes 6 DOFs per node (i.e., the drilling DOF is not ignored). Lu et al. (2015) demonstrate that the DKGQ element does not exhibit the locking problem observed with the MITC4 element. The NLDKGQ formulation builds on the DKGQ formulation to provide more accurate simulation of components exhibiting large rotations and deformations and, thus, geometric nonlinearities through use of a Lagrangian formulation. Walls used in this study exhibit modest displacement, rotation and deformation; thus only the DKQG formulation is considered in the current study.

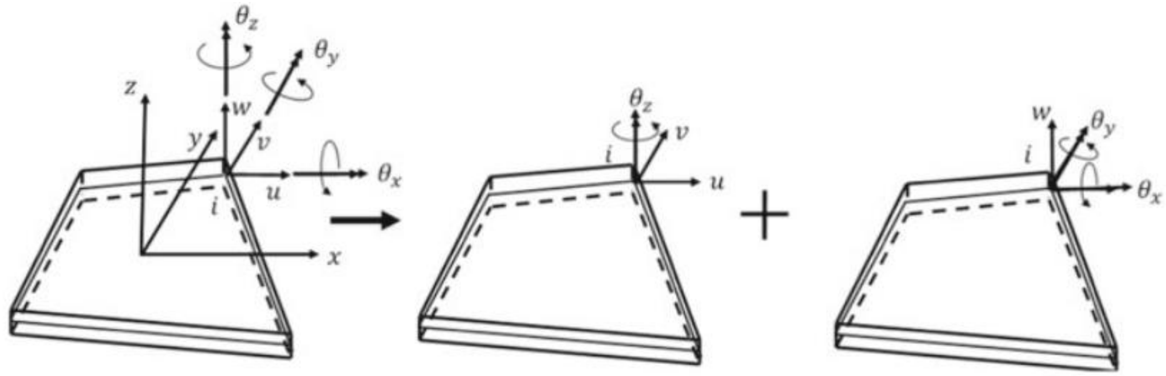

Flat shell element DKGQ and NLDKGQ | Plane membrane element GQ12 | Plate bending element DKQ

Figure 3.4 Visualization of DOFs for DKGQ and NLDKGQ

3.3 MATERIAL MODELS

Use of a layered shell element to simulate the response of a reinforced concrete wall requires definition of two-dimensional material models that simulate the response of the confined and unconfined concrete layers as well as definition of material models to represent horizontal and vertical reinforcing steel. For concrete, the OpenSees *PlaneStressUserMaterial* command is used to define a two-dimensional concrete constitutive model; the *PlateFromPlaneStress* command is used to extend the two-dimensional concrete constitutive model for use in the layered shell element. The concrete material model assumes elastic response until cracking, a fixed crack orientation once cracking occurs, and post-cracking response defined by a 1D confined or unconfined concrete stress-strain model oriented perpendicular to the crack surface combined with a shear-friction model oriented parallel to the crack surface. For reinforcing steel, a one-dimensional steel material model (OpenSees *Steel02*) is incorporated into the layered shell element using the *PlateRebar* command. The OpenSees *Steel02* material response is calibrated using the elastic modulus for steel, recommended cyclic response parameters (Pugh et al., 2015), and the yield strength and hardening stiffness provided by the researchers for each test specimen; reinforcing steel strain capacity in tension and compression are calibrated to provide accurate simulation of strength loss due to bar fracture or buckling.

The material models used in the current study and the OpenSees commands that support use of these models are discussed below.

3.3.1 Plane Stress Concrete Constitutive Model

Lu et al. (2015) developed and implemented in the OpenSees platform (OpenSees Version 3.3.0) the two-dimension plane stress concrete constitutive model "PlaneStressUserMaterial". This material model is appropriate for use with layered shell elements. The model simulates concrete response as elastic to the point at which principal tensile stress exceeds concrete tensile strength and cracking occurs. Once concrete cracking occurs, concrete is considered to be orthotropic, with concrete response defined by one-dimensional stress-strain response models in the direction normal and parallel to the fixed crack surface (Figure 3.5). To minimize mesh sensitivity associated with material softening, the softening portion of the concrete stress-strain response curve, both in compression and in tension, is defined using a mesh dependent length and a measure of energy dissipation associated with damage (Lu et al. 2015, Pugh et al. 2015, Spacone et al. 1996). The plane-stress concrete constitutive model cannot simulate increased compression strength and deformation capacity observed when concrete is subjected to compressive loading in one direction (e.g., in the plane of the concrete wall) and expansion in restrained in the orthogonal direction due to presences of confining reinforcement. To simulate the impact on concrete strength and deformation capacity of the confining reinforcement provided in the boundary element regions of most of the walls considered in this study, one-dimensional *confined* concrete material models are used to define the confined concrete compressive strength and strain at peak strength and *confined* concrete crushing energy is used to define post-peak compressive stress-strain response and the increased deformation capacity resulting from confining reinforcement. Tension response is the same for confined and unconfined concrete. For walls with confining reinforcement in boundary element regions, the layered shell elements in these regions comprise unconfined concrete layers representing cover concrete as well as confined concrete layers.

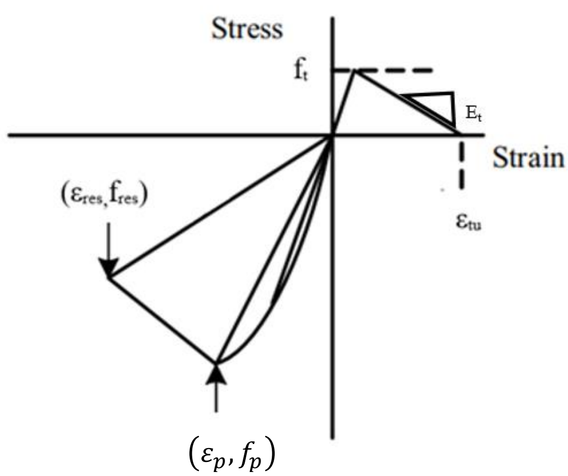

Figure 3.5 Concrete stress-strain response model perpendicular to the crack surface; confined and unconfined concrete response models have the same form, but stress and strain values defining the envelope differ.

One-dimensional concrete stress-strain response in the directions normal and parallel to the crack surface is simulated using well-established models (Figure 3.5). Concrete tensile response is simulated using a damage-type model, for which response is elastic for stress demands less than the concrete tensile strength and exhibits linear strength loss with increasing strain demand beyond the cracking strain. Concrete response in compression follows a quadratic curve to peak strength and a multi-linear envelope for strain demands exceeding that associated with maximum compressive strength. Note that for unconfined concrete, $f_p = f_c$, where f_c is measured per ASTM C39 (2024); all concrete material response model parameters defined as follows:

Concrete elastic modulus per ACI 318-25:

$E_c = 57000\sqrt{f_c}$ psi, with f_c in psi (Eq 3.1a)

$E_c = 4700\sqrt{f_c}$ MPa, with f_c in MPa (Eq 3.1b)

Concrete tensile strength per ACI 318-25,

$f_t = 4\sqrt{f_c}$ psi, with f_c in psi (Eq 3.2a)

$f_t = 0.56\sqrt{f_c}$ MPa, with f_c in MPa (Eq 3.2b)

Concrete fracture energy, which defines the area under the post peak concrete tension curve per CEB (1990),

$G_t = (0.174(D_{max})^2 - 0.0727D_{max} + 0.149)(\frac{f_c}{1450})^{0.7}$ lb/in (Eq 3.3a)

$G_t = (0.0469(D_{max})^2 - 0.5D_{max} + 26)(\frac{f_c}{10})^{0.7}$ N/m) (Eq 3.3b)

where D_{max} is the maximum aggregate size, which is defined as 0.5 inches (12.5 mm) for the current study.

Concrete strain at tensile strength loss:

$\varepsilon_{tu} = \frac{f_t}{E_c} + \frac{2G_t}{L_E f_t}$ (Eq 3.4)

Concrete strain at maximum compressive strength per Marafi et al. (2019):

$\varepsilon_p = \frac{f_p}{E_c}$ (Eq 3.5)

Confined concrete residual strength per Marfi et al. (2019):

$f_{res} = 0.2f_p$ (Eq 3.6)

Unconfined concrete residual strength per Marfi et al. (2019):

$f_{res} = 0.01f_p$ (Eq 3.7)

Unconfined concrete strain at residual strength per Marfi et al. (2019):

$\varepsilon_{res} = \frac{2G_f}{(\delta+1)f_p L_E} + \varepsilon_p \frac{\delta+1}{2}$ (Eq 3.8)

where, δ is the ratio of residual compression capacity to maximum compression strength, defined equal to 0.2 for confined concrete and 0.01 for unconfined concrete per Marafi et al. (2019), f_p is the concrete compressive strength (confined or unconfined, as appropriate) and L_E is the length of the element in the minimum principal stress direction at the onset of crushing, which is assumed to be equal to the vertical height of the element.

Unconfined concrete crushing energy per Marafi et al. (2019):

$G_{fc} = 0.0134 f_c$ k/in with f_c in psi (Eq. 3.9a)

$G_{fc} = 2 f_c$ N/mm with f_c in MPa (Eq. 3.9b)

Confined concrete has been shown to have greater strength and strain at peak strength as well as greater crushing energy. This is simulated by introducing a confined-concrete layer, with an appropriate thickness and appropriate material properties, into the layered shell element. For the confined concrete layer, concrete compressive strength and strain at peak strength, f_p and ε_p in Figure 3.5 are defined per Saatcioglu and Razvi (1992) and increased crushing energy is defined per Marafi et al. (2019). Specifically,

$$f_p = f_{cc} = k_c f_c \quad \text{(Eq 3.10)}$$

$$\varepsilon_p = \varepsilon_{cc} = k_c \varepsilon_c \quad \text{(Eq 3.11)}$$

where k_c is a confinement factor for the boundary region. For confined concrete, strain at the onset of residual compressive strength, ε_{res}, is computed using Eq. 3.8 with

$$G_f = G_{fcc} = rev * G_{fc} \quad \text{(Eq 3.12)}$$

where *rev* is the confined concrete crushing energy ratio that is calibrated as part of this study; Marafi et al. (2019) found $rev = 2.2$ to provide a best fit to experimental data when using fiber-section beam-column elements to simulate concrete wall response. Concrete response parallel to the crack surface is defined as linear elastic with shear stiffness reduced to represent slip on the crack surface:

$$\tau = G \times stc \times \gamma \quad \text{(Eq 3.13)}$$

where

$G = \frac{E_c}{2(1+v)}$ is the concrete elastic shear modulus, with $v = 0.2$ per ACI 318-25 (Eq 3.14)

stc is the cracked concrete shear retention factor, which is calibrated as part of this study, and γ is the shear deformation in the direction parallel to the crack surface.

Using the above model, when concrete principal stress exceeds the concrete tensile strength, cracks form and the concrete is treated as an orthotropic material. Shear stiffness of the cracked concrete is reduced per Eq. 3.13. As the wall develops primary and secondary cracks under loading, the stress-strain relationship is defined as follows:

$$[\sigma] = \begin{vmatrix} 1 - d_1 & 0 \\ 0 & 1 - d_2 \end{vmatrix} D_e \varepsilon_c \quad \text{(Eq 3.15)}$$

where d_1 and d_2 are the damage parameters calculated by damage evolution curves under tension and compression. These parameters equal 0 for undamaged concrete. When primary cracks form at an integration point, d_1 increases to 1 with increased crack width opening; when concrete crushing occurs d_2 increases to 1 with increased compression strain beyond the strain at peak compressive strength. σ and ε_c are the stress and strains in the direction of the principal stresses. D_e represents the elastic constitutive matrix (Lu et al. 2015).

3.3.2 Modeling Reinforcing Steel

Reinforcing steel is modeled in two ways, as a smeared horizontal steel layer within the layered shell element and using vertical truss elements. The material response of all steel is modeled using the OpenSees *Steel02* material model, which is based on the Giuffré-Menegotto-Pinto model (Menegotto and Pinto 1973, Giuffré 1970), with response parameters defined using measured response quantities and strain capacity in tension and compression reduced to account for the impact of cyclic bar buckling and loss of restraint due to concrete crushing.

The steel model requires as input steel yield strength, initial elastic modulus, and strain-hardening ratio; these quantities are provided for each wall in the Shegay et al. (2021) data set. The model requires also R0, CR1 and CR2, which are the parameters that define the transition from the elastic to the inelastic branch of the model. Figures 3.6 and 3.7 show hysteretic behavior with and without isotropic hardening in compression and tension. Figure 3.8 shows a comparison of a monotonic envelope with different values of R0 (recommendation is a value between 10 and 20). Default values for CR1 and CR2 are used (Filippou et al. 1983).

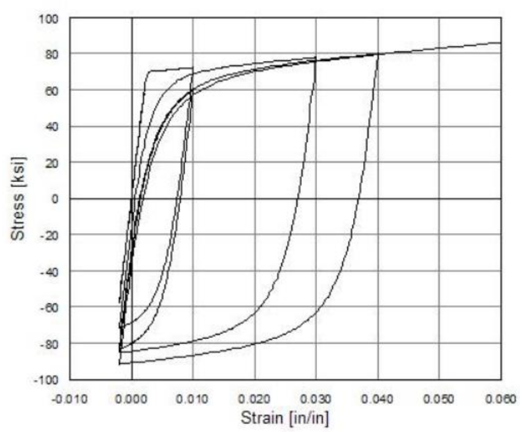

Figure 3.6 Hysteretic behavior of steel model with isotropic hardening in compression

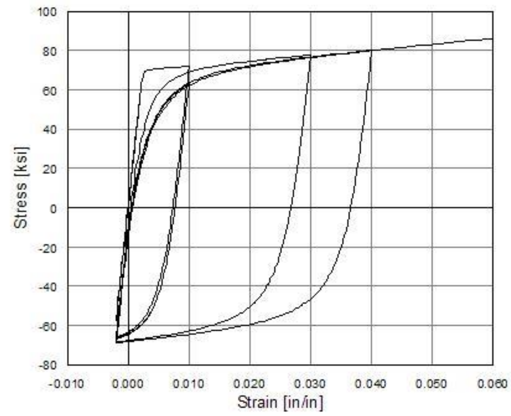

Figure 3.7 Hysteretic behavior of steel model without isotropic hardening

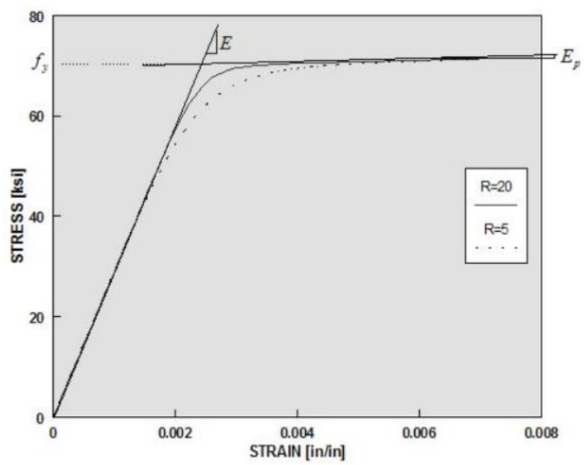

Figure 3.8 Stress vs strain behavior of steel material model for monotonically increasing strain demand

Following the recommendations of Pugh et al. (2015) and Marafi et al. (2019), the OpenSees MinMax wrapper is used to establish material strain limits; material fibers subjected to strain demands in excess of the specified strain limit are considered to "fail" and provide zero stiffness and strength for the remainder of the analysis. For both concrete and reinforcing steel, the compression strain at which material strength drops to zero is defined as the point at which the concrete surrounding the reinforcing bar reaches the compressive strain associated with concrete residual strength, ε_{res} defined in Eq. 3.8; ε_{res} is a function of the element height and concrete crushing energy, G_{fc} for unconfined concrete and G_{fcc} for confined concrete. A tensile strain limit is specified also for reinforcing steel and is defined by the steel rupture strain reduction (*srs*) parameter; the *srs* parameter is a constant less than one that reduces the measured fracture strain of the reinforcing for monotonically increasing deformation demand to account for the reduction in strain capacity observed when reinforcing steel is subjected reversed cyclic loading:

$$srs = \frac{\varepsilon_{fracture,cyclic}}{\varepsilon_{fracture,mono}} \quad \text{(Eq 3.16)}$$

Pugh et al. calibrate an energy-based tensile strain capacity parameter for reinforcing steel; while, Marafi et al. (2019) employ a tensile failure strain of 0.20 in the absence of a large body of test data. Both the confined concrete crushing strain (ε_{res} per Eq. 3.8), which is also used to define reinforcing steel strength loss due to high compression strain demand, and the steel rupture strain reduction factor (*srs* per Eq. 3.16) are calibrated as part of this study to achieve accurate simulation of onset of wall strength loss due to reinforcing steel failure.

For all of the walls included in this study, wall strength is determined by the vertical reinforcing steel and, thus, by the reinforcing steel area, material properties, and horizontal location along the wall cross-section. To improve accuracy in predicted strength and deformation capacity, vertical steel is modeled discretely using truss elements. This requires that the finite element mesh used for each wall include nodes at the horizontal location of the vertical reinforcing bars.

Horizontal reinforcement provides confinement of boundary element concrete and contributes to wall shear capacity. To accurately simulate this behavior for walls, it is not necessary to accurately locate each horizontal reinforcing bar. Thus, to reduce restrictions on model meshing and thereby reduce computational demands, horizontal reinforcement is modeled as a layer within the layered shell element that has stiffness and strength only in the horizontal direction. This is accomplished using the OpenSees *PlateRebar* function, which creates a two-dimensional plane-stress material with the appropriate material response, thickness, and orientation to represent the horizontal reinforcement. Specifically, the plane-stress material provides stiffness and strength only in the horizontal direction, and material response is a function of horizontal bar area, horizontal bar spacing, and a one-dimensional stress-strain material response model calibrated using measured horizontal steel material response parameters.

3.4 JUPYTER NOTEBOOKS FOR MODEL BUILDING

To speed modeling of the large number of planar walls included in the Shegay et al. (2021) database, two Jupyter notebooks were created to automate modeling building directly from the Shegay et al. (2021) database. These notebooks are published in the DesignSafe DataDepot (https://www.designsafeci.org/data/browser/public/designsafe.storage.community/Use%20Cas%20Products/QUOFEM) and are documented here: https://www.designsafe-ci.org/ user-guide/usecases/. The first of the two notebooks (Matlab_to_Python.ipynb) extracts, from the MATLAB (The MathWorks Inc. 2023) data structures created by Shegay et al., the data required for modeling each wall and stores these data in a structured Python (Van Rossum and Drake 2009) array. The second notebook (TCL_Script_Creator.ipynb) uses the Python array to create a tcl script (Ousterhout JK 1990) that builds the OpenSees model of the wall and executes an OpenSees analysis; the second notebook is split into nine sections that correspond to a different step in the OpenSees analysis process:

- Section 1: Initialize the model

- The model is defined to be three-dimensional with one rotational and two translational degree of freedom per axis.
- The variables, for which uncertainty will be considered, are defined

- Section 2: Define location of nodes
    - Nodes are placed at the locations of the vertical reinforcing bars along the horizontal length of the wall. If element length vs height of the wall results in a mesh that is too coarse to provide accurate results, additional nodes introduced along the horizontal length of the wall.
    - The height of each element is equal to the horizontal spacing of the nodes in boundary element to create square elements within the boundary element. This usually results in rectangular elements in the web; if the aspect ratio of web-region elements exceeds 2.0, additional nodes are introduced.
    - Note: wall specimen models extend from the top of the foundation to the height at which lateral displacement was measured. If the height at which lateral displacement was measured did not correspond to the height at which lateral load was applied, then loading was applied at the top of the wall model as a lateral load plus and an overturning moment.
- Section 3: Define material models and associated variables
    - Unconfined and confined concrete crushing energy and fracture energy are computed using element length in the vertical direction.
    - Material models are created for unconfined and confined concrete as well as for all types of reinforcing steel used in the specimen.
- Section 4: Create layered shell sections
    - A shell section comprises 5 layers: 2 cover concrete layers, 2 transverse steel layers, and 1 core concrete layer.
    - The cover concrete thickness is defined using data provided by the researcher.
    - For regions of uniform transverse reinforcement, transverse steel layer thickness is calculated as total number of transverse steel bars in the region, multiplied by the area of each bar, and divided by the vertical height of the region.
    - The cover concrete and steel thicknesses are subtracted from the total thickness of the wall to determine the thickness of the core concrete layer.
- Section 5: Define the elements
    - Elements are created layer by layer up the height of the wall using the previously defined vertical steel materials and layered shell sections
    - The Shegay et al. (2021) database includes variables that define the configuration of the boundary region on each end of the wall or identify the absences of confined boundary element regions. Thus, models represent these characteristics.
- Section 6: Define constraints
    - The bottom row of nodes is fixed for all degrees of freedom.
- Section 7: Define recorders
    - Two recorders are created to store reaction forces in the x-direction for the bottom row of nodes and displacements in the x-direction for the top row of nodes. These

data are used to generate base shear and wall drift histories as well as to enable creation of base shear force versus wall drift response histories.

  - A second group of recorders stores stress and strain histories at the four gauss points in the middle layer of concrete for all layered shell elements in the model. Theses data are used to create movies showing normal as well as principal stress and strain fields; these movies provide understanding of wall response and failure modes.
  - A third group of recorders stores the concrete crack angle at the four gauss points in the middle layer of concrete. These data are used to create movies showing the progression and orientation of concrete cracking; these movies supplement movies showing stress and strain-field histories to provide understanding of wall behavior.
  - A final group of recorders stores stress and strain data for all vertical steel truss elements. These data are used to determine onset of steel yielding as well as strength loss due to fracture or buckling of reinforcing steel.
- Section 8: Define and apply wall axial load
  - The Shegay et al. (2021) database includes the compressive axial load applied to the wall during laboratory testing; for all walls used in this study, a constant axial load was applied in the laboratory.
  - The constant axial load applied in the laboratory is simulated by applying a uniformly vertical load pattern to the nodes at the top of the wall model.
  - This uniform axial load pattern was applied via load control, with 10 steps used to apply the total load applied in the laboratory.
- Section 9: Define the cyclic lateral displacement history and conduct the analysis.
  - A cyclic lateral displacement history was defined for each test specimen by extracting, from the measured displacement history included in the Shegay et al. database, peak displacements for each half cycle (i.e., maximum positive and minimum negative displacement for each full displacement cycle) and then creating a simulated displacement history that progressed from half peak to half peak using a displacement step magnitude of 0.01 inches.
  - A lateral load pattern was created in the OpenSees model to represent the lateral load applied in the laboratory. For specimens for which lateral load was applied and measured at the same height, this lateral load pattern comprised a uniformly distributed lateral loads applied to the nodes at the top of the specimen. For specimens for which the heights of lateral load application and lateral displacement measurement were not the same, the lateral load pattern comprised lateral load plus a linearly distributed vertical load, appropriately scaled, to represent the moment associated with the vertical offset between the height above the base of the wall at which lateral load was applied in the laboratory and the height at which lateral load is applied in the analysis.
  - Lateral load (or lateral load plus moment) was applied under displacement control to match the measured lateral displacement history.
- Section 10: Create the reference file (*referenceFile.txt) that includes the variables needed for postprocessing simulation data:
  - Total number of nodes along the horizontal length of the wall

- Total number of nodes along the horizontal length of the wall that are connected to a truss element
- Total number of nodes in the file
- Total number of elements in the file
- Peaks in the horizontal displacement history at the top of the wall, in the positive direction
- Tensile strength of the concrete
- Total number of layers of concrete elements in the model
- Unique ID of the wall
- Path to the folder that contains simulation output for the wall
- Path to the tcl file for the simulation

3.5 PRELIMINARY MODEL EVALUATION

3.5.1 Mesh Size and Element Formulation Sensitivity Study

A mesh size and element formulation sensitivity study was conducted to determine the maximum element size, which could be expected to determine minimum run time, and the element formulation that could be used to achieve 1) accurate simulation of strength, stiffness, deformation capacity and failure mode and 2) a high level of reliability with respect to simulations continuing beyond the onset of strength loss. Figures 3.9 - 3.11 below show one row of elements for the three levels of mesh refined considered. In these figures, i) heavy blue lines indicate shell element edges that align with the location of truss elements representing vertical reinforcing steel along the wall cross section, ii) light blue lines indicate shell element edges in locations where there are not vertical reinforcing bars, and iii) orange elements indicate shell elements comprising confined concrete and a large volume of smeared, horizontal confining reinforcement. It should be noted that these meshes do not include cover concrete at the ends of the wall. Including this concrete, which has a thickness of less than 0.5 in. for most walls, was found in preliminary analyses to result in premature failure due to convergence issues. Mesh refinement studies were conducted using both the MITC4 and DKGQ elements.

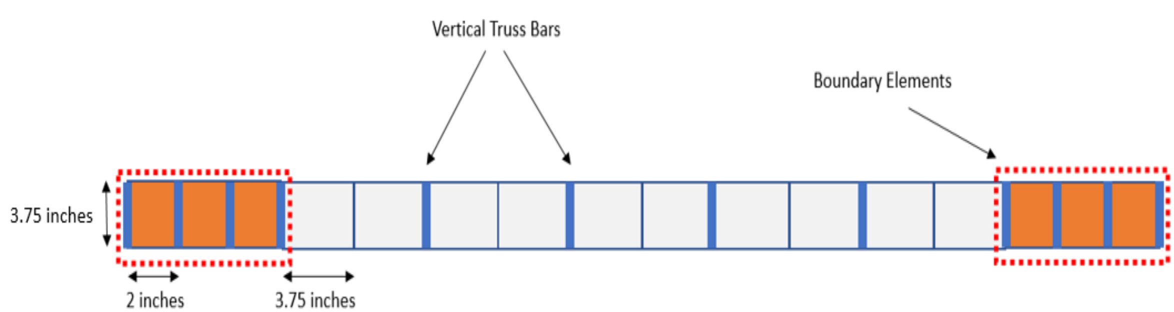

Figure 3.9 Mesh with h/l of 1 to 1.9

Figure 3.10 Mesh with h/l of 0.5 to 1.5

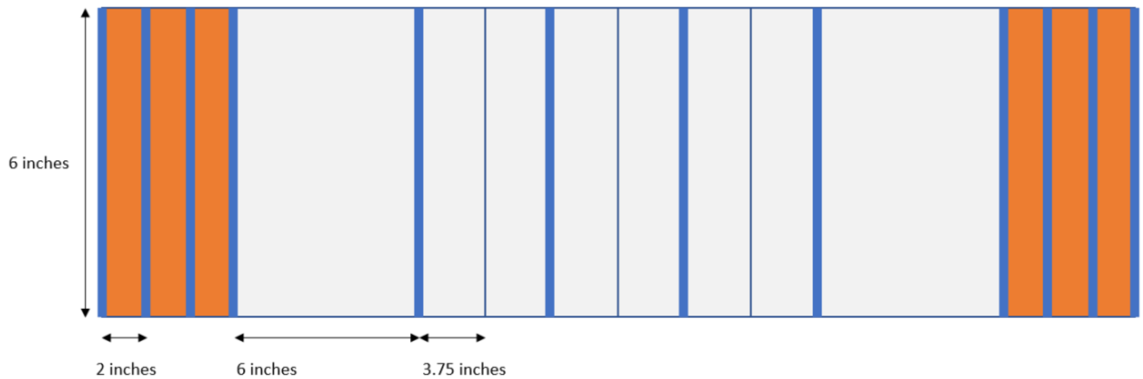

Figure 3.11 Mesh with h/l of 1 to 3

Figures 3.12 and 3.13 show simulated and measured load versus drift histories for wall RW1 computed using baseline/reference concrete and steel material model parameters with the DKGQ elements and MITC4 element and for the three levels of mesh refinement shown in Figures 3.9, 3.10 and 3.11. For both element formulations, results for meshes with elements with height-to-length (h/l) ratios ranging from 1.0 to 3.0 perform the best, with these simulations including simulation of strength loss and continuing beyond the point at which strength loss was observed in the laboratory. Simulations conducted with elements with height-to-length (h/l) ratios of less than 1.0 (green lines in Figures 3.12 and 3.13) exhibit numerical failure (i.e. solution algorithm fails to converge) at drift demand far below the drift at which strength loss was observed in the laboratory. The data in Figures 3.12 and 3.13 suggest also that models employing the DKGQ element formulation provide greater accuracy and consistency in simulating measured response over a greater range of element aspect ratios than do models employing the MITC4 element formulation. Thus, DKGQ element formulation was used with element aspect ratios greater than 1.0 for the study.

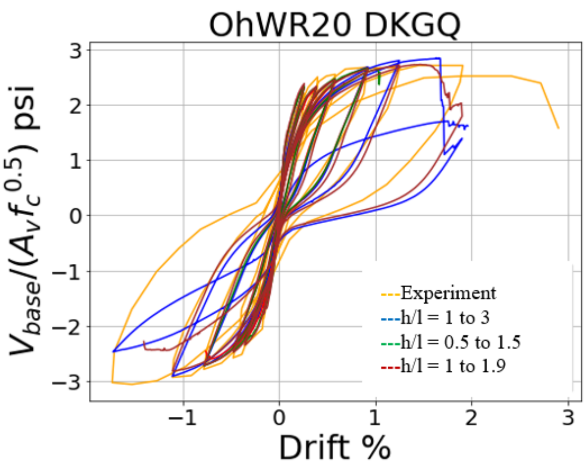

Figure 3.12 Load-Displacement as measured and as simulated using DKGQ element formulation

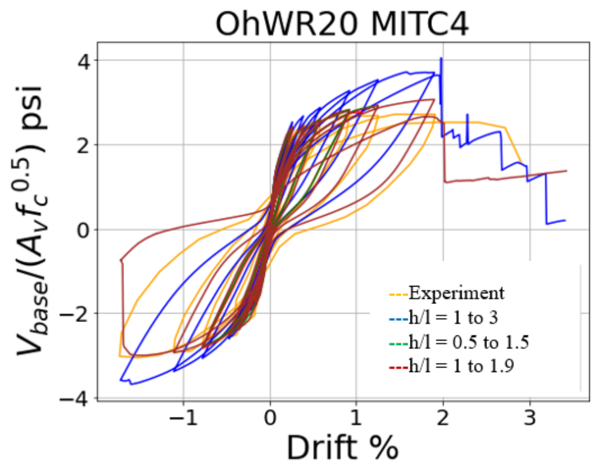

Figure 3.13 Load-Displacement as measured and as simulated using MITC4 element formulation

3.5.1.1 Mesh Size and Element Formulation Observations and Conclusions

The preliminary simulations presented above in Figures 3.12 and 3.13 provide data used to support the choice of element formulation and mesh size. Specifically, the data in Figures 3.12 and 3.13 support the following observations:

- Use of the MITC4 element can result in simulation of significant overstrength if element aspect ratio (h/l) is large.
- Use of the MITC4 element formulation requires element aspect (h/l) ratio to fall between 1 and 2 with smaller or larger aspect ratios results in inaccurate simulation of strength or failure to converge. For elements with large aspect rations (e.g., h/l = 1 to 3 in Figure 3.13), Lu et al. (2015) attributed simulation of strength exceeding that measured in the laboratory to shear locking as discussed in Section 3.2.
- Both element formulations fail to converge at displacement demands that are significantly less than that associated with significant strength loss when element aspect ratios (h/l) ranging from 0.5 to 1.5 (green lines in Figures 3.12 and 3.13) are used
- Both element formulations provide good representation of measured response when element aspect ratios of 1.0 or greater are used.

On the basis of i) the results presented above of a limited study addressing mesh size, mesh aspect ratio, and element formulation as well as ii) observations and recommendations provided in Lu et al. (2015), it was decided that the current study would employ the DKGQ element formulation with element aspect ratios (h/l) ranging from 1 to 3.

3.5.2 Comparing Simulated and Measured Response via Error Functions

Error functions were developed to quantify the accuracy with which OpenSees models simulate wall specimen response quantities measured in the laboratory. Error functions quantify the difference between simulated and measured strength, deformation capacity, and stiffness to nominal flexural strength defined as concrete reaching a strain of -0.003.

A Jupyter notebook was developed for each error function. Each notebook determines the appropriate value of the response quantity of interest using the simulated and the measured data sets and computes the error function as

$$Error = \left|\frac{simulated\ value - measured\ value}{measured\ value}\right| x100 \qquad \text{(Eq 3.17)}$$

Simulation error was quantified as follows:

- Stiffness error: Stiffness error was computed using the measured and simulated displacement at the load at which the nominal flexural strength is achieved in the simulation. For this study the nominal flexural strength was defined, per ACI 318-25, as the flexural strength of the wall section at the wall-foundation interface when the extreme concrete compression fiber reaches a compressive strain demand of -0.003 in/in.[1] The Jupyter notebook created to determine this error includes the following process steps:
    1. Identify the "index point" (i.e. step number in the simulation) at which the extreme fiber of the concrete section at the base of the wall meets or exceeds -0.003 in/in.; this is the index point at which the nominal flexural strength is reached.
    2. Identify in the simulation results files, the lateral displacement and the flexural strength of the wall at the index point. The flexural strength at the index point is considered the nominal flexural strength of the wall.
    3. Identify in the experimental data set the lateral displacement at the top of the wall at which the nominal flexural strength of the wall is achieved, in the same loading direction as was used in step 2.
    4. Compute stiffness error using simulated and measured displacements at nominal flexural strength.
- Max Strength error: Absolute maximum simulated base shear strength, which could be achieved in either the positive or the negative load direction, is compared with the maximum base shear strength, in the corresponding load direction, as measured in the laboratory test.
- Displacement capacity error: The displacement capacity, for both the measured and the simulated data sets, is defined as the displacement, on the envelope of the load-

[1] Note that this definition of nominal flexural strength differs from the definition of nominal flexural strength used by ACI 318-25 in that ACI 318 uses this concrete strain state, the assumption that reinforcing steel stress does not exceed the yield stress, and a simplified section model. For this study, simulated moment strength was computed using the element and material models presented previously.

displacement history, at which, the strength of the wall drops to 80% of maximum strength. The displacement capacity error is computed using measured and simulated displacement capacities in the loading direction in which the laboratory test specimen exhibited maximum displacement capacity. Simulated displacement capacity was found to be highly sensitive to the confined concrete crushing energy ratio or the steel rupture strain ratio used in the simulation model, depending on the failure mode. Thus, the displacement capacity error function was found to be important for calibrating these parameters.

Figures 3.14 - 3.16 show the points on the simulated (red) and measured (blue) load histories at which stiffness, max strength, and displacement capacity locations of a simulated run of RW2.

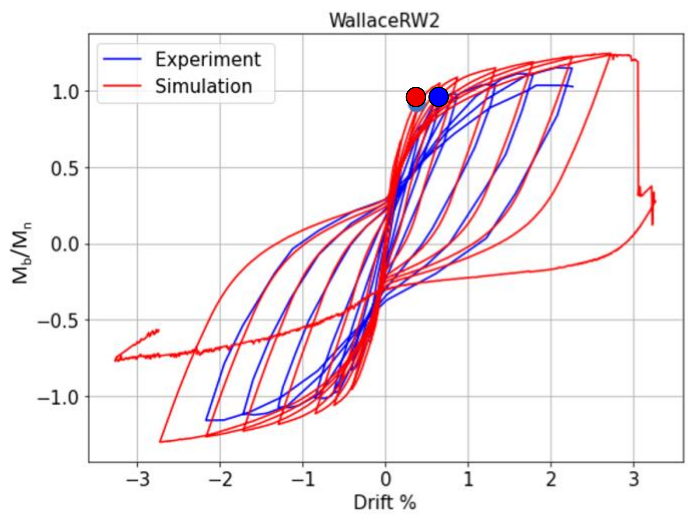

Figure 3.14 Stiffness error of 20%

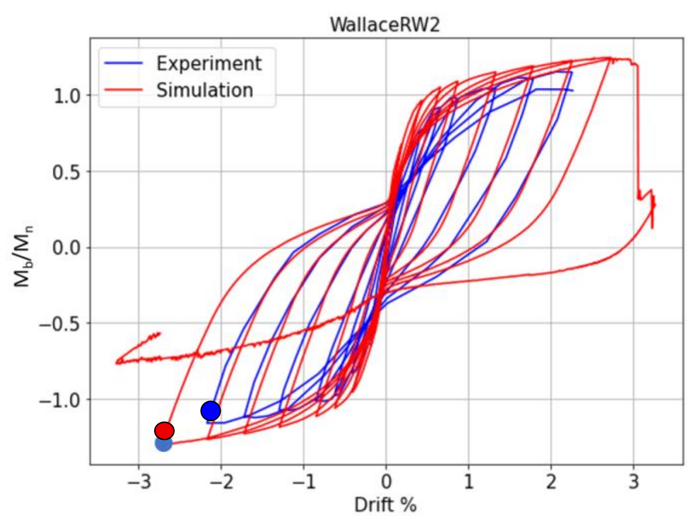

Figure 3.15 Maximum strength error of 16%

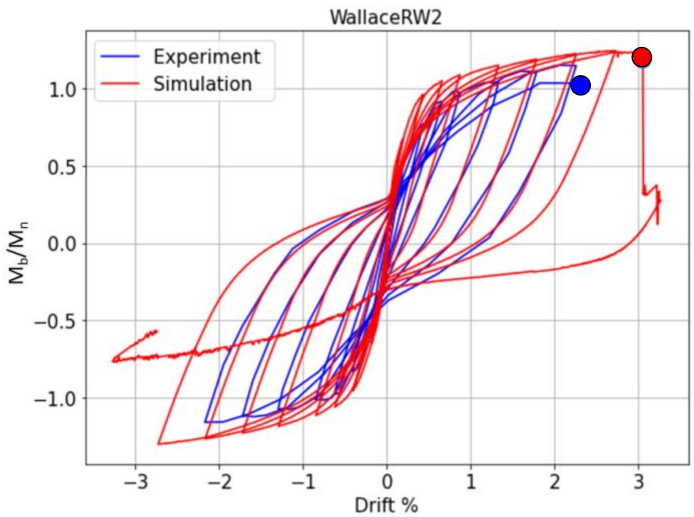

Figure 3.16 Drift capacity error of 35%

3.5.3 Failure Modes

Previous research (e.g., Lowes et al. 2019) suggests that flexure-controlled concrete walls exhibit loss of lateral load resistance due to one of three failure modes: i) *compression-buckling* characterized by strength loss due to crushing of concrete at the extreme end of the wall and simultaneous buckling of reinforcing bars, ii) *bar-rupture* characterized by fracture of previously buckled reinforcing bars, or iii) *compression-shear* charactered by crushing of concrete and buckling of reinforcing steel within the web of the wall at the interface between the unconfined interior unconfined web and confined boundary element regions of the wall. This study includes only walls exhibiting compression-buckling and bar-rupture failure modes.

To determine the simulated wall failure mode, the simulated concrete and steel stress and strain histories for concrete shell elements and vertical reinforcing steel bars at the extreme ends of the of the wall, at the base of the wall, were extracted from the recorders data sets. These data were processed to identify i) the simulation index point at which a quadrature point for the confined concrete layer in the bottom row of layered shell elements develops a compressive strain that exceeds the strain at which residual compression strength is reached and ii) the simulation index point at which the tensile strain in a reinforcing steel element exceeds the tension rupture strain.

Figure 3.17 shows data for RW1, for which the simulated and observed failure modes were both compression-buckling. Figure 3.18 shows data for RW2, for which the simulated and observed failure modes were both bar rupture.

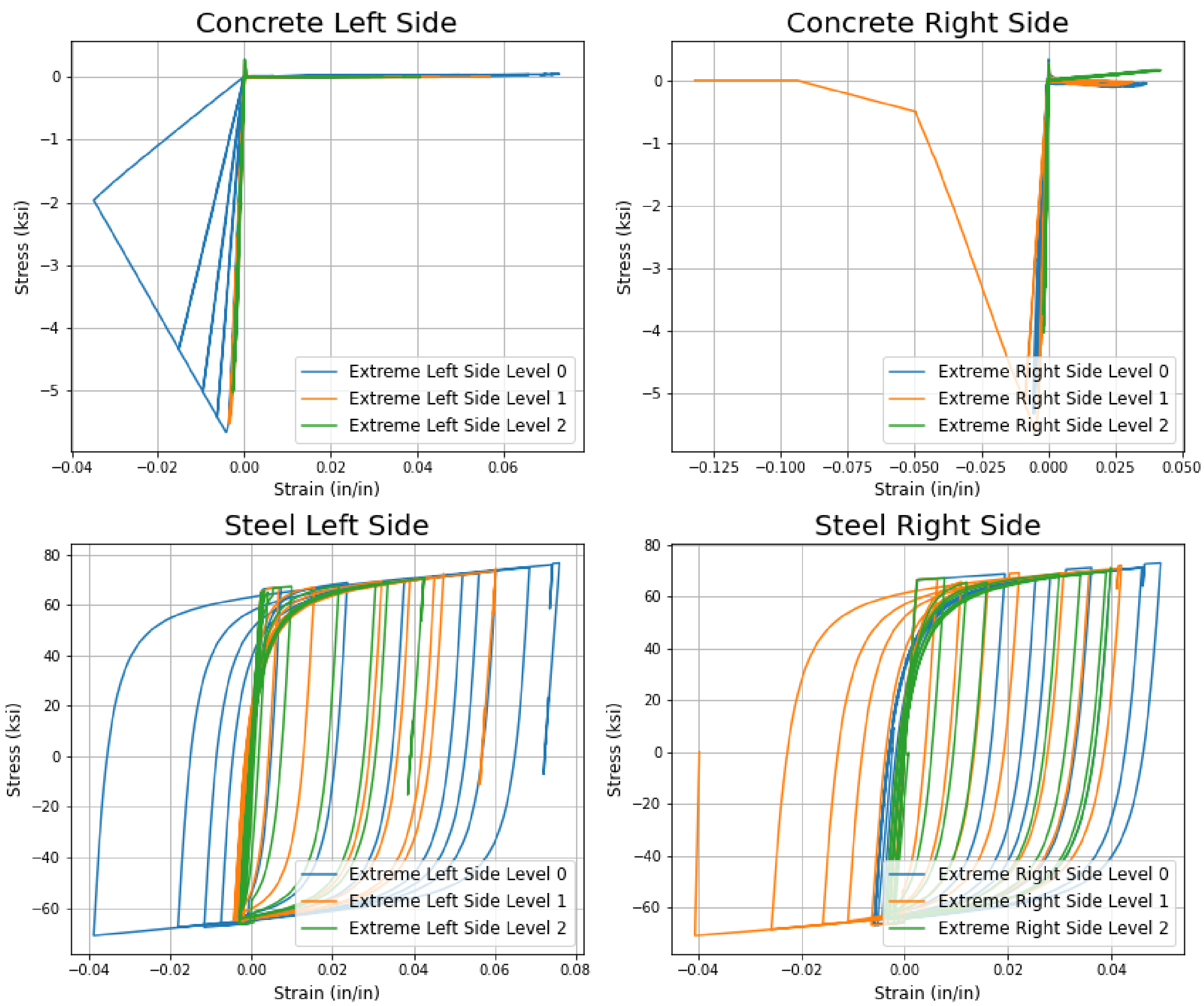

Figure 3.17 Visualization of wall failure for Compression Buckling Failure (Wall Specimen RW1)

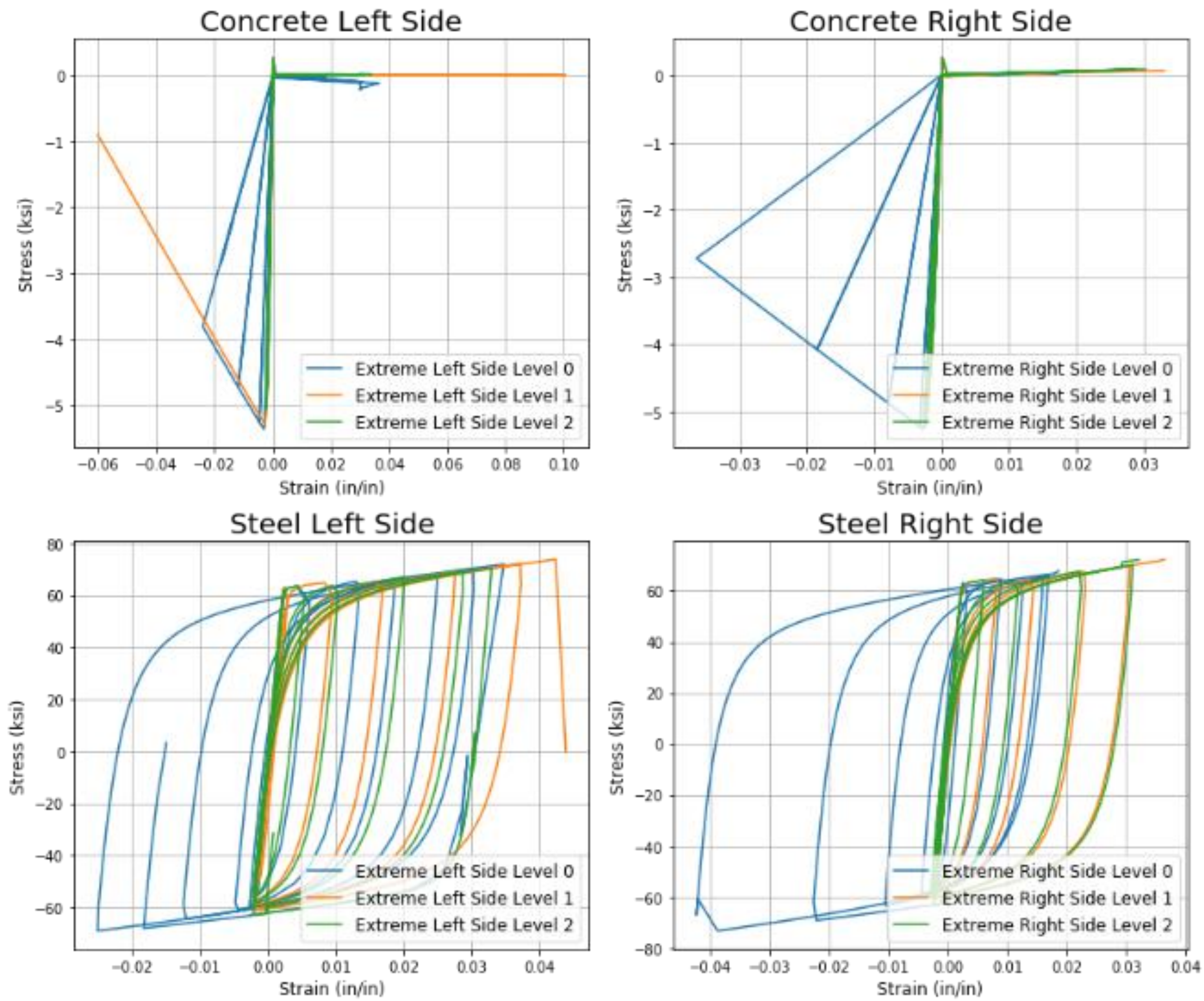

Figure 3.18 Visualization of wall failure for bar Rupture Failure (Wall Specimen RW2)

3.6 SUMMARY

A review of previous research to develop and apply a breadth of finite element formulations and material models suggests that layered shell element models are an ideal tool for simulating the nonlinear response of planar and nonplanar walls exhibiting flexure-controlled response under combined axial and lateral loading. The three layered shell element formulations available for use in OpenSees Version 3.3.0 (DKGQ, NLDKGQ, and MITC4) paired with the two-dimensional concrete constitutive model, PlaneStressUserMaterial, and a commonly-used one-dimensional reinforcing steel model, steel02, were investigate for use in simulating the response of planar concreate walls exhibiting compression- and tension-controlled failure modes under constant axial and cyclic lateral loading. Results of the preliminary investigation included identification of a preferred OpenSees modeling approach for walls where large deformations are not expected. Specifically, the DKGQ model formulation was identified as the preferred element formulation, due to the MITC4 element demonstrating poor performance for meshes with large element aspect ratios. The two-dimensional PlaneStressUserMaterial concrete material model and one-dimensional steel02 reinforcing steel model were found to provide good simulation of concrete and reinforcing steel response when paired with the preferred layered shell element. Error functions were defined for use in assessing the accuracy with which wall stiffness, strength and deformation capacity is simulated. Also in this chapter, a series of Jupyter notebooks are introduced that facilitate the creation of tcl scripts that build OpenSees models of the wall test specimens introduced in Chapter 2, execute OpenSees simulations of these walls using the axial load and lateral displacement histories applied in the laboratory, and enable visualization of simulation results and comparison of simulated and measured response histories.

4 TOOLS

4.1 INTRODUCTION

This chapter presents the computing infrastructure, software, and computational workflows used to accomplish the research presented in this document. Three software platforms were used to complete this project: 1) the opensource finite element analysis platform OpenSees (McKenna 1997, McKenna et al., 2010), for which finite element formulations and constitutive models are presented in Chapter 3, 2) the quoFEM software (McKenna et al. 2025) developed by the NHERI SimCenter (Deierlein et al. 2020), which includes unique algorithms for uncertainty quantification and parameter estimation as well as leverages 3) the Dakota software developed by Sandia National Laboratory (Adams et al. 2021). Use of these software platforms was enabled via use of NHERI DesignSafe computing resources (Rathje et al. 2017) which maintains the DataDepot, in which the Shegay et al. (2021) experimental data set is archived, provides access to the high-performance computing resources at the Texas Advanced Computing Center (TACC), provides research data storage, and provides access to a Jupyter Hub that was used to create and execute a series of Jupyter notebooks (Kluyver et al. 2016) that were developed for this project to support model building, visualization of simulation results, and model assessment.

4.2 COMPUTATIONAL INFRASTRUCTURE

In 2015, the National Science Foundation (NSF) funded the Natural Hazard Engineering Research Infrastructure (NHERI) program to provide infrastructure to support natural hazard engineering research. The NHERI SimCenter and the NHERI DesignSafe facility are two of 11 research infrastructure facilities funded through the NSF NHERI program. The SimCenter "provides next-generation computational modeling and simulation software tools, user support, and educational materials to the natural hazards engineering research community with the goal of advancing the nation's capability to simulate the impact of natural hazards on structures, lifelines, and communities." The NHERI DesignSafe facility enables users to employ state-of-the-art computational methods to advance natural hazard engineering and science, including providing users with access to the high-performance computing resources at the Texas Advanced Computing Center (TACC), providing research data storage, maintaining the DataDepot for publication of natural hazard data sets, and providing access to a Jupyter Hub and Jupyter notebooks.

Specific SimCenter and DesignSafe resources used for the current student include the following:

1. The DataDepot platform for publishing and archiving natural hazard data and/or accessing data published and archived by others.

2. Secure and expansive data storage space for data that are developed by natural hazard research teams during ongoing research projects, with the expectation that some of these data will ultimately be published in the Data Depot.

3. Access to the following software: OpenSees Version 3.3.0, quoFEM, Dakota, Jupyter Hub and Jupyter Notebooks, and Python (Van Rossum and Drake 2009).

4. Access to HPC resources at the Texas Advanced Computing including the Stampede2 supercomputer used in conjunction with quoFEM and OpenSees.

5. The use of Jupyter Hub on DesignSafe to utilize the Jupyter Notebooks created for this research.

4.3 SOFTWARE

The software used for this research are OpenSees Version 3.3.0, quoFEM developed by the NHERI SimCenter, and, via quoFEM, Dakota developed by Adams et al. at Sandia National Laboratory. The current study also uses the HPC resources and the Jupyter Hub provided by the NHERI DesignSafe facility. Specifically, quoFEM is used to utilize Dakota as well as other embedded algorithms to accomplish parameter estimation and sensitivity analysis of OpenSees models; Jupyter notebooks, the Python scripting language, and the DesignSafe Jupyter Hub are used to create OpenSees models and visualize simulation results.

OpenSees is the open-source software platform originally developed by McKenna (1997) and published by McKenna, Scott and Fenves (2000) for simulating the earthquake response of structural and geotechnical systems. OpenSees can be used on a local machine or executed on HPC systems such as DesignSafe. The original OpenSees framework has been greatly enhanced by community contributions of new element and material formulations, solution algorithms, and utilities. This study employs OpenSees Version 3.3.0., including the 1D steel02 material model and truss elements that are included in the OpenSees platform. The current study also employs the following OpenSees components developed by Lu et al. (2015) and included in OpenSees Version 3.3.0: the DKGQ layered shell element, the 2D plane stress concrete material model *PlaneStressUserMaterial*, and the *PlateFromPlaneStress* utility function that creates 2D material layers for use with layered shell elements such as DKGQ from 2D constitutive models such as the *PlaneStressUserMaterial*.

The quoFEM software provides a user-friendly interface to uncertainty quantification codes and software, including the Dakota software. The Dakota software provides "iterative systems analysis methods", which include: optimization with gradient and non-gradient based methods; uncertainty quantification with sampling, reliability, stochastic expansion, and epistemic methods; parameter estimation using nonlinear least squares (deterministic) or Bayesian inference (stochastic); and sensitivity/variance analysis with design of experiments and parameter study methods" for use in conjunction with a wide range of simulation tools. For the current study, quoFEM is used to facilitate use of Dakota with OpenSees; specifically, to facilitate use of Dakota to accomplish a sensitivity analysis and parameter estimation for OpenSees models. The primary workflow for the current study comprises running quoFEM from the user's local desktop, with each quoFEM "run" comprising identification of random variables, creation of a Dakota input file to conduct the requested analyses, and sending the job to nodes on the Stampede2 supercomputer. The quoFEM / Dakota analyses are i) sensitivity analysis and ii) parameter estimation. Section 4.4 provides further discussion of the probability and analysis theory and methods embedded in Dakota, the computational workflows, and the quoFEM interface. Details of the use of quoFEM for the current project are provided in Section 4.5.

Jupyter notebooks and Python are used to create tcl scripts (Ousterhout, J.K., 1990) that drive the OpenSees analyses. OpenSees was used rather than OpenSeesPy (Zhu et al. 2018) because the concrete material model developed by Lu et al. has not been incorporated into OpenSeesPy. Jupyter notebooks can be downloaded locally to a computer and used as a web application to create code and documentation. Jupyter Notebook is also available through the DesignSafe cloud servers. Data that are stored in the DesignSafe Data Depot can be accessed through the DesignSafe Jupyter Hub and immediately analyzed, which accelerates the workflow. Currently, quoFEM is only available as a desktop app, which slows the workflow because quoFEM input files need to reside on the local drive. It is expected that future development activities will enable quoFEM to be used through Jupyter notebooks on DesignSafe. A discussion of the workflow, Python code, and output of the Jupyter notebooks that were developed for this project is provided in Section 4.6. Details of the Jupyter notebooks developed for the current study are presented in Section 4.4.

4.4 JUPYTER NOTEBOOKS

Three groups of Jupyter notebooks were created for this project; these notebooks i) create OpenSees models of the walls in the dataset and execute OpenSees simulations, ii) visualize simulation results, and iii) compute error functions characterizing the accuracy with which measured response quantities are simulated. Individual notebooks are described below, published at https://github.com/stokljos/thesis/tree/main/notebooks, and available via DesignSafe Use Cases https://www.designsafe-ci.org/user-guide/usecases/overview/.

4.4.1 Notebooks for OpenSees Simulations

The first group of two notebooks can be used to accomplish OpenSees simulations of each wall in the data set. The first notebook (Notebook 1.1: Matlab_to_Python.ipnyb) maps the MATLAB data characterizing wall test specimens and loading protocols into Python, and the second notebook (Notebook 1.2: TCL_Script_Creator.ipynb) creates OpenSees models of each wall as well as executes OpenSees analyses of each wall subjected to its laboratory loading protocol. The second group of Jupyter notebooks comprises five notebooks that accomplish post processing of simulation data.

4.4.1.1 Notebook 1.1: MATLAB to Python

The primary function of Notebook 1.1: MATLAB to Python.ipynb is to create a Python list that stores all of the data from the Shegay et al. (2021) MATLAB data structure that are required to build and execute OpenSees analyses of the 33 planar walls that are used in the current study. For each wall extracted from the Shegay et al. dataset, this notebook creates a unique name and a unique index number; these identifiers are used throughout the analysis. The "unique name" is a combination of 1) the last name of the researcher who conducted the laboratory testing and published the laboratory data and 2) the identifier assigned to each wall specimen by the researcher. For example, Wallace and Thomsen (1995) conducted laboratory testing and published laboratory data for a wall specimen that they identified as RW1; thus, this wall specimen is given the unique name "WallaceRW1". Each wall specimen is assigned a unique index number, somewhat randomly, based on the order in which the data were entered into the Shegay MATLAB data structure. For example, the WallaceRW1 wall was assigned the index 33. When 33 is provided as input to Notebook 1.2, a Python list is created that stores all relevant data for 'WallaceRW1' for use in subsequent notebooks.

The data that are retrieved from the MATLAB data structure and stored in the Python list for use in model building include the following:

1. **Wall geometry:** including height, thickness, in-plan length, shear span defined as the moment at the base of the wall divided by the shear at the base of the wall, thickness of cover concrete, and aspect ratio.

2. **Reinforcement layout:** including, for horizontal and vertical bars, locations of the vertical bars, bar diameters, bar spacing of bars, and reinforcement ratios.

3. **Steel material data:** including, for each unique bar size, yield strength, ultimate strength, strain at yield, and strain at ultimate strength.

4. **Concrete material data**: including, concrete (boundary and web regions) compressive strength and strain at compressive strength. Compressive strength for concrete is that measured in the lab; compressive strength for confined concrete as well as strain at maximum strength for unconfined and confined concrete are calculated and/or prescribed values.

5. **Response data**: axial load, lateral load, and displacement history.

4.4.1.2 Notebook 1.2: TCL_Script_Creator

Notebook 1.2: TCL_Script_Creator.ipynb requires the user to input one or more wall indexes. For each wall, the output is a tcl script that can be used to create and execute an OpenSees analysis of the wall as well as two *.txt files that support analysis and postprocess analysis data.

For each wall index listed in Notebook 1.2, Notebook 1.1 is executed with the wall index to retrieve a Python list of data characterizing the wall and the load and displacement histories employed in the laboratory.

Chapter 3 provides a summary of each section of Notebook 1.2 as well as the three other files that are created with the OpenSees model file; these files comprise a text file that includes the experimental displacement capacity, the experimental maximum strength, and a reference file that provides information required for use with post-processing notebooks. These text files are used with quoFEM, as discussed in Section 4.3.

4.4.2 Notebooks for Post Processing

Four notebooks (Notebook 2.1: XmlReader, Notebook 2.2: DisplacementLoadHistory, Notebook 2.3: br_or_cb.ipynb, and Notebook 2.4: movies.ipynb, support postprocessing of the OpenSees analysis data. Notebook 2.1 reads the xml files generated by OpenSees and extracts and processes the data that are used by Notebooks 2.2, 2.3 and 2.4.

4.4.2.1 Notebook 2.1: xml Reader

Notebook 2.1: xml_Reader.ipynb requires as input a file named *referenceFile.txt, where * is a unique identifier for the analysis. This file is created with the *.tcl file that is the "input" file used to execute the OpenSees analysis and is placed in the same folder as the *.tcl file and all "output" files created during execution of the OpenSees analysis. xml_Reader.ipynb extracts data, from the simulation output files, that are required for the data visualization notebooks.

Some of the output data from the simulation are recorded in xml files. The xml format is used to save data storage space, text files used to store data would be two to five times larger than the xml files. A typical xml file for concrete stress at each point along the solution path ranges from 200 MB to 1 GB and comprises thousands of lines of data. Notebook 2.1 extracts data form the xml files required for use with other notebooks that accomplish data post processing and visualization tasks.

The xml_Reader.ipynb notebook extracts specific data from the xml files and writes these to a Python variable. For example, this notebook extracts, from the *.xml files in which element stress and strain data are recorded, concrete stress and strain in the y-direction, concrete stress and strain in the x-direction and shear stress and strain data for each element and places these data in correspondingly named array that can be used by another post-processing notebook.

Following are the names of the variables and a description of the data that are included in each XML output file utilized by Notebook 2.1:

- FULLWALL_elementsmat*fib$sig.xml and FULLWALL_elementsmat*fib$eps.xml store stress and strain data for all layered concrete shell elements in the model for material * and fiber $ at all integration points. Multiple FULLWALL*.xml files are created to capture stress and strain data for all integration points in the element.

- FIRST3LEVELS_elementsmat*fib3sig.xml and FIRST3LEVELS_elementsmat1fib3sig.xml store stress and strain data for the first three rows of layered concrete shell elements in the model, for all four quadrature points, and for "fiber 3" which is the middle concrete layer and is the confined concrete layer in the boundary elements. This is used to save time for post-processing when stress and strain data are required only for the more heavily loaded bottom section of the wall.
- trusssig.xml and trussseps.xml store stress and strain data for all vertical reinforcing bars in the wall
- Crack_elementsmat1fib3crack.xml stores the simulation step number at which the middle concrete layer, for each quadrature point in each layered shell element, cracks and angle from the horizontal axis of the concrete crack surface. These data are used to visualize the progression and orientation of concrete cracking during the analysis.

The *referenceFile.txt file, which is created when the model is created, contains approximately 10 lines that define values used in postprocessing the simulation data. These include the number of nodes along the base of the wall, the total number of nodes in the wall model, and the total number of elements in the wall model. These data are unique to each wall model and are used to parsing the data for visualizing simulation results.

4.4.2.2 Notebook 2.2: Visualization of load-displacement history

Notebook 2.2: LoadDisplacement.ipynb creates figures showing measured and simulated load displacement histories for each test specimen. The input for this notebook includes two simulation output files, basereact.txt and topdisp.txt, and measured data retrieved from the appropriate MATLAB files. The *.txt simulation files include the horizontal reaction force at the base of the wall and the horizontal displacement at the top of the wall. Using these data, a simulated response history is generated characterizing base moment versus displacement at the top of the specimen. The experimental base-moment versus drift at the top of the specimen response history as measured in the laboratory is retrieved from the MATLAB file. As shown in Figure 4.1, the measured and simulated data are converted to unitless quantities by dividing measurement and simulated base moment by the ACI 318 nominal flexural strength of the wall, M_n and by converting displacement at the top of the wall to drift by dividing displacement by the height from the base of the wall to the point at which the lateral displacement of the wall is measured in the laboratory and in the simulation. It should be noted that the number of points used to define the experimental and simulation normalized load versus drift histories differ due to added points to the simulation history to achieve converged solutions for each solution point on the simulated load-displacement history.

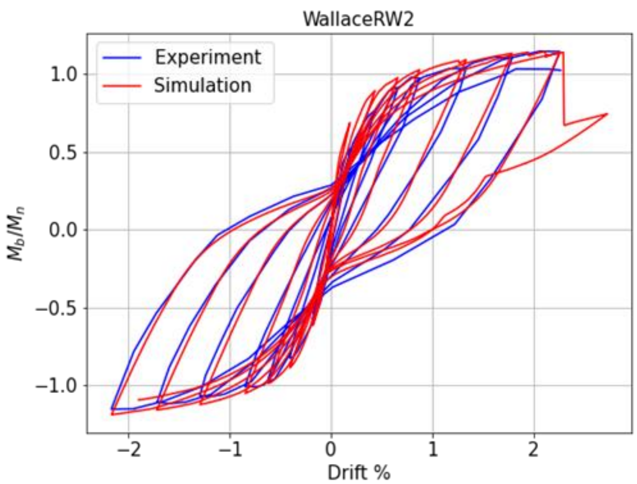

Figure 4.1 Load-Drift plot comparison from the experiment and simulation

4.4.2.3 Notebook 2.3: Assessment of Wall Failure Mode

Notebook 2.3: br_or_cb.ipynb processes simulation data to plot concrete and steel element material response histories and to determine if the simulated failure mode for the wall is a compression- or a tension-type failure. The notebook takes as input the stress and strain histories at each quadrature point in each concrete element for the bottom three rows of elements as well as the stress and strain histories for all vertical steel bars in the first 3 rows of concrete elements. These data are used to create plots showing the stress-strain histories for concrete element quadrature points and reinforcing steel elements near the bottom of the wall, including at the horizontal ends of the wall, where material yielding and failure could be expected to occur. Notebook 2.3 provides as output plots of concrete quadrature point vertical stress-strain response and vertical reinforcing steel stress-strain response.

Notebook 2.3 also provides as output the simulated failure mode for the wall, which is defined as either concrete crushing and simultaneous reinforcement bucking (CB) or reinforcing steel fracture due to prior cycles of high compression strain demand, which could be expected to produce bar buckling (BR). Bar rupture failure is identified when a phase of monotonically increasing steel tensile strain produces a drop, to zero, of steel stress. Concrete crushing failure is identified when increasing concrete compressive strain demand results in loss of concrete compressive strength. In the laboratory, extreme concrete compression strain demand is typically accompanied by compression buckling of reinforcing steel; in the model reinforcing steel loses compressive strength at the compressive strain demand at which concrete compressive strength drops to the residual compression strength. Figure 4.2 show samples of simulated stress strain histories for quadrature points closest to the base of the wall in concrete elements at the horizonal perimeter of the wall and for vertical reinforcing steel elements near the base of the wall and at the horizontal ends of the wall. Simulated failure of concrete and steel was found to occur typically at the bottom most quadrature point and element, respectively; however considering data for several layers of quadrature points was found to be useful in evaluating wall response.

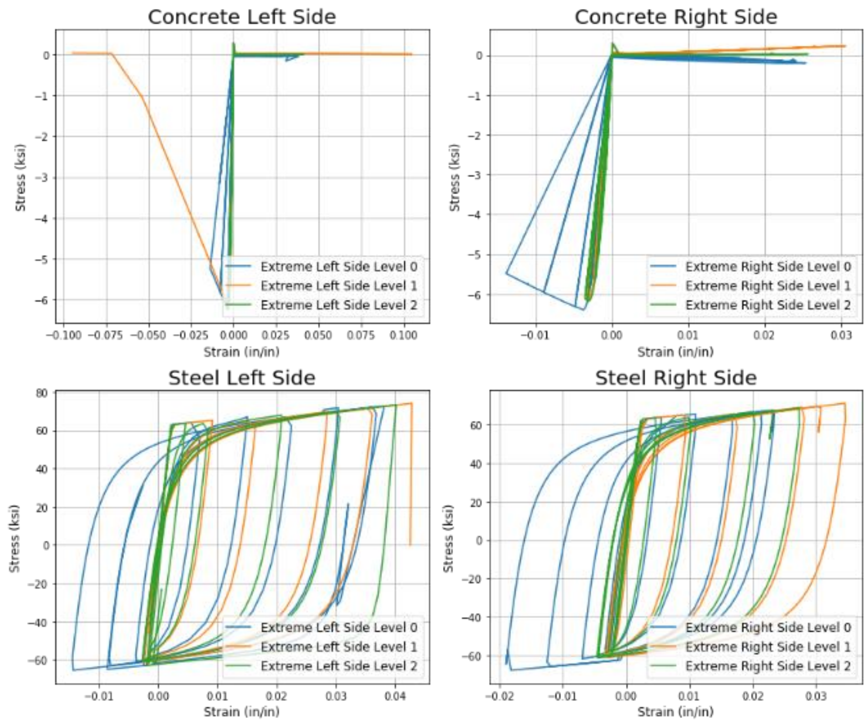

Figure 4.2 Stress strain response histories for extreme concrete and steel fibers

4.4.2.4 Notebook 2.4: Movies

Notebook 2.3: Movies.ipynb requires as input the stress and strain arrays generated using Notebook 2.1; these are the simulated stress and strain histories for every concrete element quadrature point and every reinforcing steel element in the model. Notebook 2.3 creates an interactive plotting tool that can provide movies of the simulated concrete stress and strain field histories for the entire wall. The plotting interface comprises two plots of simulated concrete stress of strain fields placed side by side with a dropdown menu above each one to select which stress/strain value to be plotted and a slide bar at the bottom that identifies the point in the simulation history for which data are shown (Figure 4.3). The user can manually slide the bar to choose unique points during the simulation history or choose auto scroll, which slides through the cyclic history. The user can choose to view normal stress/strain in the vertical direction or shear stress/strain as well as minimum or maximum principal stresses and strains. This tool for visualizing simulation results enables the user to understand how these fields evolve as the wall is subjected to the cyclic displacement history and, thereby, provides improved understanding of the load-transfer mechanism and failure mode.

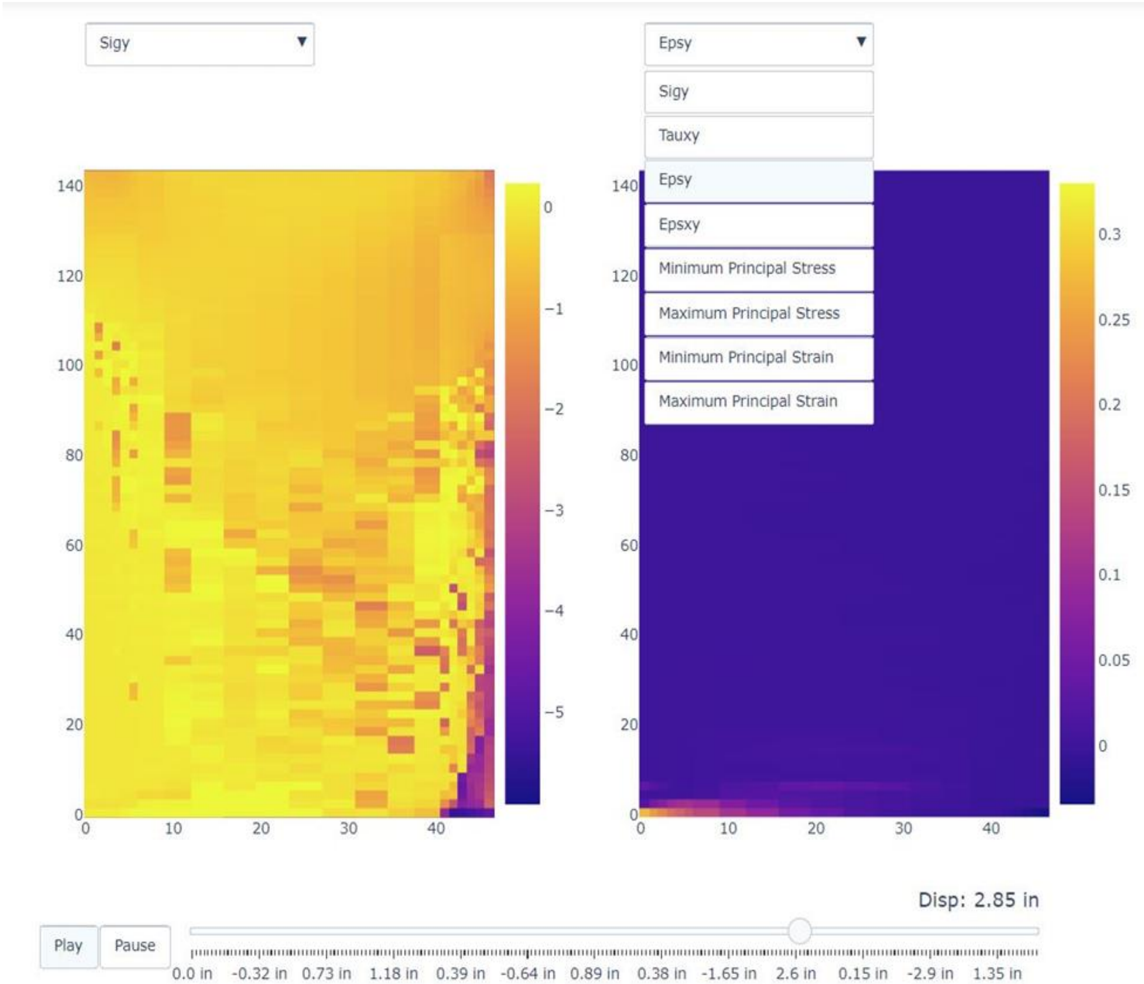

Figure 4.3 Wall stress profile of drift history

4.4.2.5 Notebook 2.5: Concrete Crack Angle

Notebook 2.5: CrackedModel.ipynb requies as input the crack xml files and creates as output a figure showing the angle of the concrete crack at each cracked quadrature point at the end of the analysis. Figure 4.4 provides an example of the notebook output. These crack orientation data can be compared with crack patterns observed in the laboratory to evaluate the accuracy of the simulation. These data also provide understanding of the orientation of the principal stress fields at the point of crack initiation. The concrete material model includes two recorders that provide, for each quadrature point, i) output indicating whether or not the concrete has cracked and 2) the concrete crack angle. Notebook 2.5 first builds an image of the wall mesh and then creates a short line parallel to the crack surface at the node closest to the quadrature point; this results in pairs of crack markers at most nodes. It should be noted that within the material model, once a crack forms, the orientation of the crack surface is fixed for the remainder of the analysis.

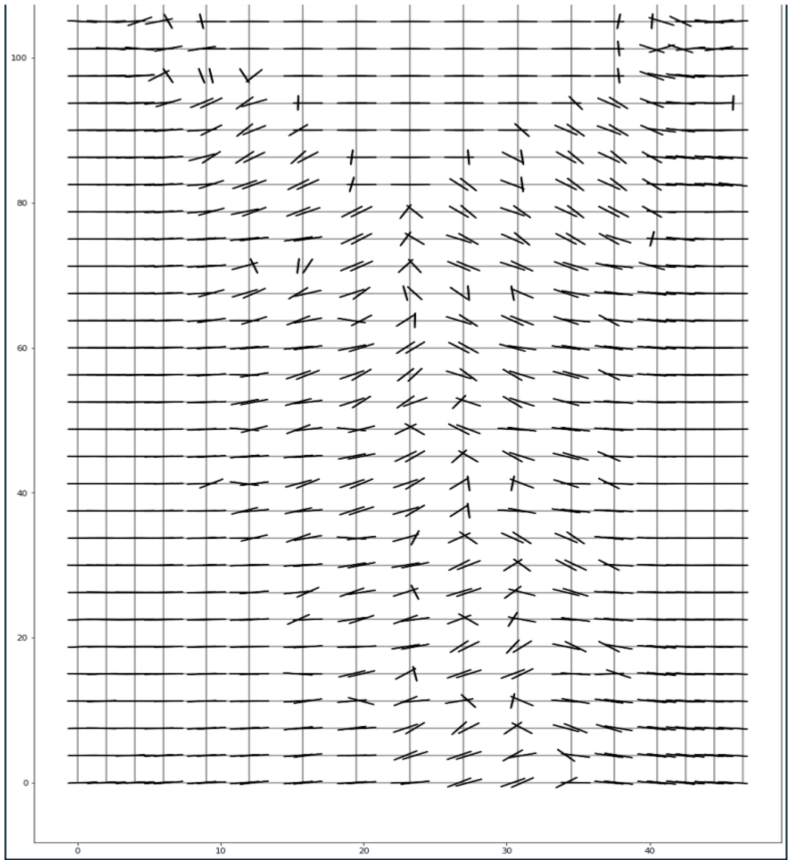

Figure 4.4 Example of crack angle presentation for concrete elements.

4.4.3 Notebooks 3.1 through 3.4

The last group of Jupyter notebooks compute error functions that quantify the different between measured and simulated response quantities. There are four unique notebooks in this group that compute the difference between the measured and simulated i) stiffness, ii) maximum strength, iii) displacement capacity, and iv) envelope to the cyclic response history. Specifics of these notebooks follow:

4.4.3.1 Notebook 3.1: Stiffness Error

Notebook 3.1: StiffnessError.ipynb defines the error in simulated initial stiffness. Initial stiffness is defined by the load-displacement point at which the extreme concrete compression fiber reaches a strain of -0.003. This strain value is used in the ACI 318 Code (ACI Committee 318, 2025) to define loading to the nominal flexural strength of the wall, M_n. Because the experimental data do not include the load and displacement at which maximum concrete compressive strain at the base of the wall reaches -0.003, the stiffness error is instead defined using the measured displacement, $d_{n,m}$, and simulated displacement, $d_{n,s}$, at which the nominal flexural strength of the wall is achieved:

$$Error_{stiffness} = \left|\frac{k_{simulated} - k_{measured}}{k_{measured}}\right| = \left|\frac{\frac{M_n}{d_{n,s}} - \frac{M_n}{d_{n,m}}}{\frac{M_n}{d_{n,m}}}\right| = \left|\frac{d_{n,m} - d_{n,s}}{d_{n,s}}\right| \qquad \text{(Eq 4.1)}$$

4.4.3.2 Notebook 3.2: Maximum Strength Error

Notebook 3.2: StrengthError.ipynb defines the error in simulated maximum strength. Measured data are analyzed to find the maximum load, in either the positive or negative loading direction, sustained by the specimen during testing. Then, the simulation data are searched to find the maximum simulated load, in the same loading direction as the maximum measured load was recorded. The strength error is computed as follows:

$$Error_{strength} = \frac{F_{max_{simulated}} - F_{max_{measured}}}{F_{max_{measured}}} \qquad \text{(Eq 4.2)}$$

with measured and simulated forces acting in the same load direction.

4.4.3.3 Notebook 3.3: Displacement Capacity Error

Notebook 3.3: DriftCapacityError.ipynb defines the error in the simulated displacement capacity, with displacement capacity defined as the displacement at which the component strength drops to 80% of maximum strength with increasing displacement demand. Displacement capacity is computed using displacement and strength data for a single loading direction Notebook 3.3 searches through the measured data to find the displacement at strength loss from maximum greater than 20% with increasing displacement demand $\left(D_{max_{measured}}\right)$, searches through the simulation data to find the displacement at which simulated onset of strength loss occurs in that same direction, and computes the displacement capacity error as follows:

$$Error_{displacement\_capacity} = \frac{D_{max_{simulated}} - D_{max_{measured}}}{D_{max_{measured}}} \qquad \text{(Eq 4.3)}$$

4.4.3.4 Notebook 3.4: quoFEM

The final Jupyter notebook creates a quoFEM post processing script. This script duplicates code in Notebooks 3.2 and 3.3 to determine simulated max strength and displacement capacity and provides as output the ratios of i) simulated maximum strength divided by measured maximum strength and ii) simulated displacement capacity divided by measured displacement capacity.

4.5 QUOFEM

The quoFEM (McKenna et al. 2023, Deierlein et al. 2020) software developed by the NHERI SimCenter was used to facilitate uncertainty quantification and model parameter estimation for the current study. The quoFEM application provides a user-friendly interface to three uncertainty quantification and parameter estimation computational "engines": the Dakota software, which is developed and maintained by Sandia National Laboratory, and the SimCenterUQ and UCSD-UQ engines, which were developed as part of the NHERI Simcenter project. The current study uses only the Dakota software and the sensitivity analysis and parameter estimation methods that are included in the Dakota software.

4.5.1 quoFEM Sensitivity Analyses

Initially, quoFEM Sensitivity Analyses were performed, using the Dakota Nataf transformation algorithm, to assess the impact on simulated response of variation in the uncertain model parameter defining shear retention on the cracked concrete surface. This parameter was investigated first because variation of the shear retention was found to result in variation in maximum simulated strength.

Use of the quoFEM software requires definition of the following to complete an analysis:

- name of the random variable
- distribution to be assigned to the variable and distribution parameters
- input file
- output file
- quantity of interest in the output file

For this first application of quoFEM, a sensitivity analysis was conducted to assess the variability of the maximum simulated strength given uncertainty in model input parameter shear retention factor (*stc*); the model parameter was assumed to have a uniform distribution within practical limits for the model (0.01 to 0.15). Figures 4.5 through 4.9 show definition of the analysis and input quantities using the quoFEM GUI; Figure 4.7 identifies the shear retention factor (*stc* in Eq. 3.13 and Figure 4.7) as varying from 0.01 to 0.15.

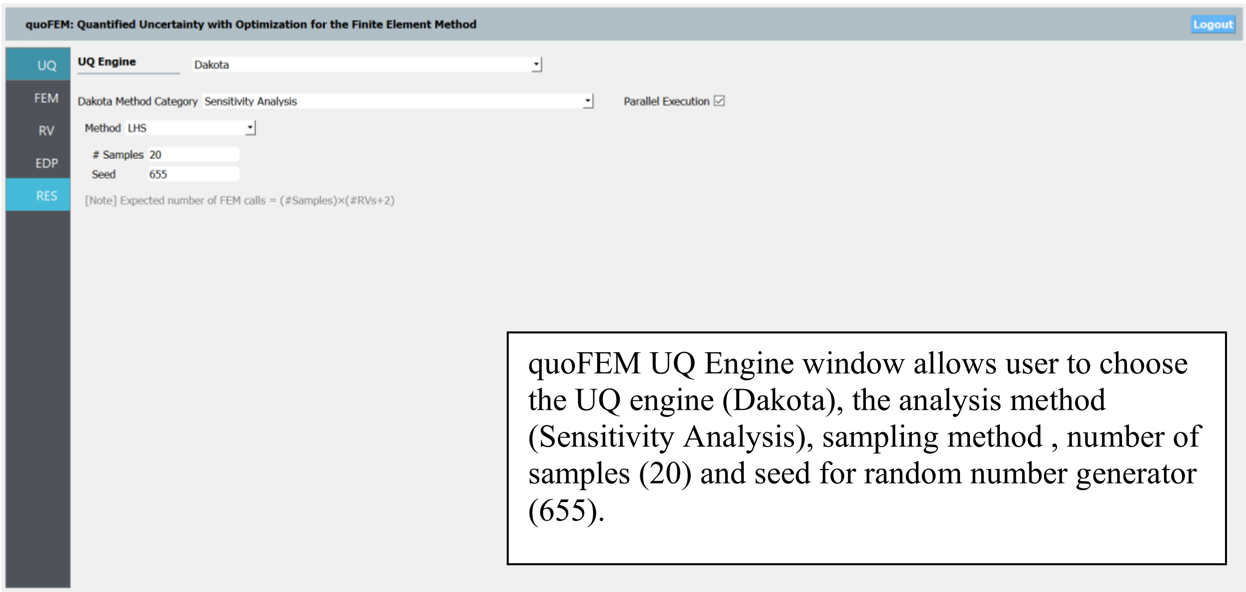

Figure 4.5 quoFEM sensitivity set up

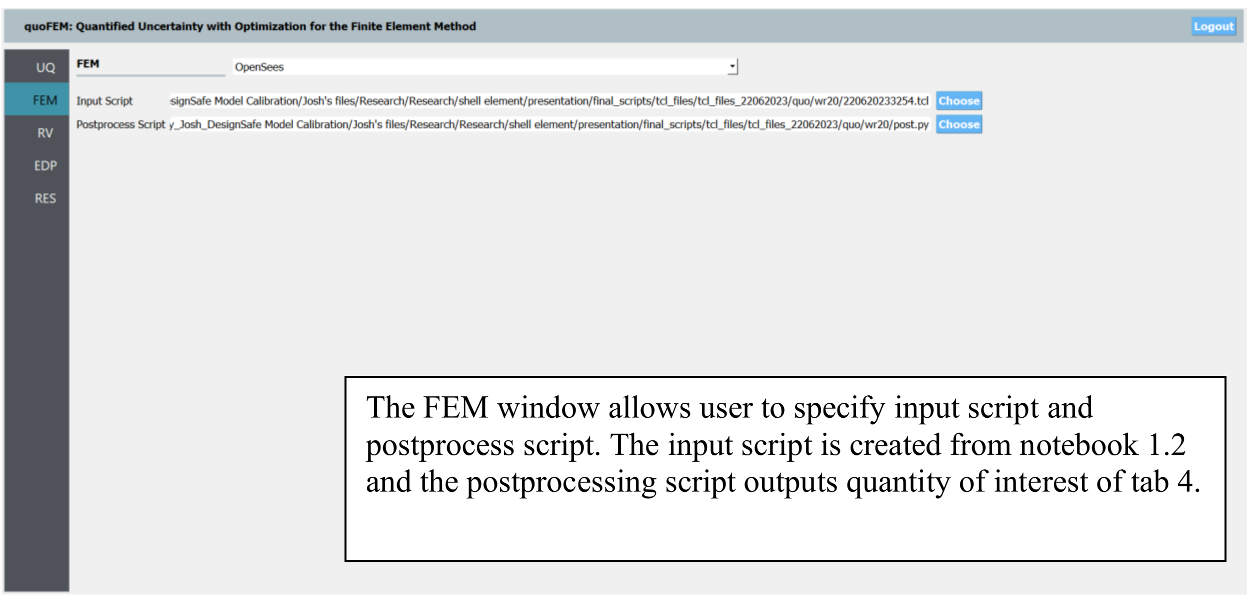

Figure 4.6 quoFEM sensitivity FEM set up

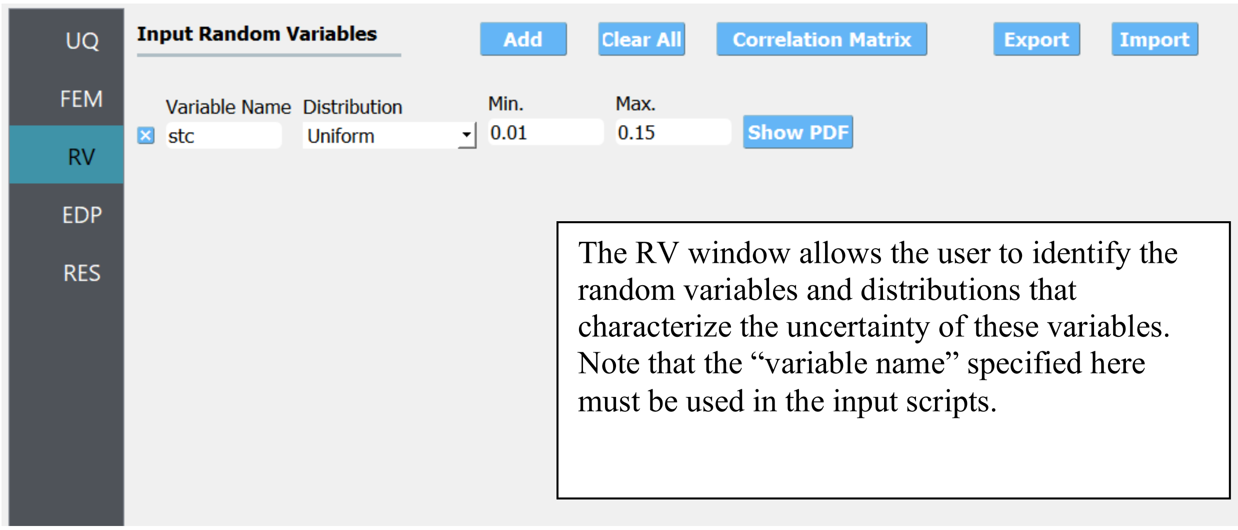

Figure 4.7 quoFEM sensitivity variable definition

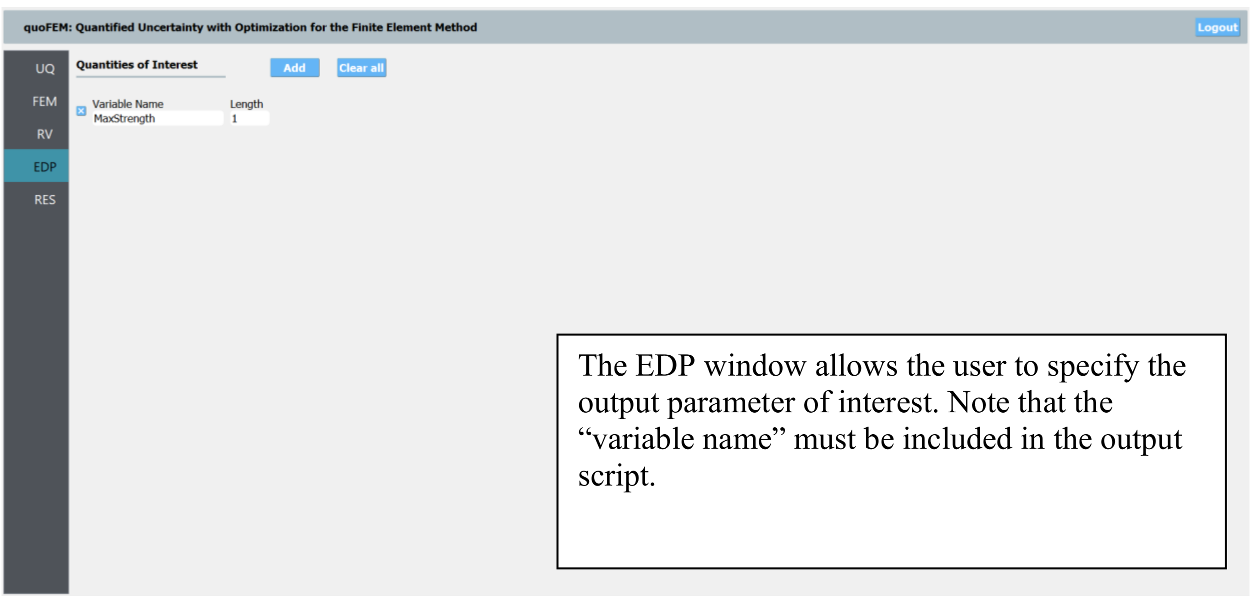

Figure 4.8 quoFEM sensitivity QoI set up

Figure 4.9 quoFEM Results

A single quoFEM run to investigate the impact of model parameter uncertainty was found to take between 1 and 5 hours using a PC with a i7-10700 CPU @2.9GHz with 8 cores, 16 logical processor and 16 GB RAM. Time variation depended on the the number of elements used to model the wall. The results in Figure 4.9 show the sensitivity of the simulated strength to variation in the shear retention factor (*stc*) used in the concrete material model; specifically the data show that increasing the shear retention factor for the concrete crack surface increases the simulated strength of the wall. Note that each simulation is stored in a zip file on the DesignSafe data depot. That file can be extracted and further post processing can be down through Jupyter to understand how certain parts of the model are behaving due to the change in the parameter.

4.5.2 quoFEM Parameter Estimation

Two algorithms are available in the SimCenter quoFEM software, the OPT++GuassNewton algorithm and the NL2SOL algorithm. Additional information about these algorithms is provided in the Dakota User's Manual (Adams et al., 2021).

The first algorithm consists of the Gauss-Newton Hessian approximation with full Newton optimization algorithms. The exact objective function value, exact objective function gradient, and the approximate objective function Hessian are defined from the least squares term values and gradients and are passed to the full-Newton optimizer. As for all of the Newton-based optimization algorithms in OPT++, unconstrained, bound-constrained, and generally-constrained problems are supported. However, for the generally-constrained case, a derivative order mismatch exists in that the nonlinear interior point full Newton algorithm will require second-order information for the nonlinear constraints whereas the GuassNewton approximation only requires first order information for the least squares terms.

The NL2SOL algorithm is a secant-based least-squares algorithm that is q-superlinearly convergent. It adaptively chooses between the Gauss-Newton Hessian approximation and this approximation augmented by a correction term from a secant update. NL2SOL tends to be more robust (than conventional Gauss-Newton approaches) for nonlinear functions and "large residual" problems, i.e., least-squares problems for which the residuals do not tend towards zero at the solution.

When setting up a parameter estimation on quoFEM, it follows the sensitivity analysis workflow except for the first tab which will define the parameter estimation. The method will either be OPT++GuassNewton or NL2SOL, then max iterations of the estimation can be set and a convergence tolerance. The user will also add a calibration file which will hold the value(s) of the result the user is trying to get to for the output of the post processing file (Figure 4.10).

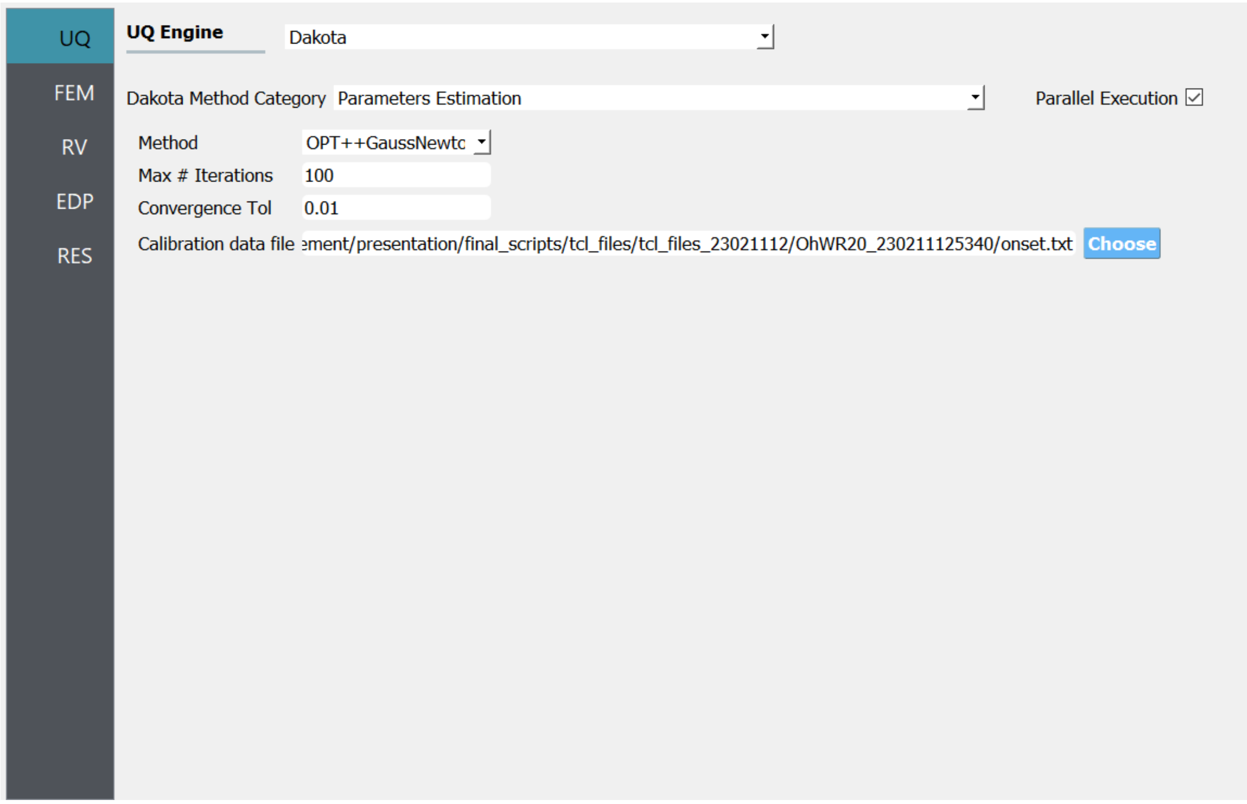

Figure 4.10 quoFEM parameter estimation set up

In the instance of using a model where the parameters cannot be reliably estimated, there is the gradient free parameter estimation. This method minimizes the function based on how the function values are evaluated. The exact pattern search algorithm this method uses is called *'coliny_pattern_search'*.

For a non-gradient parameter estimation, the user will select Optimization under 'Dakota Method Category' and use the 'Derivative-Free Local Search" method. The gradient free parameter estimation follows the same workflow as sensitivity analysis and parameter estimation expect for the first tab. The following is an explanation of each input seen in Figure 4.11:

1. Initial step size: this defines the initial size of the offsets used in the pattern search algorithm

2. Contraction factor: this specifies the ratio of the reduction in the offset size used in the pattern search algorithm

3. Max # model evals: This is a termination criterion. This specifies the maximum number of model evaluations allowed during the search for the optimum parameter values. This sets the total computational budget for the pattern search algorithm.

4. Max # iterations: This is a termination criterion. This specifies the maximum number of iterations allowed in the optimization algorithm. During each iteration of the algorithm, several model evaluations occur in parallel.

5. Variable tolerance: This is a termination criterion. This specifies the maximum permitted change in the value of the parameters being estimated from one iteration to the next.

6. Convergence tolerance: This is a termination criterion. This specifies the maximum permitted change in the value of the objective function from one iteration to the next.

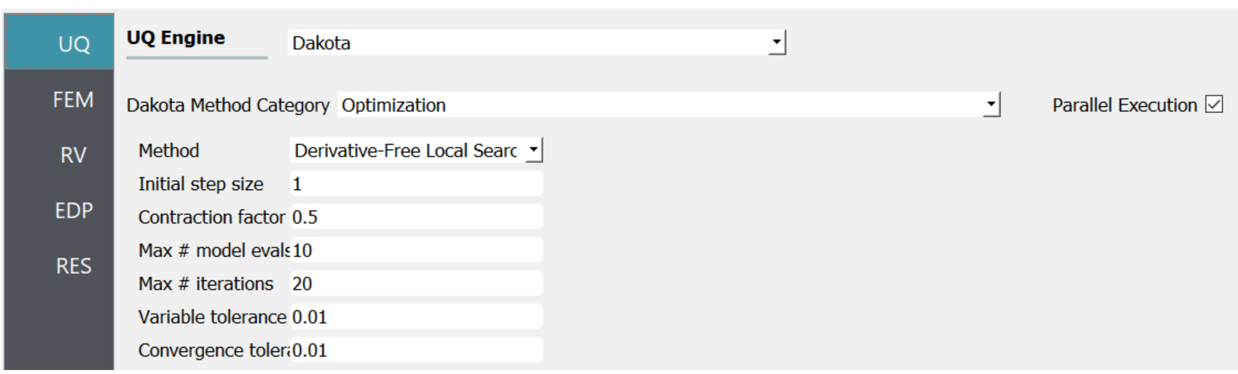

Figure 4.11 Non-gradient parameter estimation set up

4.6 WORKFLOW

There are four workflows to consider; i) local desktop for single OpenSees run and post process (Figure 4.12), ii) Jupyter Hub single OpenSees run and post process (Figure 4.13), iii) quoFEM setup and run (Figure 4.14), iv) post-quoFEM Jupyter Hub process (Figure 4.15). Each workflow has its own purpose and use in the research being presented. Each workflow can be represented by the flow charts at the end of the section. The following will discuss each workflow in detail.

The first workflow is for the purpose of getting quick results. Unlike on DesignSafe where jobs are put in a queue to run, on a desktop with OpenSees downloaded the job starts immediately. The main goal of this workflow is to see how changing a variable or convergence script affects the results of the simulation. Since it is running on a local desktop/laptop, a single run will be slower than on TACC computers, but the setup and process will be quicker.

To start the workflow it is assumed the user has OpenSees and Jupyter notebook installed and apart of file path environmental variables and the scripts used for this research downloaded. The first step is to run Jupyter notebook in the folder where the scripts are located. Once the Jupyter notebook browser is up, the model creator script is selected. In this script, the only user input is the index number(s) for the wall that will be modeled. For specific wall indices see Appendix C. There are options to create a single wall or multiple walls at once in the script. Once these models have been created, they will be stored in a subfolder of tcl_files (If this folder is not already created, one will be created in the same directory as the script). The subfolder is named after the year, month, day, and hour represented in seconds and if multiple walls were created they will all be stored in the subfolder with their corresponding unique id and date. Next step is to go to each wall folder and run OpenSees in folder path by typing "source *filename*.tcl" and hitting enter. Once OpenSees has finished, Jupyter notebooks are used by selecting a postprocessing script to run. All postprocessing images or interactive graphs will be stored in the corresponding wall folder.

The second workflow is for the purpose of running a single wall or multiple walls without requiring any memory or RAM from a local desktop or laptop. It has a similar workflow as the first one, but everything is done through the Jupyter hub on DesignSafe. To get the Jupyter hub, a user needs to sign into DesignSafe, select Workspace then Tools & Applications and then click on Jupyter (not HPC). The options are then to select updated Jupyter image or classic Jupyter image. The scripts are created in the classic Jupyter image, therefore this is the option that is selected. Assuming that the scripts are copied to the users local file system on Design Safe, the same workflow above is followed except when using OpenSees. The file path of wall to simulate is selected followed by selecting the OpenSees script and input necessary information for the job and then running it. The rest of the workflow will mirror above. Only difference is this will be on the users local DesignSafe system.

The third and fourth workflows could be a single workflow but they are split up into a desktop workflow for quoFEM which is setup and run, and then a DesignSafe workflow for quoFEM which is the postprocessing.

Since quoFEM is an application that is directly installed to local computer, the wall that will be used on quoFEM needs to be created on the local computer. So the first part of workflow #1 is used to create the model, followed by the use of the Python error function (for max strength or displacement capacity) and corresponding text file for calibration for the input files in quoFEM. After following section 4.3.3 for a sensitivity analysis or 4.3.4 for a parameter estimation, the job is executed.

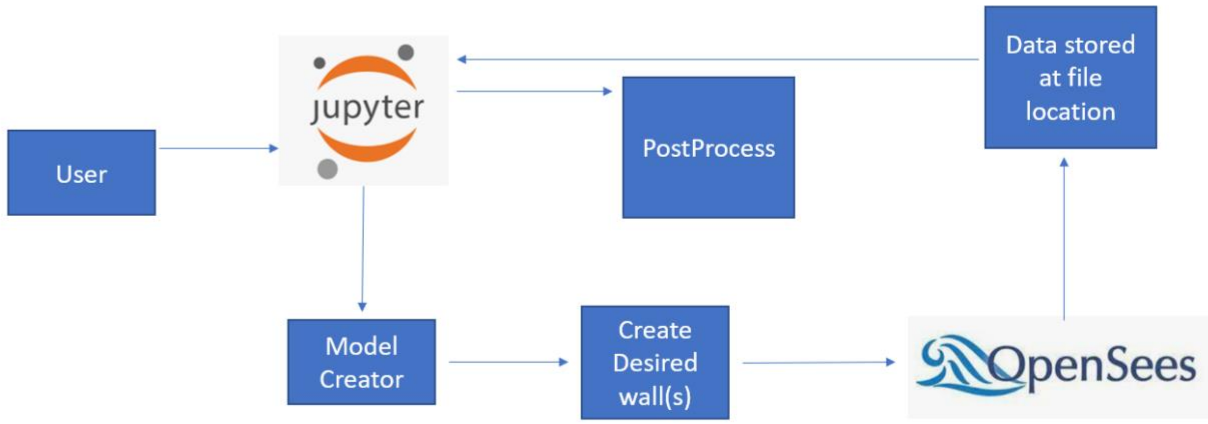

Figure 4.12 Local run

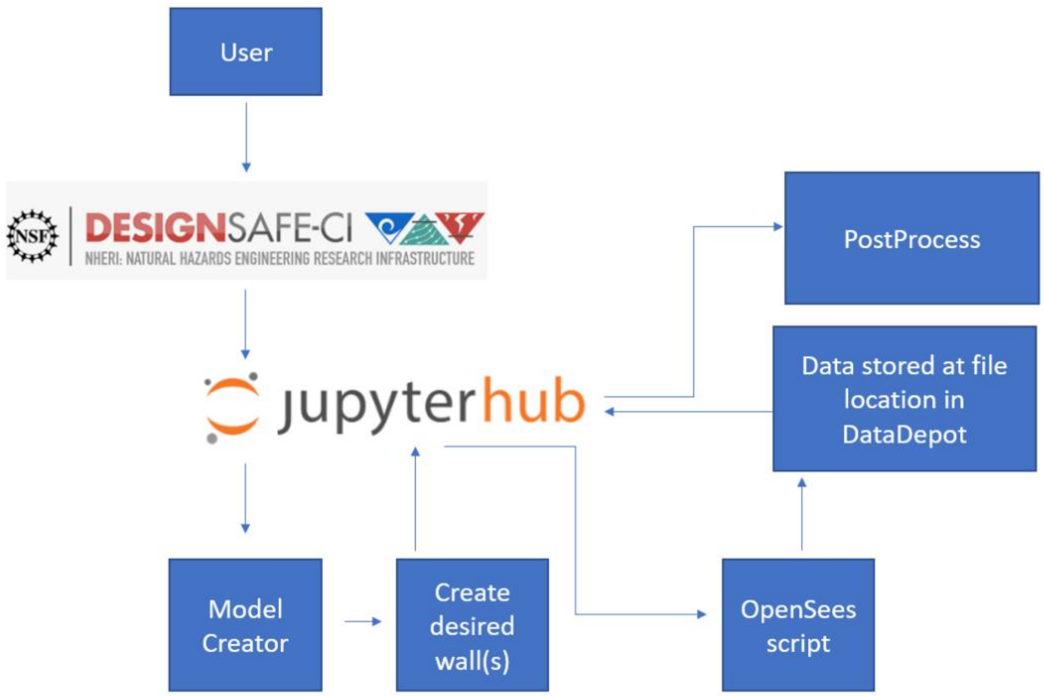

Figure 4.13 Setting up OpenSees on DesignSafe

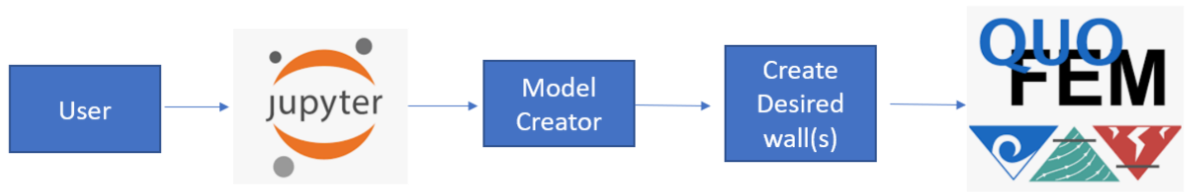

Figure 4.14 Setting up a quoFEM job

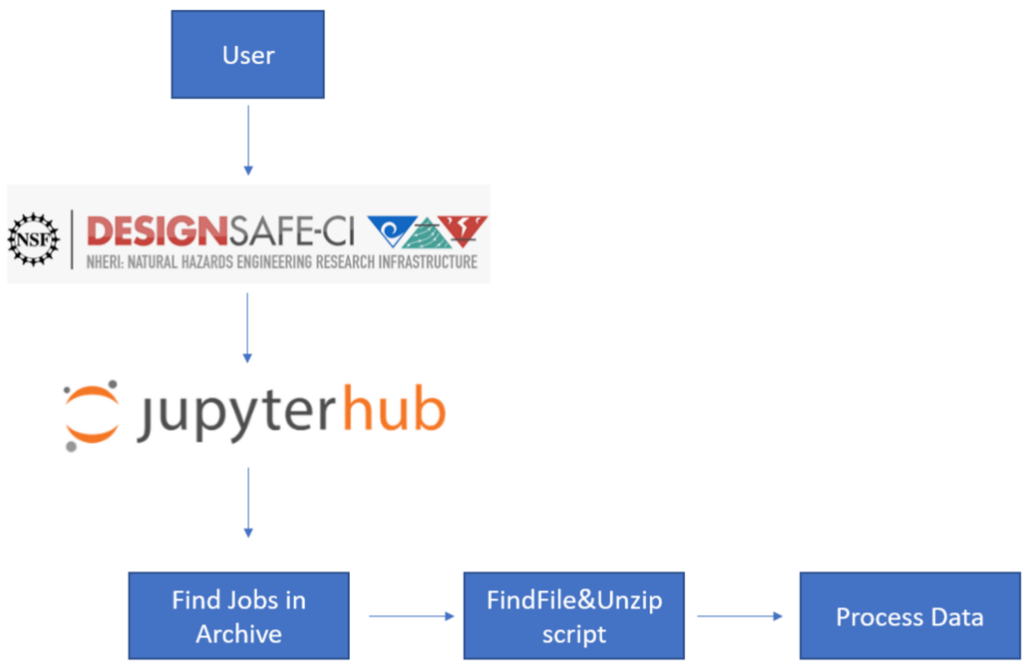

Figure 4.15 Post quoFEM Jupyterhub processing

4.7 SUMMARY

This chapter presented the software that was utilized in this research and described the Jupyter notebooks that assisted in building the model, post processing the data and created the error functions that aid a quoFEM run, and described the multiple workflows that can be used on a local machine and on the SimCenter workbench. The next chapter will conduct sensitivity analysis and parameter estimations for the calibration set and use the preferred values in the validation set to determine if the model can accurately predict strength and drift capacity of the various wall models.

5 CALIBRATION AND VALIDATION

5.1 INTRODUCTION

This chapter presents the calibration and validation of three concrete wall model parameters that are not well-defined by experimental data: the cracked concrete shear retention factor (*stc* in Eq. 3.13), the ratio of confined to unconfined concrete crushing energy (*rev* in Eq. 3.12), and the reinforcing steel cyclic rupture strain reduction factor (*srs* in Eq. 3.16). Calibration and validation are accomplished using the calibration and validation data sets extracted from the Shegay et al. (2018) experimental data set presented in Chapter 2; each of the data sets (calibration and validation) spans a range of specimen design parameters and includes an approximately equal number of specimens exhibiting the compression-buckling failure mode and the buckling-rupture failure mode. The quoFEM software developed by the SimCenter (McKenna et al. 2025, Deierlein et al. 2020) is used to support the calibration process.

The calibration process uses only the specimens in the calibration data set. Calibration starts with, for each specimen in the calibration data set, calibration of the shear retention factor (*stc*) to achieve accurate simulation of wall specimen strength. Then, for walls exhibiting compression-buckling failure, the ratio of unconfined to confined concrete crushing energy (*rev*) is calibrated, and for walls exhibiting buckling-rupture failure, the steel rupture strain reduction factor (*srs*) is calibrated. Regardless of failure mode, this second step in the calibration process seeks the model parameter value that results in accurate simulation of drift capacity, defined as the drift at onset of significant strength loss. Average values for the three critical model parameters are computed for the entire calibration dataset. These average values are *evaluated* by using them to simulate the response of each of the specimens in the calibration data set and comparing simulated with measured response quantities. The average model parameters are *validated* via comparison of simulated with measured response quantities for the validation data set, which comprises approximately half of the experimental test specimens used in this study, spans a range of specimen design parameters, and includes approximately an equal number of specimens exhibiting the compression-buckling failure mode and the buckling-rupture failure mode.

The calibration and validation processes and results are presented in Sections 5.2 through 5.5 of this report as follows. Section 5.2 discusses the error functions used in the calibration and validation processes and their use with the quoFEM software. Section 5.3 presents calibration of the shear retention factor, crushing energy ratio, and steel rupture strain ratio using quoFEM and the calibration data set. Section 5.4 presents simulation results, for the calibration data set, computed using the average values of the model parameters; results include simulated and measured load-displacement histories as well as simulated material strain-strain histories at critical locations in the wall specimens and concrete stress fields at critical points in the load-displacement history. Section 5.5 compares simulated and measured response quantities for the validation data set, with simulated values computed using the average calibrated model parameter values.

5.2 ERROR FUNCTIONS

The error functions presented in Chapter 4 were used with quoFEM to determine preferred values for the shear retention factor (*stc*), ratio of confined to unconfined crushing energy (*rev*), and steel rupture strain reduction factor (*srs*):

$$Error = \frac{Quantity_{\,simulated} - Quantity_{measured}}{Quantity_{measured}} x\ 100 \qquad \text{(Eq. 5.1)}$$

Preliminary evaluation of the model in Chapter 3, indicated that the shear retention factor (*stc*) has significant impact on maximum wall strength; this is attributed to the fact that larger values of shear retention result in increased shear transfer parallel to concrete crack surfaces, which can increase wall strength. Thus, this parameter was calibrated to achieve accurate simulation of wall strength (i.e., *Quantity* in Eq. 5.1 is wall strength). Previous research (Pugh et al. 2015, Marafi et al. 2019) demonstrates that the ratio of confined to unconfined concrete crushing energy (*rev*) and steel rupture strain (function of *srs*) determine simulated deformation capacity. Thus, wall displacement capacity was used in the error function defined by Eq 5.1 to calibrate these quantities. The following sections present the model parameter values that were found, using quoFEM, to result in minimum errors in simulated strength and displacement capacity.

5.3 MODEL PARAMETER CALIBRATION

The section presents the use of the wall calibration data set presented in Chapter 2 to calibrate three model parameters that are not well-defined by experimental data. Concrete shear retention factor (*stc*) is calibrated to achieve accurate simulation of wall strength (Section 5.3.1), and the ratio of confined to unconfined concrete crushing energy (*rev*) and the steel rupture strain (function of *srs*) are calibrated to achieve accurate simulation of wall deformation capacity (Section 5.3.2).

5.3.1 Shear Retention Factor Calibration

The concrete crack shear retention factor (*stc* in Eq. 3.13) was calibrated first, using the entire calibration data set, because preliminary analyses demonstrated that this value determines simulated maximum strength, regardless of failure mode. Eq. 5.1 was used to compute the error measure for calibration of the shear retention factor, with the variable $Quantity$ in Eq 5.1 defined by the maximum base shear strength measured in the laboratory and computed in the OpenSees simulation. Preliminary analyses showed that a shear retention factor in excess of 0.2 typically resulted in convergence problems and/or excessive strength. Thus, in the final shear retention factor calibration study, shear retention factors ranging from 0.01 to 0.15 were considered.

Table 5.1 lists the shear retention factor that was found to provide the most accurate simulation of wall strength for each wall in the calibration data set. The average shear retention factor for all specimens in the calibration data set is 0.056 with a COV of 67%. Twelve of the 16 walls had shear retention factors ranging from 0.02 to 0.06. Wall C10 tested by Shegay et al. (2018) and walls W8 and W9 tested by Hube et al. (2014) required relative high shear retention values to achieve measured wall flexural strength; a detailed review of these test programs did not identify factors that might have contributed to the high shear retention factors. The lowest shear retention values were computed for walls tested by Liu (2004); these low values are consistent with final results (Table 5.1) that show flexural strength of the Liu walls being overpredicted when the average shear retention factor for the full data set was used for all walls. The average shear retention factor for the entire calibration data set, *stc* = 0.056, was used for all models for all subsequent analyses. Use of this average value for all of the walls in the calibration data set results in an average error in predicted wall strength of 8.4%. This average error is not considered to be significantly larger than the average error in predicted strength, 1.3%, which was computed when the best *stc* for each individual wall was used to simulate the strength of that wall. The accuracy and precision of wall strength simulated using *stc* = 0.056 for all walls in the calibration and in the validation data sets is discussed in detail in Sections 5.4 and 5.5.

Table 5.1 Calibration Results: Shear Retention Factor

Author	ID	Shear Retention Factor (*stc*) Required to Accurately Simulate Strength	Simulated Strength Error Using Wall-Specific Shear Retention Factor (%)	Observed Failure Mode[2]
Dazio	WSH1	0.058	0.14	BR
Dazio	WSH3	0.046	0.04	BR
Wallace	RW1	0.034	0.80	BR
Wallace	RW2	0.060	0.20	CB
Liu	W1	0.010	0.20	CB
Liu	W2	0.022	0.16	BR
Lu	C1	0.039	1.00	BR
Lu	C2	0.037	0.40	BR
Lu	C3	0.039	0.40	BR
Tran	S38	0.060	0.10	CB
Oh	WR20	0.056	0.20	CB
Hube	W8	0.140[1]	12.3	CB
Hube	W9	0.136[1]	4.20	CB
Zhang	SW7	0.024	0.37	CB
Zhang	SW9	0.030	0.21	CB
Shegay	C10	0.107[1]	0.22	CB
	Average	0.056	1.3%	
	COV	69%		

1. Result is an outlier, but was included in calculating sample average and COV.
2. BR indicates that the wall exhibited a buckling-rupture failure mode in which lateral strength loss is due to buckling of vertical reinforcement followed by bar rupture under load reversal; CB indicates that the wall exhibited a compression-buckling failure mode in which lateral strength loss results from simultaneous concrete crushing and reinforcement buckling in the extreme fibers of the wall compression zone.

5.3.2 Steel Rupture Strain Ratio and Crushing Energy Ratio Calibration

The steel rupture strain ratio (srs in Eq. 3.16) and confined concrete crushing energy ratio (rev in Eq. 3.12) determine onset of significant strength loss for walls exhibiting steel-controlled buckling rupture (BR) failure and concrete-controlled crushing-buckling (CB) failure, respectively. Chapter 3 presents the results of studies by Pugh et al. and Marafi et al. to calibrate, evaluate, and validate steel rupture strain ratio and confined concrete crushing energy ratio to enable accurate simulation of onset of lateral strength loss, using fiber-type beam-column elements, for planar reinforced concrete walls subjected axial and cyclic lateral loading.

For the current study, the unconfined concrete crushing energy, $G_{fc} = 0.0134 f_c$ k/in with f_c in psi ($G_{fc} = 2 f_c\ N/mm$ with $f_c$in MPa), recommended by Pugh et al. and used by Marafi et al. is adopted (Eq. 3.9) and the confined concrete crushing energy ratio, $rev = \left(G_{fcc}/G_{fc}\right)$ is calibrated to provide accurate simulation of onset of strength loss, using the layered shell element, for walls exhibiting CB failure. The reinforcing steel rupture strain ratio (*srs*), which defines the reduction in steel rupture strain due to reversed cyclic loading, is calibrated to achieve accurate simulation of onset of strength loss for walls exhibiting BR failure.

The *rev* and *srs* values recommended by Pugh et al. for use with beam column elements are used as the starting values for the quoFEM parameter estimation study for the layered shell element, with walls exhibiting a BR failure used to calibrate the steel rupture strain ratio (*srs*) and walls exhibiting a CB failure used to calibrate the crushing energy ratio (*rev*).

Each quoFEM run on the TACC Stampede supercomputer has an allowed maximum runtime of 48 hours; jobs are automatically terminated, and results lost, when the run time exceeds 48 hours. Preliminary analyses for the current study resulted in maximum runtimes, for individual walls in the calibration dataset, of approximately five (5) hours. Thus, parameter estimation runs were submitted in batches of ten, and batched jobs were submitted in parallel. It should be noted that if the run time for one of these "batched" jobs exceeded the 48-hour limit, only the data for the final wall specimen in the dataset are lost.

Figures 5.1 and 5.2 show the error value for sequential parameter estimation analyses using quoFEM for two walls exhibiting BR and CB failure modes; individual data points are numbered for wall specimen RW1 to show the estimation process and sequence of analyses. These data show the optimization function seeking a minimum error by using parameter values on either side of the user-specified initial value to determine which direction will increase the error and which direction will decrease the error. The algorithm continues this approach, using results from all previous runs, until the user-defined error function falls below the convergence tolerance or the maximum number of simulations is reached. These data show also that the optimization continues until the error is less than 0.01 and a strategy of increasing and decreasing values is employed to speed convergence on the correct value. Data for calibration of walls RW1 and RW2 exhibit this well. Data for wall W9 (Figure 5.2) show an increase in the error at a crushing energy ratio (*rev*) of approximately 2.1; this inconsistency in the convergence path was found to be common and was typically due to the OpenSees simulations failing to converge to a solution for the given model parameters. The parameter estimation algorithm used for this study was found to be capable of overcoming inconsistencies in the solution path resulting from simulations “failing to converge” by simply progressing to the next preferred trial value; initial parameter estimation efforts using gradient-based methods were found to fail when this situation arose.

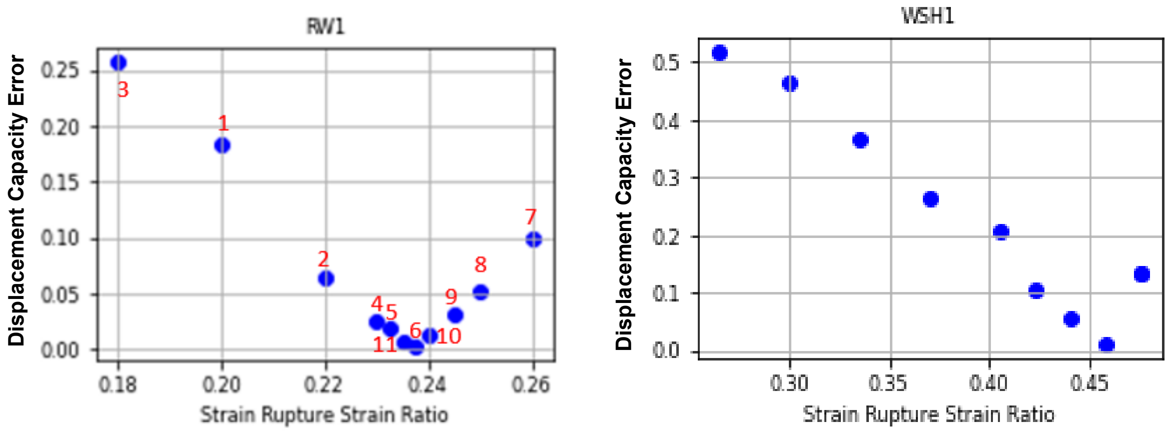

Figure 5.1 Parameter Estimation Results for RW1 and WSH1

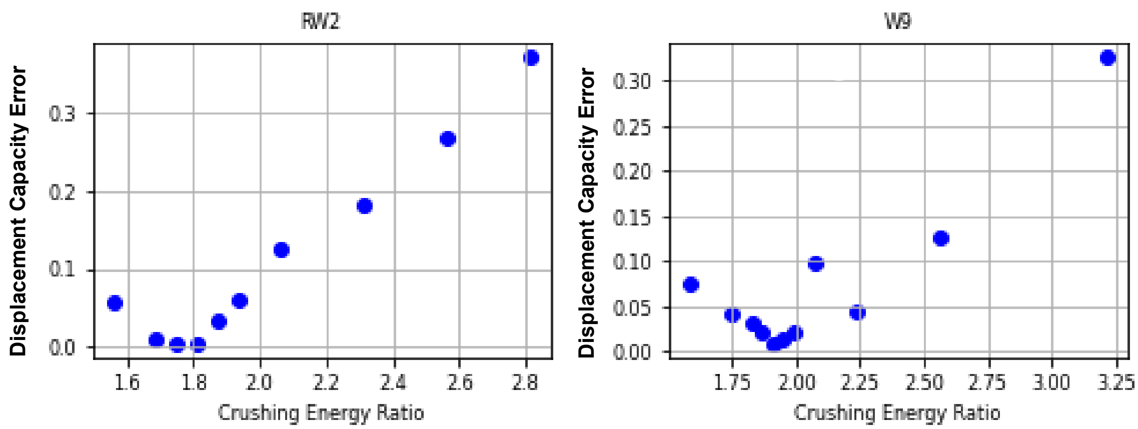

Figure 5.2 Parameter Estimation Results for RW2 and W9

Table 5.2 presents the results of the parameter estimation analyses for each wall. The data in Table 5.2 show that 12 of 16 analyses converged; exceptions were WSH1 and W2 (BR failures) and C10 and W8 (CB failures). Data for walls WSH1, W2, and C10 were used to compute recommended values for subsequent use because the complete output file for these analyses showed that i) the models were sensitive to the parameters being calibrated, and ii) the calibration process was converging to a solution as the parameter of interest was varied, but that the parameter estimation algorithm failed to localize to a single value that resulted in an error value that met the convergence tolerance within the 48 hour runtime allotted to the job. Data in Table 5.2 also show that the drift capacity of wall specimen W8 was not sensitive to the crushing energy, and review of the complete output file did not suggest that the solution was converging; thus, data for specimen W8 were not used to compute the recommended crushing energy value.

Table 5.2 Calibration Results: Steel Rupture Strain Ratio (srs) and Concrete Crushing Energy Ratio ($rev = G_{fcc}/G_{fc}$)

ID	Steel Rupture Strain Ratio (srs)	Error (%)	ID	Crushing Energy Ratio ($rev = G_{fcc}/G_{fc}$)	Error (%)
WSH1	0.46[1]	1.20	**RW2**	1.81	0.40
WSH3	0.32	0.90	**S38**	2.56	0.90
RW1	0.24	0.30	**WR20**	3.11[1]	1.00
W2	0.15	3.00	**W1**	1.93	0.60
C1	0.26	0.50	**W8**	3.0[2]	97.0
C2	0.30	0.60	**W9**	1.91	1.00
C3	0.29	0.10	**C10**	6.4[1]	1.70
			SW7	2.05	0.80
			SW9	1.35	0.20
Avg	0.29	0.94		2.64	0.83
COV	33%			61%	

1. Result is an outlier but was included in calculating sample average and COV. 2. Result in an outlier and was not used to calculate sample average.

5.4 SIMULATION OF THE WALL CALIBRATION DATA SET USING AVERAGE CALIBRATED MODEL PARAMETESR

The average values for the model parameters presented in Tables 5.1 and 5.2 and repeated below were used to simulate the response all walls in the calibration data set.

- Shear retention factor, per Eq. 3.13, stc = 0.056
- Steel rupture strain ratio, per Eq. 3.16, srs = 0.29
- Confined concrete crushing energy, per Eq. 3.12, $rev = \frac{G_{fcc}}{G_{fc}} = 2.64$

Table 5.3 lists measured and simulated response quantities of interest for the walls in the calibration data set and provides statistics for the dataset.

Table 5.3 Simulation results for calibration data set

		Stiffness to M_n			Maximum Strength			Deformation Capacity			Failure Mode	
Author	**Wall ID**	**Exp. Δ_{Mn}**	**Sim. Δ_{Mn}**	**Error[2] (%)**	**Exp. Mb/Mn**	**Sim. Mb/Mn**	**Error (%)**	**Exp. Δ_u**	**Sim. Δ_u**	**Error (%)**	**Exp.**	**Sim.**
		-	-	--	--	--	--	%	%	--	--	--
Dazio	**WSH1**	0.39	0.65	-40.0	1.03	1.01	-1.9	1.04	0.69	-33.7	BR	BR
Dazio	**WSH3**	0.56	0.80	-30.0	1.10	1.10	0.0	2.03	1.83	-9.9	BR	CB
Wallace	**RW1**	0.58	0.89	-34.8	0.99	1.12	13.1	2.10	2.57	22.4	BR	CB
Liu	**W2**	0.80	0.98	-18.4	0.99	1.27	28.3	2.87	4.72	64.5	BR	CB
Lu	**C1**	0.62	1.35	-54.1	0.98	1.34	36.7	2.46	2.59	5.3	BR	BR
Lu	**C2**	0.11	0.66	-83.3	1.08	1.12	3.7	1.23	1.39	13.0	BR	BR
Lu	**C3**	0.15	0.59	-74.6	1.05	1.11	5.7	0.82	1.09	32.9	BR	BR
Wallace	**RW2**	0.79	0.79	0.0	1.14	1.18	3.5	2.25	2.29	1.8	CB	BR
Tran	**S38**	0.46	0.78	-41.0	1.32	1.30	-1.5	3.10	3.34	7.7	CB	CB
Oh	**WR20**	0.19	0.46	-58.7	1.04	1.06	1.9	2.45	1.65	-32.7	CB	CB
Liu	**W1**	0.95	0.87	9.2	1.01	1.20	18.8	3.05	2.78	-8.9	CB	CB
Hube	**W8**	0.5	0.83	-39.8	1.48	1.25	-15.5	2.71	3.7	36.5	CB	CB
Hube	**W9**	0.37	0.57	-35.1	1.18	1.25	5.6	2.68	4.08	52.2	CB	BR
Zhang	**SW7**	0.34	0.51	-33.3	1.12	1.30	16.1	2.00	3.15	57.5	CB	BR
Zhang	**SW9**	0.27	0.30	-10.0	1.37	1.72	25.5	2.00	4.01	100.5	CB	--
Shegay	**C10**	0.15	0.21	-28.6	1.22	1.15	-5.7	0.85	0.61	-28.2	CB	CB
Average[3]				-36%	1.13	1.22	8.4%	2.10	2.53	18%	Failure Mode Simulated w/ 56% Accuracy	
Std. Dev.				25%			14%			38%		

Quantities in Table 5.3 are defined as follows:

- Stiffness: Simulation of initial stiffness is evaluated using the simulated and the measured drift at the top of the wall specimen at the load level corresponding to the wall developing nominal flexural strength, M_n. For the current study, nominal flexural strength is defined per ACI 318-25 as flexural strength when the concrete element at the base of the wall develops a compressive strain of -0.003. The simulated drift at M_n is compared with the measured drift at the same load level and in the same loading direction. Specifically,

[2] Stiffness to M_n is evaluated using the measured and simulated displacements at the top of the wall when the wall first develops nominal flexural strength, per ACI 318-25, at the base of the wall (see Section 3.5.2).
[3] The average error is computed as the simple average of the percentage error.

$$Error_{stiffness} = \frac{\frac{M_n}{\Delta_{sim}} - \frac{M_n}{\Delta_{exp}}}{\frac{M_n}{\Delta_{exp}}} = \frac{\Delta_{exp} - \Delta_{sim}}{\Delta_{sim}} \qquad \text{(Eq. 5.2)}$$

- Strength: Maximum simulated and measured strength is compared with maximum measured strength. Specifically,

$$Error_{strength} = \frac{M_{max_{sim}} - M_{max_{exp}}}{M_{max_{exp}}} \qquad \text{(Eq. 5.3)}$$

- Deformation capacity: Measured and simulated deformation capacities are defined as the drift at the point at which the wall exhibits a strength loss of 20% from maximum strength.

$$Error_{deformation\ capacity} = \frac{\Delta_{20\%_{sim}} - \Delta_{20\%_{exp}}}{\Delta_{20\%_{exp}}} \qquad \text{(Eq. 5.4)}$$

- Failure Mode: Walls are labeled as exhibiting either a compression buckling failure (CB) or a bar rupture (BR) failure. A compression buckling failure is characterized by concrete and steel compression strain exceeding the concrete crushing strain, resulting in concrete and steel strain dropping to zero. A bar rupture failure is characterized by reinforcing steel tensile strain exceeding the rupture strain, resulting in steel stress dropping to zero.

The data in Table 5.3 show that, using average values for shear retention factor (*stc*), steel rupture strain ratio (*srs*), and confined concrete crushing energy (*rev*), wall stiffness is not accurately predicted (average error of -36%) but that strength is accurately predicted (average error less than 10%) and deformation capacity is predicted with an average error of less than 20%. Specifically:

- ***Simulation of stiffness to M_n***: Simulated stiffness to M_n is substantially lower and simulated displacement at M_n is significantly higher, than that measured in the laboratory. This is represented in Table 5.3 as simulated drift at M_n exceeding measured drift at M_n. Underprediction of concrete component "initial" stiffness is atypical, as most modeling approaches ignore some of the mechanisms that introduce flexibility in the laboratory (e.g., concrete shrinkage cracking and slip at the concrete-steel interface) and, as a result, overpredict the initial stiffness of concrete components.

  The primary explanation for under-prediction of specimen stiffness in the current study is likely computing stiffness on the basis of displacement at M_n, the "nominal flexural strength" defined by tension reinforcement carrying yield stress and the maximum vertical concrete compressive strain in the wall reaching -0.003, rather than at the lower load/displacement level of "yield strength", defined by reinforcing steel carrying its tensile yield strain of 0.002. Prior to reinforcement yielding, reduction in wall stiffness (i.e.. nonlinear response) is due almost entirely to i) concrete cracking under mechanical loading and shrinkage induced stresses and ii) modest slip at the concrete-steel interface within the wall and the foundation. While almost all models simulate concrete cracking under mechanical load, few models explicitly simulate bond-slip at the concrete-steel interface or shrinkage cracking, and this typically leads to over-prediction of "initial" wall stiffness.

Once reinforcement yields, but before nominal flexural strength is reached, wall deformation is a function of a large number of complex nonlinear response mechanisms: the nonlinear response of the yielding reinforcing steel under cyclic loading, significant concrete cracking, modest nonlinear concrete compression response due strain demands that approach the strain defining nominal flexural strength (-0.003), opening and imperfect closing of concrete cracks, shear transfer and slip on concrete cracks, and increased slip at concrete-steel interface within the wall and the foundation. Some, but not all of these response mechanisms are included in the model.

Thus, the under prediction of wall initial stiffness observed in this study is attributed to inaccuracy in modeling the impact on component stiffness of the multiple nonlinear response mechanism that develop in the load interval between reinforcement yielding (the point at which many studies assess initial stiffness of concrete components) and the extreme concrete fiber reaching a compressive strain of -0.003 (the point at which "initial" stiffness was computed for this study).

- ***Simulation of maximum strength:*** On average wall strength is accurately predicted with an average error of less than 10% and a standard deviation in this error of 14%. These error measures are consistent with previous efforts to calibrate and validate concrete wall models (e.g., Pugh et al. 2015, Lowes et al. 2019, Lowes et al. 2020). Error in simulated strength may be attributed to myriad factors including aspects of wall construction and response that are not accurately represented in the model (e.g., shrinkage cracking and bond slip) as well as model inaccuracy (e.g., simplified representation of horizontal reinforcement and coarse mesh size). Here it should be noted also that the error in simulated wall strength is correlated with the error in simulated deformation capacity ($R^2 = 0.19$). Thus, some of the error in simulated strength can be attributed to the fact that i) the walls exhibit hardening in the post yield regime and ii) where wall deformation capacity is overpredicted, strength is also overpredicted due to this hardening (Figure 5.3 below shows this).

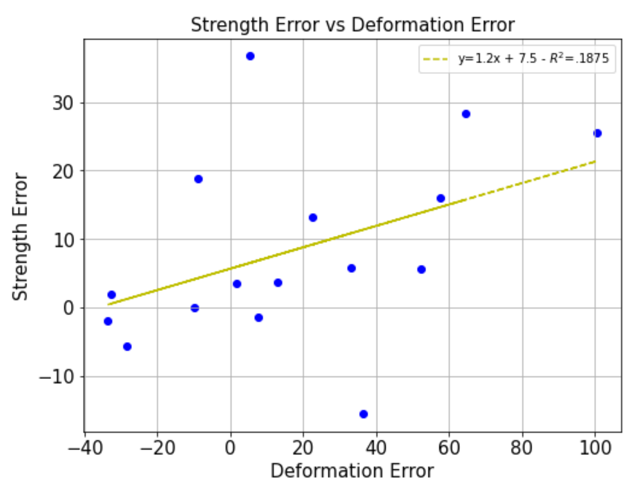

Figure 5.3 Strength error versus deformation error

Simulation of deformation capacity: On average, simulated deformation capacity exceeded measured capacity for the calibration data set by 18%, with standard deviation of 38%. These values are higher than is desirable but are not inconsistent with previous efforts to calibrate models for simulating the deformation capacity of flexure-controlled concrete walls subjected to cyclic loading (e.g., Pugh et al. 2015, Lowes et al. 2019, Lowes et al. 2020). These errors are likely due to factors identified in the previous sections as potentially resulting in reduced accuracy in simulation of wall stiffness and strength.

Simulation of failure mode: Failure mode was accurately simulated for only 56% of the test specimens. These results are poorer than observed with other modeling approaches (e.g., Pugh et al. 2015, Lowes et al. 2019, Lowes et al. 2020), and warrant further investigation.

5.4.1 Simulated and measured load-displacement histories for walls in the calibration data set

Figures 5.4 and 5.5 provide simulated and measured load-displacement histories for all of the walls in the calibration data set, with simulations using the average shear retention factor (*stc* = 0.056), steel rupture strain ratio (*srs* = 0.29), and confined concrete crushing energy (*rev* = 2.6) computed for the calibration data set. Specifically, Figure 5.4 provides data for walls exhibiting bucking rupture failure in the laboratory, and Figure 5.5 provides data for walls exhibiting compression-buckling failure. These figures graphically demonstrate the accuracy and precision of the model, with some simulations providing *very good* representation of wall response (e.g., wall specimens WallaceRW1, WallaceRW2), some providing *good* representation of response (e.g., DazioWSH1, DazioWSH3, TranS38, OhWR20), and all providing *quite good* representation of the shape of the hysteretic response curves, including the extent to which the hysteretic response shows substantial pinching, and associated energy dissipation (e.g., Dazio WSH3, Wallace RW1, LuC1, LuC2, LiuW1, ZhangWangSW7, ZhangWangSW9).

5.4.2 Stress-strain and stress field data for walls in the calibration data set

Figures 5.6 through 5.8 provide additional simulation data for three test specimens for which simulated failure was determined by reinforcing steel buckling and rupturing (BR) and by simultaneous concrete crushing and steel buckling (CB). Specifically, data are provided for each specimen showing i) simulated and measured normalized base moment demand versus drift history, ii) simulated stress-strain histories for the two extreme concrete element quadrature points at the bottom of the wall (i.e., quadrature points that are the farthest left in the farthest left element and farthest right in the farthest right element at the bottom of the wall), iii) stress-strain histories for the two extreme reinforcing steel elements (i.e., farthest left and farthest right) at the base of the wall, and iv) the simulated concrete element vertical stress fields at three points along the envelope of the load-drift history: when the wall is loaded to nominal strength, at a load point between nominal strength and failure, and at incipient failure.

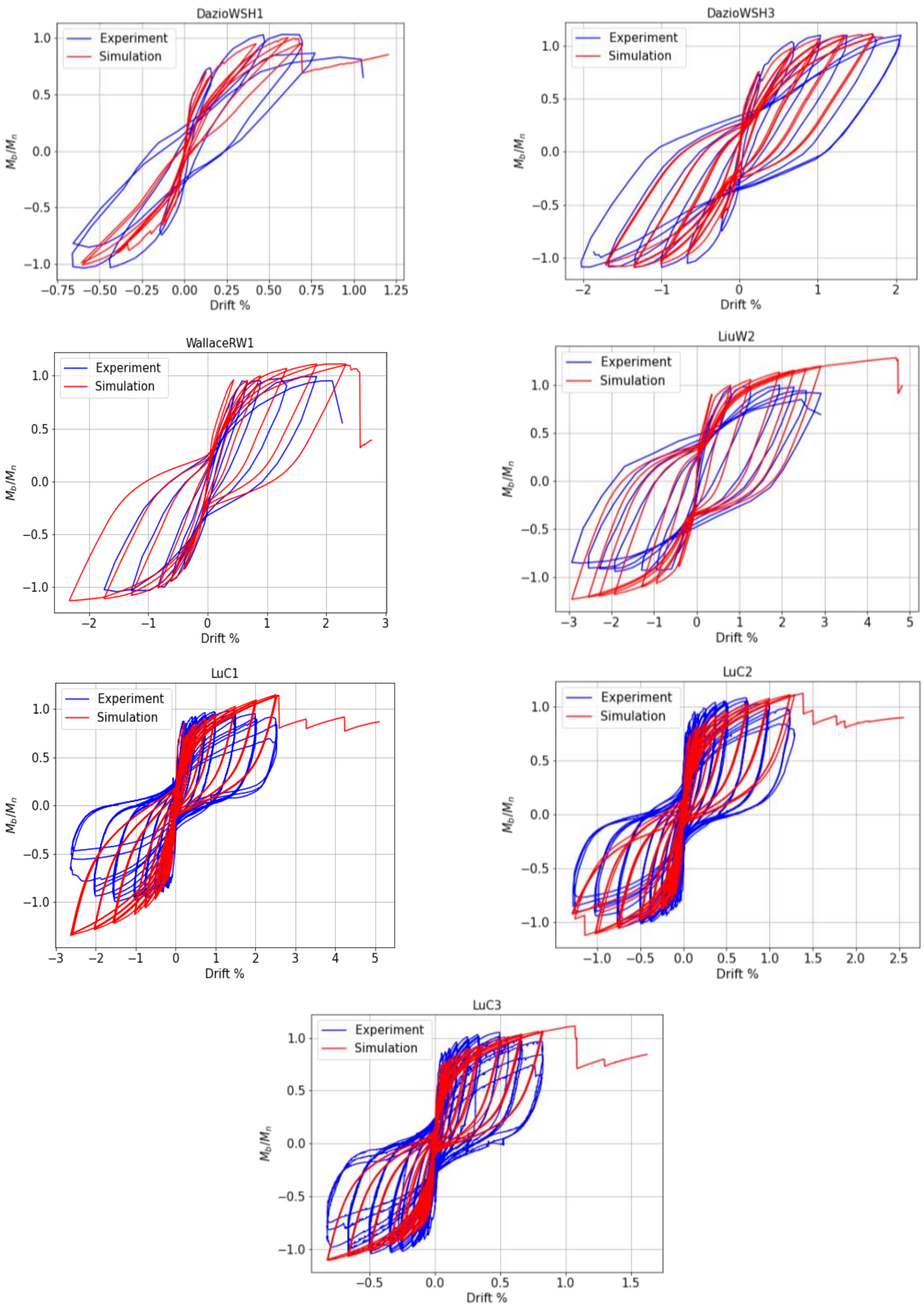

Figure 5.4 Calibration data set: Simulated and measured response for walls that exhibited BR failure in the laboratory.

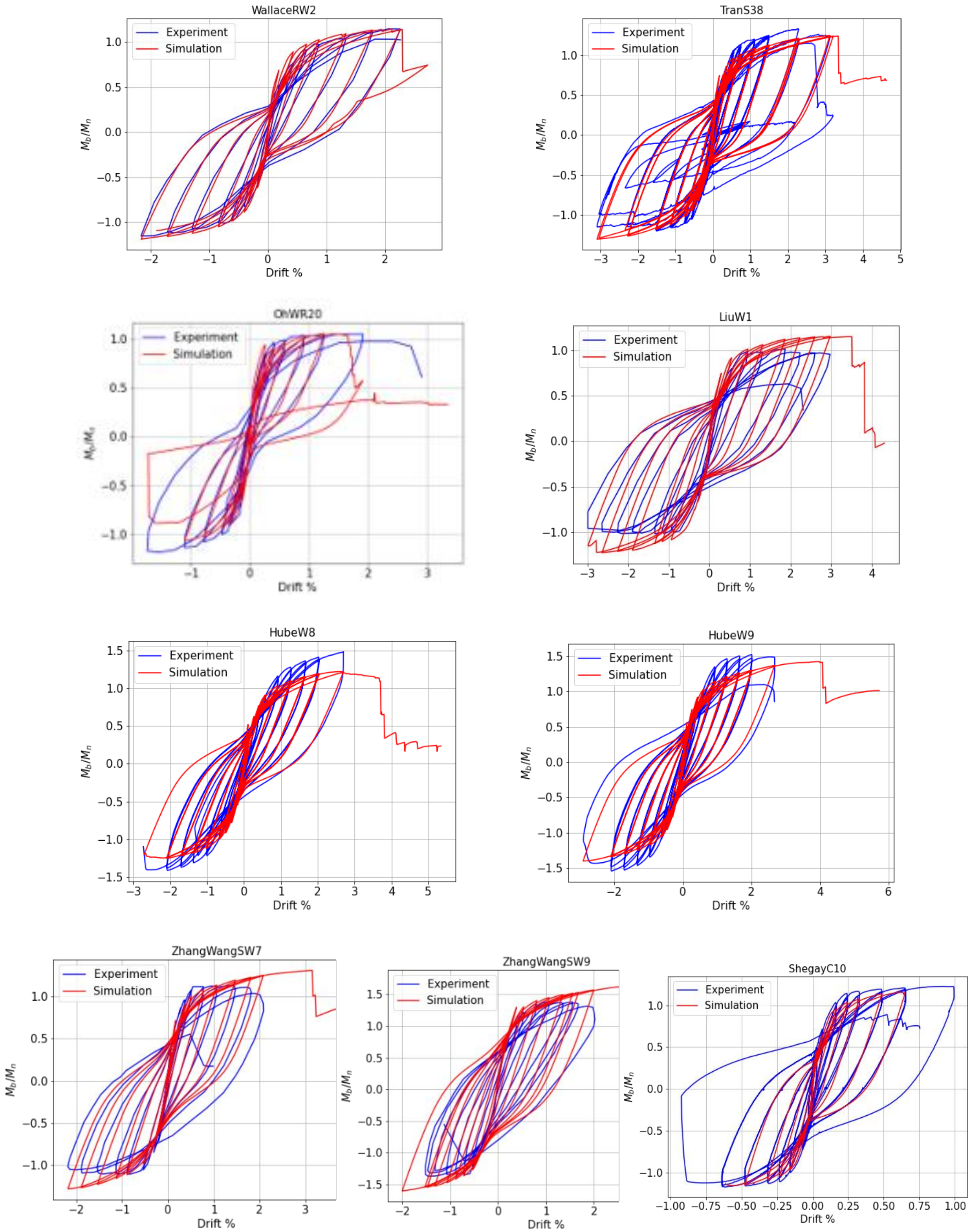

Figure 5.5 Calibration data set: Simulated and measured response for walls that exhibited CB failure in the laboratory.

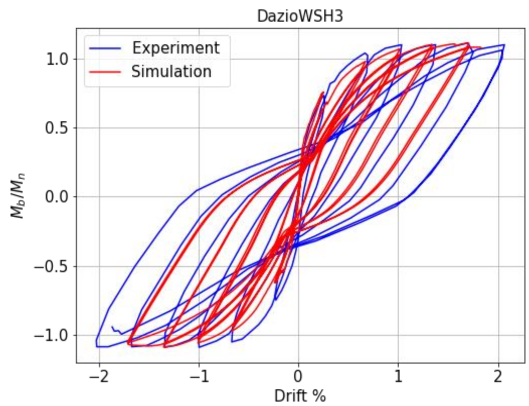

a) Measured and simulated load-deformation response histories

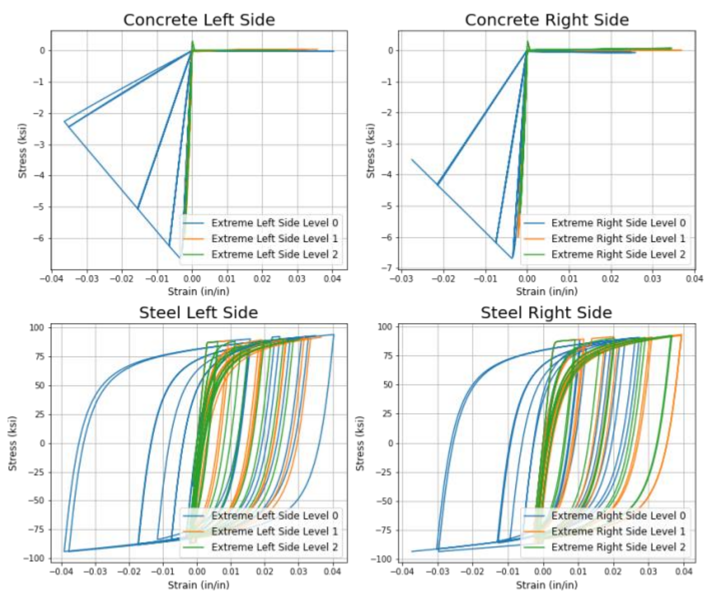

b) Simulated stress-strain histories for extreme concrete elements and reinforcing bars at the base of the wall

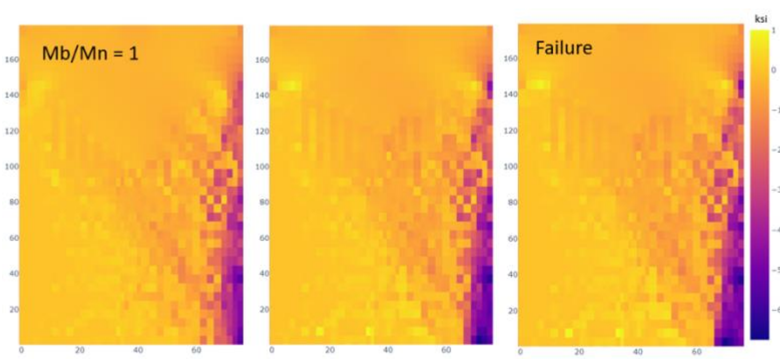

c) Vertical concrete stress profile for M_b/M_n = 1, midpoint of the test, and incipient failure.

Figure 5.6 Wall specimen WSH3: failure in the lab is BR; simulated failure is CB.

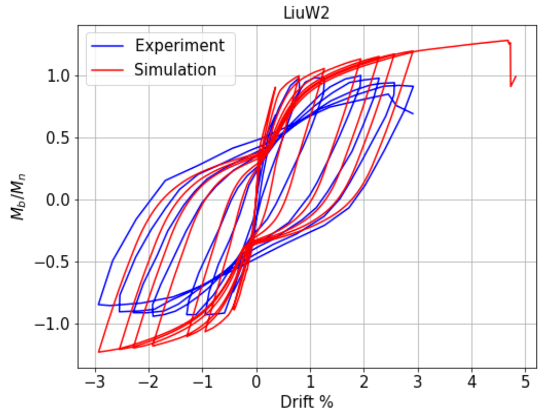

a) **Measured and simulated load-deformation response histories**

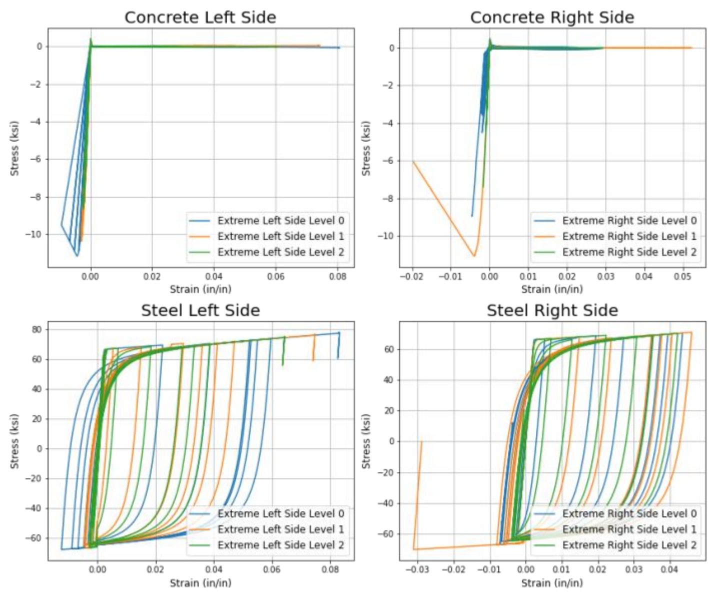

b) **Simulated stress-strain histories for extreme concrete elements and reinforcing bars at the base of the wall**

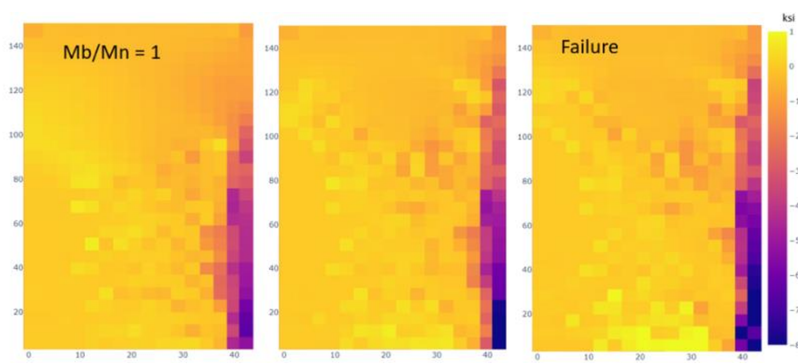

c) **Vertical concrete stress profile for M_b/M_n = 1, midpoint of the test, and incipient failure.**

Figure 5.7 Wall specimen LiuW2: failure in the lab is BR; simulated failure is CB.

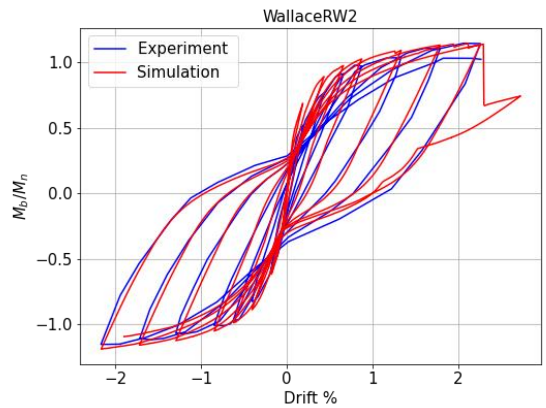

a) Measured and simulated load-deformation response histories

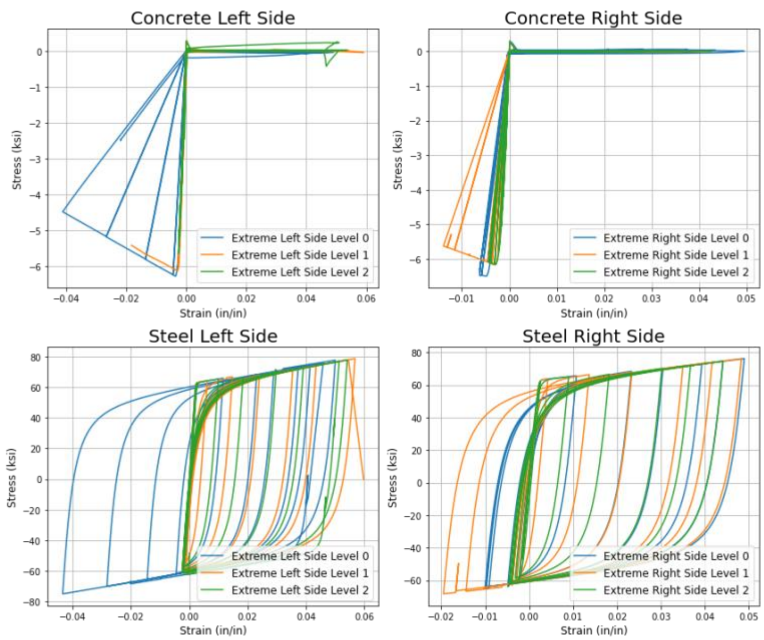

b) Simulated stress-strain histories for extreme concrete elements and reinforcing bars at the base of the wall

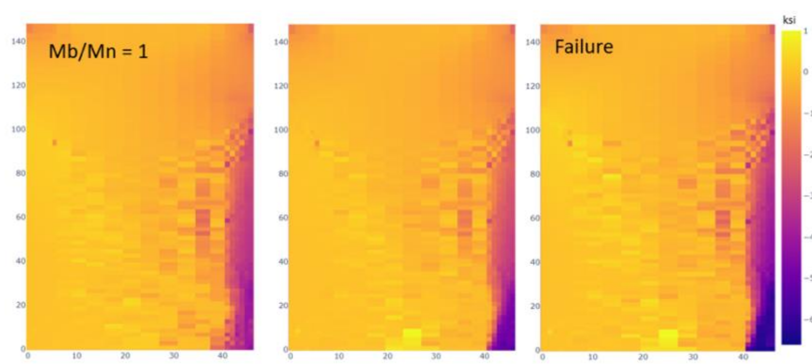

c) Vertical concrete stress profile for M_b/M_n = 1, midpoint of the test, and incipient failure.

Figure 5.8 Wall specimen RW2: failure in the laboratory is CB; simulated failure is BR

Data in Figures 5.6 and 5.7 provide additional understanding of simulated response for walls WSH3 tested by Dazio et al. and W2 tested by Liu et al., for which simulated failure was compression-buckling (CB).

- Data in Figure 5.6b show the extreme concrete fibers tracing the post-peak soften envelope of the concrete stress-strain curve through multiple load-unload-reload cycles that push the response further down the compression softening curve. Similarly, data in Figure 5.6c show the element at the bottom right corner of the wall carrying the maximum compressive stress in the wall when the wall achieves nominal flexural strength (Mb/Mn = 1) and the location of maximum compressive stress shifting towards the middle of the wall as the element(s) at the bottom right corner of the wall begins to fail and lose compressive strength.
- Data in Figure 5.7b show concrete strain demands in excess of that corresponding to maximum compressive strength, load-unload-reload cycles that trace the softening region of the stress-strain envelope in compression, and a single concrete compression cycle, associated with the final load cycle, that takes the extreme concrete element quadrature point from strain less than that associated with peak strength through peak compression strength and beyond into the post-peak softening regime.
- Data in Figure 5.7c show that a coarser mesh was used for simulation of specimen W2 than was used for specimen WSH3. These data show also concrete compressive strength loss occurring in the element above the base of the wall. Compression failure above the bottom of the wall is common in the laboratory and in simulations. It results from the boundary conditions at the base of the wall acting to confine the concrete in this region and, thereby, increase concrete compressive strength and push the compression failure region higher up the edge or the wall.
- For specimens WSH3 and W2, data in Figures 5.6b and 5.7b support classification of the these walls as compression-buckling (CB) failures, with the stress-strain histories for the extreme reinforcing bars at the base of the wall showing reinforcing steel elements unloading towards at end of the simulation, to equilibrate the concrete compressive strength loss, rather than losing strength with increasing strain demand, which would be indicative of a buckling-rupture (BR) failure.

Concrete and reinforcing steel data for Wall RW2 (Figure 5.8), for which a buckling-rupture (BR) failure was simulated, are very similar to those in Figure 5.6 and 5.7. However, the stress-strain response for the extreme bar on the left side of the wall (Figure 5.8b) clearly shows loss of strength with increasing strain demand during the last cycle of the load-displacement history, when there is simulated strength loss with increasing displacement demand towards the right side of the wall (Figure 5.8a). Additionally, the concrete compressive stress field (Figure 5.8c) does not show regions of concrete compressive strength loss during the final failure cycle. These data support the characterization of the simulated failure as buckling-rupture (BR).

The data presented in Figures 5.6, 5.7 and 5.8 are provided for all walls in Appendix D.

5.5 SIMULATION OF THE WALL VALIDATION DATA SET USING CALIBRATED MODEL PARAMETERS

Response histories for the walls in the *validation* set were computed using the preferred model values determined from the calibration study: a shear retention factor (*stc*) of 0.056, a steel rupture strain reduction factor (*srs*) of 0.29, and a crushing energy ratio (*rev*) of 2.6. Wall specimen stiffness, strength, and deformation capacity simulated using these values are compared with measured quantities in Table 5.4. Measured and simulated load-drift histories are provided in Figures 5.2 and 5.3

Table 5.4 Simulation results for validation data set

		Stiffness to M_n			Strength			Deformation			Failure Mode	
Author	**Wall ID**	**Exp. Δy**	**Sim. Δy**	**Error[4] (%)**	**Exp. Mb/Mn**	**Sim. Mb/Mn**	**Error (%)**	**Exp. Δ_u**	**Sim. Δ_u**	**Error (%)**	**Exp.**	**Sim.**
		--	--	--	--	--	--	%	%	--	--	--
Dazio	**WSH2**	0.63	0.79	-20.3	1.13	1.15	1.8	1.42	0.98	-31.0	BR	BR
Dazio	**WSH5**	0.28	0.65	-56.9	1.10	1.09	-0.9	1.35	0.85	-37.0	BR	CB
Shegay	**A10**	0.17	0.21	-19.0	1.24	1.16	-6.5	0.98	0.58	-40.8	BR	CB
Lu	**C4**	0.21	0.32	-34.4	0.78	1.11	42.3	1.47	1.85	25.9	BR	BR
Lu	**C5**	0.18	0.85	-78.8	1.19	1.41	18.5	1.94	2.26	16.5	BR	CB
Lu	**C6**	0.24	0.77	-68.8	1.03	1.09	5.8	1.2	1.22	1.7	BR	BR
Segura	**WP6**	0.11	0.21	-47.6	0.94	1.16	23.4	0.9	0.46	-48.9	BR	BR
Segura	**WP7**	0.25	0.18	38.9	1.06	1.12	5.7	0.96	0.54	-43.8	BR	CB
Dazio	**WSH6**	0.37	0.57	-35.1	1.18	1.25	5.9	2.07	1.81	-12.6	CB	BR
Oh	**WR10**	0.36	0.56	-35.7	1.09	1.26	15.6	2.82	1.74	-38.3	CB	CB
Shegay	**A14**	0.16	0.18	-11.1	1.20	1.2	0.0	0.79	0.45	-43.0	CB	CB
Shegay	**A20**	0.08	0.12	-33.3	1.44	1.38	-4.2	0.65	0.44	-32.3	CB	CB
Tran	**S63**	0.61	0.54	13.0	1.21	1.15	-5.0	3.0	1.31	-56.3	CB	CB
Zhang	**SW8**	0.16	0.36	-55.6	1.53	1.59	3.9	1.5	2.38	58.7	CB	BR
Hube	**W5**	0.17	0.36	-52.8	1.92	1.25	-34.9	1.1	1.91	73.6	CB	CB
Hube	**W7**	0.49	0.77	-36.4	1.27	1.17	-7.9	2.3	3.1	34.8	CB	CB
Lowes	**PW4**	0.41	0.29	41.4	1.53	1.86	21.6	0.6	0.82	36.7	CB	CB
Average[5]				-29%	1.23	1.26	-5%	1.47	1.33	8%	Failure Mode Predicted with 65% Accuracy	
Std. Dev.				34%			17%			41%		

[4] Stiffness to M_n is evaluated using the measured and simulated displacements at the top of the wall when the wall first develops nominal flexural strength, per ACI 318-25, at the base of the wall (see Section 3.5.2).
[5] The average error is computed as the simple average of the percentage error.

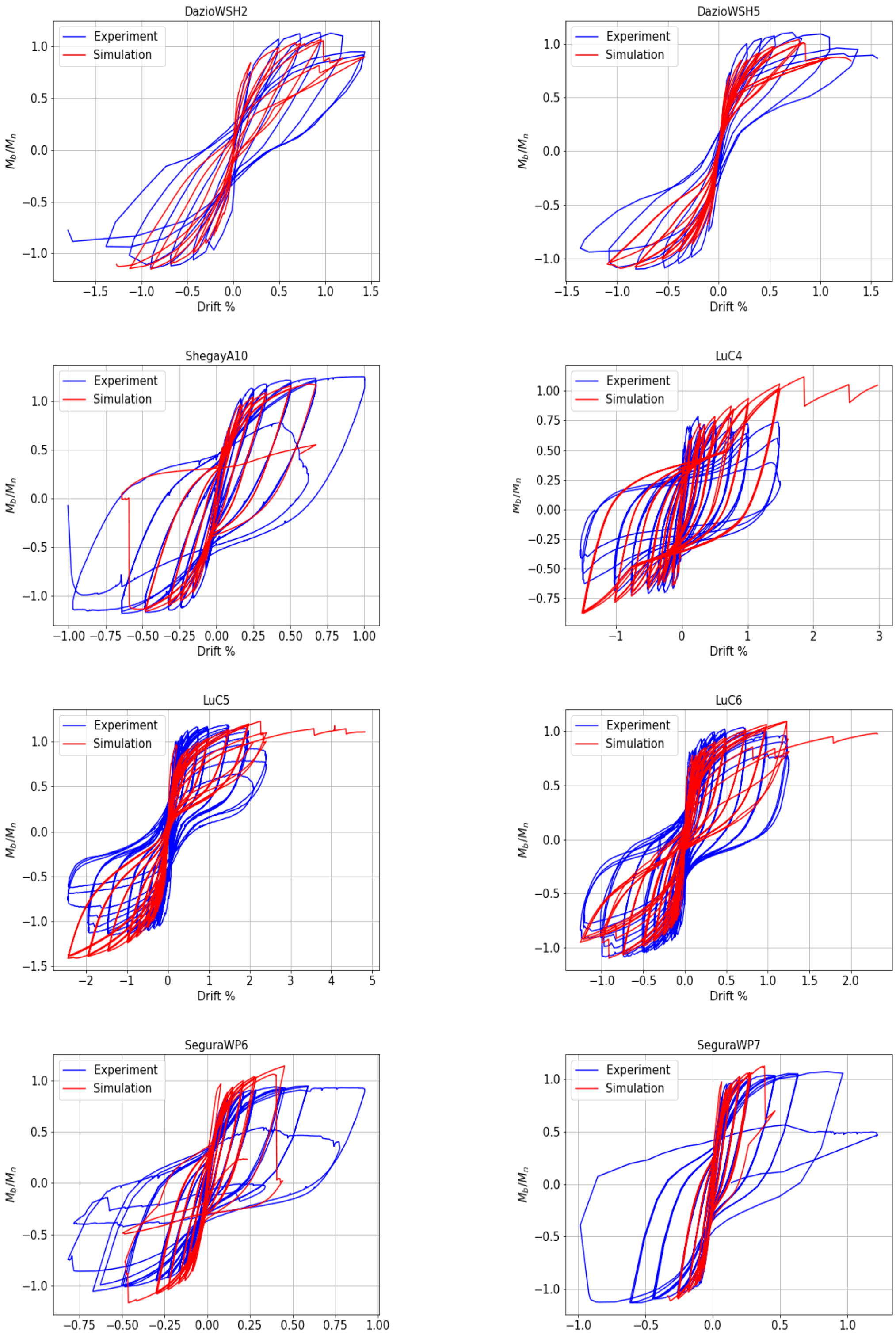

Figure 5.9 Validation Data Set: Simulated and measured response for walls that exhibited BR failure in the laboratory. Note that not all simulated failures are BR (see Table 5.4).

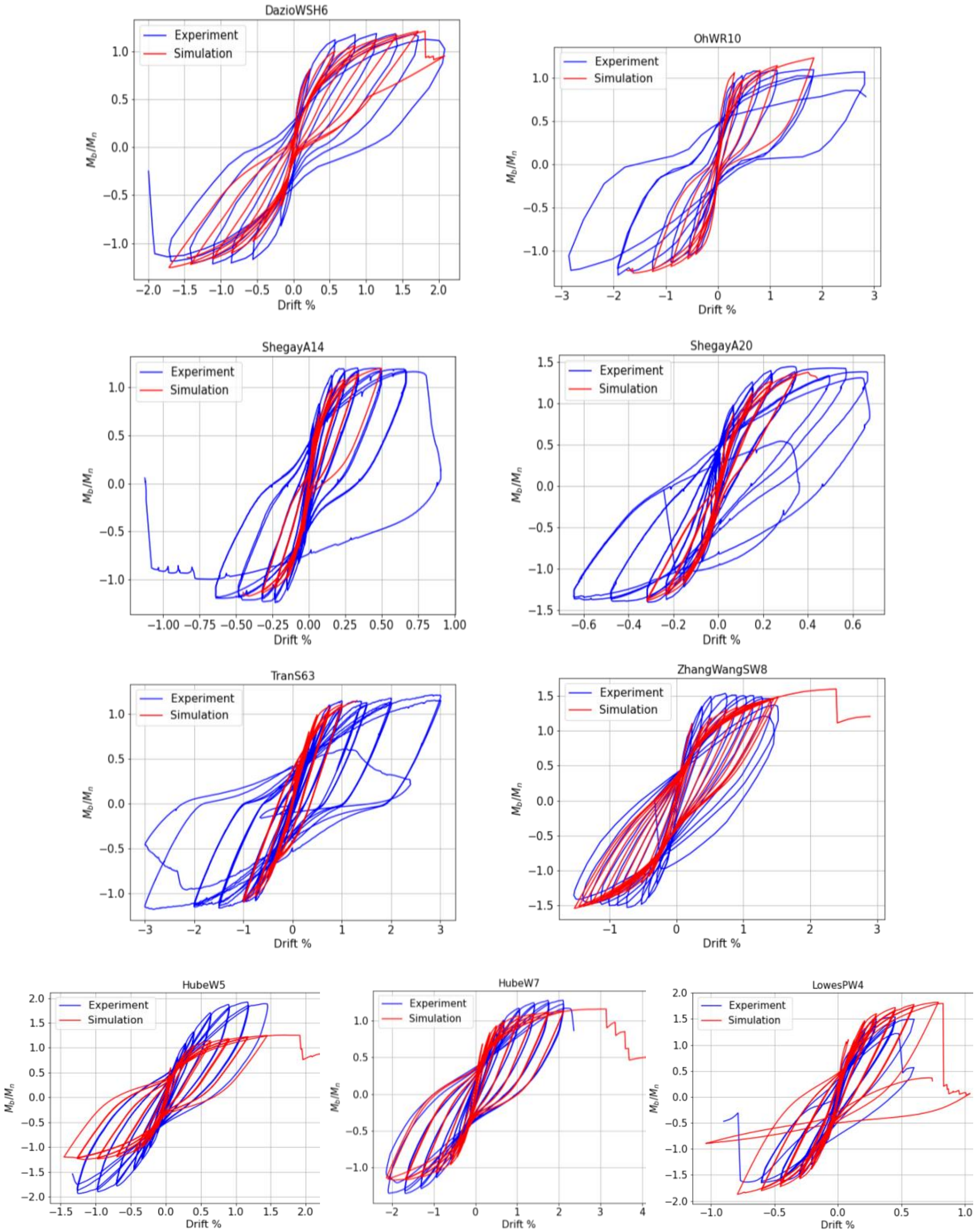

Figure 5.10 Validation data set: Simulated and measured response for walls that exhibited CB failure in the laboratory. Note that not all simulated failures are CB (see Table 5.4).

The data in Table 5.4 and Figure 5. and 5.3 support the following observations about the model:

- Displacement at nominal flexural strength is significantly over predicted; correspondingly stiffness to nominal flexural strength is significantly underpredicted. Both are predicted with a high level of uncertainty.
- Strength is simulated with a high level of accuracy and reasonably high level of precision.
- Deformation capacity is simulated accurately but imprecisely with an average error in simulated deformation capacity of -8% and a standard deviation of 41%.
- Failure mode is correctly simulated for 65% of the test specimens.

The primary observations above regarding average errors and standard deviations in these errors for the validation data set are similar to those made for the calibration data set, when average model parameter values are used for all specimens in the calibration data sets.

5.6 SUMMARY

This chapter presents use of the experimental data presented in Chapter 2, combined with software tools presented in Chapter 4, to i) calibrate material model parameters that are not well defined by material tests but are required to define the OpenSees layered shell element model presented in Chapter 3 and to ii) validate the calibrated model. Experimental data are divided into two data sets of approximately equal size, a *calibration* data set comprising 16 specimens and a *validation* data set comprising 17 specimens. Using the 16 tests in the calibration data set, the following model parameters were determined to provide the best fit to the data:

- Concrete shear retention factor, stc = 0.056 = $\tau/(G\gamma)$ per Eq. 3.13, defines shear capacity parallel to the cracked concrete surface, which affects simulated strength.
- Steel rupture strain reduction factor, $srs = 0.29 = \varepsilon_{fracture,cyclic}/\varepsilon_{fracture,mono}$ per Eq. 3.16, defines the reduction in steel tensile strain capacity resulting from cyclic loading and determines deformation capacity for walls exhibiting tension-controlled flexural failure.
- Confined concrete crushing energy ratio, $rev = 2.6 = G_{fcc}/G_{fc}$ per Eq. 3.12, defines the increase in concrete compression strain capacity resulting from the use of confining reinforcement in wall boundary element regions and affects deformation capacity for walls exhibiting compression-controlled flexural failure.

Using the calibration data set, average values were computed for each of the above model parameters, and these average values were used to simulate the response of each of the walls in the calibration and in the validation data sets. For walls in the *calibration* data set, average errors in simulated response quantities are as follows:

- simulated displacement at nominal flexural strength: -36%
- simulated maximum strength: 8.0%,
- simulated deformation capacity: 18%

and the failure mode is correctly simulated for 60% of the test specimens. Using the calibrated model parameters for all walls in the *validation* data set, average errors in simulated response quantities are as follows:

- simulated displacement at nominal flexural strength: -29%,
- simulated maximum strength: 5.0%,
- simulated deformation capacity: -8.0%

and the failure mode is correctly simulated for 65% of the test specimens.

Standard deviations for all simulated response quantities are relatively large. Strength is the most precisely simulated quantity, with a standard deviation on the simulation error of 14% for the calibration data set and 17% for the validation data set. The standard deviations for the stiffness and deformation capacity errors are 25% and 38%, respectively, for the calibration data set and 34% and 41% for the validation data set.

6 CONCLUSIONS

The research presented in this report employed data for planar concrete walls extracted from the experimental database assembled by Shegay et al. (2021) of laboratory tests of reinforced concrete walls as well as the quoFEM software tool developed by the SimCenter (McKenna et al. 2023, Deierlein et al. 2020), computing resources provided by DesignSafe (Rathje et al. 2017), and the OpenSees platform (McKenna 1997, McKenna et al. 2010) to evaluate, calibrate, and validated a modeling approach, which utilized the planar concrete constitutive model and layered shell element developed and implemented in OpenSees version 3.3.0 by Lu et al. (2015), for use in the simulating the response of planar reinforced concrete walls exhibiting flexure-controlled response when subjected to constant axial and cyclic lateral loading in the laboratory.

The primary objectives of the study were:

1. Develop a modeling technique that utilizes the layered shell elements, planar concrete constitutive model and other commonly used element formulations and material constitutive models (e.g., steel) available in the OpenSees platform to simulate the nonlinear response of planar walls subjected to multi-dimensional loading.

2. Create and publish a Jupyter notebook (Kluyver et al. 2016) based computational framework for building wall models, executing OpenSees simulations, and visualizing simulation results that utilizes NHERI DesignSafe computing resources as well as NHERI SimCenter computational tools.

3. Use the computational framework, a published data set (Shegay et al. 2021), and SimCenter and DesignSafe software and computational resources to evaluate the shell-element models for simulating wall response as well as to calibrate the wall model to provide accurate simulation of stiffness, strength, deformation capacity, failure mode, and cyclic response for a large set of test specimens with a range of design and load characteristics.

4. Provide recommendations and calibrated model parameters to advance modeling of flexure-controlled reinforced concrete walls subjected to constant axial and cyclic lateral loading.

5. Evaluate the functionality of DesignSafe and SimCenter computational resources and tools and provide feedback to drive advancement of these resources.

6.1 RESEARCH SUMMARY

6.1.1 Model Calibration and Validation

Modeling recommendations were developed for use in simulating the stiffness, strength, deformation capacity and failure mechanisms for planar concrete walls exhibiting flexure-controlled response when subjected reversed cyclic lateral loading and constant gravity loading. These recommendations utilize the material models and element formulation developed and incorporated in the OpenSees 3.3.0 platform by Lu et al.

The three shell element formulations available in the OpenSees platform were evaluated: DKGQ and NLDKGQ developed and implemented in OpenSees by Lu et al. (2015) and MITC4 formulated by Dvorkin and Bathe (1984) and implemented in OpenSees by Love (1996). The DKGQ element was found to be the most stable and least prone to artificial strength gain due to the combination of a planar membrane element and a plate bending element. The DKGQ layered shell element was used in combination with the PlaneStressUserMaterial developed by Lu et al. and other material models, element formulations, and utility functions available in OpenSees.

Data for thirty-three laboratory tests of planar walls exhibiting flexure-controlled response under constant axial load and cyclic lateral loading were extracted from the Shegay et al. database for use in the current study. These data were split into a calibration data set (16 walls) and a validation data set (17 walls). The calibration data set was used with the quoFEM software to calibrate concrete and reinforcing steel material model parameters that determine the simulated stiffness, strength and deformation capacity of concrete walls. Specifically the following model parameters were calibrated:

- Concrete shear retention factor, which defines shear response parallel to the concrete crack surface and determines wall strength, was found to have a preferred value of *stc* = 0.056.
- Confined concrete crushing energy, which determines strength loss for walls exhibiting failure due to simultaneous concrete crushing and steel buckling (compression-controlled) failure, was found to have a preferred value of *rev* = 2.56
- Reinforcing steel strain capacity reduction factor, which determines strength loss for walls exhibiting failure due to fracture of previously buckled reinforcing steel (tension-controlled) failure, was found to have a preferred value of *srs* = 0.29

Using the calibrated model parameters, the average error in simulated wall response quantities for walls in the *calibration* and *validation* data sets are presented in Table 6.1. These data indicate a

- Stiffness: Simulated stiffness to nominal flexural strength is, on average, significantly lower than measured in the laboratory and there is high variability in ratio of simulated to measured displacement at the nominal flexural strength of the wall, M_n per ACI 318-25. As discussed in Section 5.4, these results are attributed to evaluating simulated stiffness using measured and simulated displace at nominal flexural strength rather than at first yield of the flexural reinforcement.

- Strength: For both the calibration and validation data sets, maximum strength is accurately and reasonably precisely simulated, with average errors and standard deviations on this error simulation of 8.0% and 14% for the calibration data set and 5.0% and 17% for the validation data set. Accurate and precise simulation of strength is common for reinforced concrete walls (e.g., Pugh et al. 2015, Lowes et al. 2019, Lowes et al. 2020)
- Deformation capacity: For both the calibration and validation data sets, deformation capacity is simulated, on average, with acceptable accuracy and with an accuracy that is consistent with previous studies (e.g., Pugh et al. 2015, Lowes et al. 2019, Lowes et al. 2020). The standard deviation on simulated deformation capacity indicates an uncertainty and variability in the simulated deformation capacity higher than is desirable.
- Failure mode: Failure mode is simulated with less accuracy than is desirable and with less accuracy than has been observed in previous studies (e.g., Pugh et al. 2015, Lowes et al. 2019, Lowes et al. 2020). The inaccuracy in simulated failure mode is somewhat surprising given the acceptable accuracy with which deformation capacity is simulated. Further research is required to determine the specific aspects of the modeling approach used in this study that contribute to poor representation of failure mode.

Table 6.1: Average errors and standard deviation of that error for the *calibration* and *validation* data sets when average calibrated model parameters are used for all walls

Response Quantity	Calibration Data Set		Validation Data Set	
	Average error	Standard deviation	Average error	Standard deviation
Displacement at M_n	-36%	25%	-29%	34%
Maximum strength	8.0%	14%	-5.0%	17%
Deformation capacity	18%	38%	8.0%	41%
Failure mode correctly simulated	60%		65%	

6.1.2 SimCenter Software, DesignSafe Resources and Jupyter Notebooks

Integral to the research project was the use of OpenSees version 3.3.0, Jupyter notebooks (Kluyver et al. 2016), the quoFEM software developed by the NHERI SimCenter to support sensitivity analysis and model calibration, and NHERI DesignSafe computing and data-storage resources.

A series of Jupyter notebooks was created to automate creation, execution and evaluation of OpenSees models of each wall test specimen included in the study. These notebooks were used on the JupyterHub on DesignSafe, where they supported access of HPC resources and direct access to archived folders from quoFEM jobs. During the course of the project, hundreds of OpenSees models were created for each wall to investigate different element formulations and levels of mesh refinement as well as to calibrate model parameters to achieve accurate simulation of observed response. Thus, the notebooks and DesignSafe resources were integral to the success of the project. These notebooks are published in GitHub and the DesignSafe DataDepot.

The SimCenter quoFEM software was used as a Windows application on a PC to calibrate the model parameters that were not easily defined using fundamental material and design characteristics. A quoFEM sensititivy analysis was used with the calibration data set to determine the preferred value for cracked concrete shear retention (*stc*). For calibration of the confined concrete crushing energy ratio (*rev*) and the reinforcing steel rupture strain capacity ratio (*srs*), the quoFEM gradient-based parameter estimation algorithm was used initially to determine the preferred value of this parameter; however, this algorithm was found not to work well for this particular project and the non-gradient-based parameter estimation method was used instead to calibrate the concrete crushing energy ratio (*rev*) and steel rupture strain reduction factor (*srs*).

Using a calibration data set comprising 16 test specimens, the preferred values for the shear retention factor, steel rupture strain ratio, and the crushing energy ratio were determined for each specimen and then averaged across the calibration data set. These values were then used to simulate the response of the 17 walls in the validation data set. Data in Table 6.1 provide the results of these simulations. Average errors and standard deviations on these average errors are approximately the same for the calibration and validation data sets.

7 REFERENCES

ACI Committee 318 (2025). *Building Code Requirements for Structural Concrete (ACI 318-25) and Commentary*. Farmington Hills, MI.

Adams, B.M., Bohnhoff, W.J., Dalbey, K.R., Ebeida, M.S., Eddy, J.P., Eldred, M.S., Hooper, R.W., Hough, P.D., Hu, K.T., Jakeman, J.D., Khalil, M., Maupin, K.A., Monschke, J.A., Ridgway, E.M., Rushdi, A.A., Seidl, D.T., Stephens, J.A., Swiler, L.P., and Winokur, J.G., "Dakota, A (2021). *Multilevel Parallel Object-Oriented Framework for Design Optimization, Parameter Estimation, Uncertainty Quantification, and Sensitivity Analysis: Version 6.15 User's Manual, Sandia Technical Report SAND2020-12495*. Sandia Laboratory.

Ahmed K, Lowes LN, Lehman DE (2023). "Investigation of the Behavior of Slender Reinforced Concrete Walls with Complex Configurations Using Nonlinear Finite Element Analysis" *Resilient Cities and Structures* 2(1):120-142. DOI: 10.1016/j.rcns.2023.02.010

ASTM C39/C39M-24 (2024) Standard Test Method for Compressive Strength of Cylindrical Concrete Specimens, ASTM INTERNATIONAL.

Berry M, Lehman DE, Lowes LN (2008). "Lumped-Plasticity Models for Performance Simulation of Bridge Columns." *ACI Structural Journal* 105 (3). https://doi:10.14359/19786.

Comité Euro-International du Béton (1990). *CEB-FIP Model Code 1990*, Thomas Telford, London, UK, 1990, 437 pp.

Dazio A Beyer K, Bachman H (2009). "Quasi-Static Cyclic Tests and Plastic Hinge Analysis of RC Structural Walls." Engineering Structures 31 (7): 1556–71. https://doi:10.1016/j.engstruct.2009.02.018.

Deierlein GG, McKenna F, Zsarnóczay A, Kijewski-Correa T, Kareem A, Elhaddad W, Lowes LN, Schoettler MJ, Govindjee S. (2020). "A Cloud-Enabled Application Framework for Simulating Regional-Scale Impacts of Natural Hazards on the Built Environment." *Frontiers in Built Environment*. 6:558706. https://doi: 10.3389/fbuil.2020.558706

Dvorkin EN, Bathe KJ (1984). "A continuum mechanics based four node shell element for general nonlinear analysis." Engineering Computing: 1, 77-88.

Giuffrè A (1970). "Il Comportamento Del Cemento Armato per Sollecitazioni Cicliche Di Forte Intensità." *Giornale Del Genio Civile* 28: 1–20.

Hube MA, Marihuén A, de la Llera JC, Stojadinovic B (2014). "Seismic behavior of slender reinforced concrete walls" *Engineering Structures* 80: 377-388. https://doi.org/10.1016/j.engstruct.2014.09.014

Kluyver, T., Ragan-Kelley, B., Perez F., Granger, B., Bussonnier, M., Frederic, J., Kelley, K., Hamrick, J., Grout, J., Corlay, S., Ivanov, P., Avila, D., Abdall, S., Willing, C. (2016). "Jupyter Notebooks – a publishing format for reproducible computational workflows." *Positioning and Power in Academic Publishing: Players, Agents and Agendas,* F. Loizides and B. Schmidt (Eds.), pp. 87–90. DOI: 10.3233/978-1-61499-649-1-87.

Liu H. (2004). "Effect of Concrete Strength on the Response of Ductile Shear Walls." MS Thesis. Dept. of Civil Engineering and Applied Mechanics, McGill University.

Love, E (1996). "OpenSees implementation of 4-node shell element formulation developed by Bvokin and Bathe"

Lowes, LN, Lehman, D.E., Birely, A.C., Kuchma, D.A., Marley, K.P., Hart, C.R. (2012). "Earthquake Response of Slender Planar Concrete Walls with Modern Detailing" *Engineering Structures* Vol. 43: p 31-47.

Lowes LN, Lehman DE, Baker C (2020) "SP-339-11: Recommendations for Modeling the Nonlinear Response of Flexural Reinforced Concrete Walls Using Perform." *ACI SP-339*, Farmington Hills: American Concrete Institute.

Lowes LN, Lehman DE, Whitman Z (2019). "Investigation of failure mechanisms and development of design recommendations for flexural reinforced concrete walls." *Engineering Structures* (186):323-335. https://doi.org/10.1016/j.engstruct.2019.01.122

Lu, Y., Henry, R. S., Gultom, R., & Ma, Q. T. (2017). Cyclic testing of reinforced concrete walls with distributed minimum vertical reinforcement. *Journal of Structural Engineering,* 143(5), 04016225-1-04016225–17. https://doi.org/10.1061/(ASCE)ST.1943- 541X.0001723.

Lu XZ, Xie LL, Guan H, Huang YL, Lu X (2015). "A shear wall element for nonlinear seismic analysis of super-tall buildings using OpenSees," *Finite Elements in Analysis & Design* 98: 14-25. https://DOI: 10.1016/j.finel.2015.01.006

Marafi N, Ahmed K, Lehman D, Lowes LN (2019). "Variability in Seismic Collapse Probabilities of Solid- and Coupled-Wall Buildings" *Journal of Structural Engineering*. https://doi.org/10.1061/(ASCE)ST.1943-541X.0002311

McKenna F (1997). "Object oriented finite element analysis: Frameworks for analysis algorithms and parallel computing". *Dissertation*. University of California, Berkeley.

McKenna F, Scott MH, Fenves GL (2010). "Nonlinear Finite-element Analysis Software Architecture using Object Composition" *Journal of Computing in Civil Engineering* 24(1): 95-107.

McKenna F, Yi S, Satish AB, Zsarnoczay A, Gardner M, Elhaddad W (2025). NHERI-SimCenter/quoFEM: Version 4.1.0 (v4.1.0). Zenodo. https://doi.org/10.5281/zenodo.14583957

Menegotto M, Pinto PE (1973). "Method of analysis of cyclically loaded RC plane frames including changes in geometry and non-elastic behavior of elements under normal force and bending." *Preliminary Report IABSE*, vol 13.

NIST (2013). "Recommendations for Seismic Design of Reinforced Concrete Wall Buildings Based on Studies of the 2010 Chile Earthquake," NEHRP Consultants Joint Venture for the National Institute of Standards and Technology, Gaithersburg, MD, Tech. Rep. No. GCR 13-917-25.

NZS (Standards New Zealand) (2006). "Concrete structures standard (Amendment 2)." Wellington, New Zealand.

Oh YH, Sang WH, and Le LH (2002). "Effect of Boundary Element Details on the Seismic Deformation Capacity of Structural Walls." *Earthquake Engineering & Structural Dynamics* 31 (8): 1583–1602. https://doi:10.1002/eqe.177.

Orakcal K, Wallace J. (2006). "Flexural Modeling of Reinforced Concrete Walls - Experimental Verification." ACI Structural Journal 103(2). https://doi:10.14359/15177.

Ousterhout, J.K., (1990) "TCL: An Embeddable Command Language," *Proceedings of the 1990 Winter USENIX Conference*, pp 133-146. ftp://ftp.smli.com/pub/tcl/tclUsenix90.ps.

Palermo D, . Vecchio FJ (2007). "Simulation of Cyclically Loaded Concrete Structures Based on the Finite-Element Method." *Journal of Structural Engineering* 133(5):728–38. https://doi:10.1061/(ASCE)0733-9445(2007)133:5(728).

Ministry of Construction, People's Republic of China (1992). *Technical Specification for Concrete Structures of Tall Building (JGJ 3-92)*. China Architecture & Building Press.

Pugh J (2012). "Numerical Simulation of Walls and Seismic Design Recommendations for Walled Buildings." *Ph.D. Dissertation*, Seattle, WA: Dept. of Civil and Environmental Engineering, University of Washington.

Pugh, JS, Lowes LN, Lehman DE (2015). "Nonlinear line-element modeling of flexural reinforced concrete walls" *Engineering Structures* 104: 174-192. https://doi.org/10.1016/j.engstruct.2015.08.037

Python Software Foundation (2022). "Python Language Reference". https://www.python.org.

Rathje, E., Dawson, C. Padgett, J.E., Pinelli, J.-P., Stanzione, D., Adair, A., Arduino, P., Brandenberg, S.J., Cockerill, T., Dey, C., Esteva, M., Haan, Jr., F.L., Hanlon, M., Kareem, A., Lowes, L., Mock, S., and Mosqueda, G. (2017). "DesignSafe: A New Cyberinfrastructure for Natural Hazards Engineering," *ASCE Natural Hazards Review*, https://doi:10.1061/(ASCE)NH.1527-6996.0000246.

Saatcioglu M, Razvi SR (1992). "Strength and Ductility of Confined Concrete." *Journal of Structural Engineering* 118: 1590-1607.

Segura C. (2017). "Seismic Performance Limitation of Slender Reinforced Concrete Structural Walls" *Ph.D. Dissertation*. *UCLA*. ProQuest ID: Segura_ucla_0031D_16051.

Segura CL, Wallace JW (2018). "Seismic Performance Limitations and Detailing of Slender Reinforced Concrete Walls." *ACI Structural Journal* 115(3): 849-859. doi: 10.14359/51701918.

Shegay A, Motter C, Henry R, Elwood K, Lowes LN, Lehman DE. (2018). "Impact of Axial Load on the Seismic Response of Rectangular Walls." *Journal of Structural Engineering*" 10.1061/(ASCE)ST.1943-541X.0002122.https://doi.org/10.1061/(ASCE)ST.1943-541X.0002122

Shegay A, Birely A, Elwood K, Henry R, Lehman DE, Lowes LN, Motter C, Pugh J (2021). "UoA-UW Reinforced Concrete Wall Database." DesignSafe-CI. https://doi.org/10.17603/ds2-r12q-t415 v1.

Spacone E, Ciampi V, Filippou FC (1996). "Mixed Formulation of Nonlinear Beam-Finite Element." *Computers and Structures* 58(1): 71–83.

The MathWorks Inc. (2022). MATLAB version: 2022b, Natick, Massachusetts: The MathWorks Inc. https://www.mathworks.com

Tran TA (2012). "Experimental and Analytical Studies of Moderate Aspect Ratio Reinforced Concrete Structural Walls." *Ph.D. Dissertation*. UCLA Dept. of Civil and Environmental Engineering.

Van Rossum G., Drake FL (2009). The Python Language Reference, Release 3.10.X Python Software Foundation.

Wallace JW, Thomsen JH, (1995). "Seismic Design of RC Structural Walls. Part II: Applications." *Journal of Structural Engineering* 121(1): 88–101. https://doi:10.1061/(ASCE)0733-9445(1995)121:1(88).

Wond PS, Vecchio FJ, Trommels H (2013). *Vector2 & Formworks User's Manual*. Toronto, ON: Vector Analysis Group.

Zhang Y, Wang, Z. (2000). "Seismic behavior of reinforced concrete shear walls subjected to high axial loading" *ACI Structural Journal* (97): 739-750.

Zhu M, McKenna F, Scott MH (2018). "OpenSeesPy: Python library for the OpenSees finite element framework" *SoftwareX* (7): 6-11. https://doi.org/10.1016/j.softx.2017.10.009

Appendix A Material and Wall Demands

Table A.1 Material properties for wall data set

Author	ID	Material								
		f'_c	$f_{y,be}$	$E_{s,be}$	$f_{u,be}$	$\epsilon_{u,be}$	$f_{y,v}$	$E_{s,v}$	$f_{u,v}$	$\epsilon_{u,v}$
		ksi	ksi	ksi	ksi	in/in	ksi	ksi	ksi	in/in
Dazio et al.	WSH1	6.53	79.38	29000	89.91	0.046	84.64	29000	87.12	0.023
Dazio et al.	WSH2	5.87	84.57	29000	108.40	0.077	70.33	29000	77.52	0.058
Dazio et al.	WSH3	5.69	87.16	29000	105.22	0.077	82.55	29000	101.55	0.073
Dazio et al.	WSH5	5.55	84.66	29000	103.61	0.079	75.26	29000	81.03	0.055
Dazio et al.	WSH6	6.61	83.54	29000	97.88	0.073	84.66	29000	103.61	0.079
Liu	W1	4.80	66.38	29000	91.41	0.180	67.35	29000	84.25	0.165
Liu	W2	10.25	66.38	29000	91.41	0.180	67.35	29000	84.25	0.165
Lowes et al.	PW4	4.27	67.10	29000	109.50	0.120	75.70	29000	77.00	0.055
Thomsen et al.	RW1	4.58	63.00	29000	93.00	0.100	65.00	29000	85.00	0.080
Thomsen et al.	RW2	4.93	63.00	29000	93.00	0.100	65.00	29000	85.00	0.080
Oh et al.	WR20	4.77	65.12	29000	89.49	0.176	47.72	29000	64.54	0.176
Oh et al.	WR10	5.05	65.12	29000	89.49	0.176	47.72	29000	64.54	0.176
Shegay et al.	C10	4.74	78.76	29000	98.34	0.160	73.53	29000	94.71	0.143
Shegay et al.	A10	4.74	78.76	29000	98.34	0.160	73.53	29000	94.71	0.143
Shegay et al.	A14	6.18	78.76	29000	98.34	0.160	73.53	29000	94.71	0.143
Shegay et al.	A20	6.34	78.76	29000	98.34	0.160	73.53	29000	94.71	0.143
Tran	S38	6.83	68.40	29000	88.90	0.150	65.30	29000	95.90	0.122
Tran	S63	7.05	69.20	29000	92.40	0.144	64.20	29000	102.60	0.190
Zhang et al.	SW7	4.82	58.74	29000	70.49	0.120	44.24	29000	53.08	0.120
Zhang et al.	SW8	5.20	62.66	29000	75.19	0.120	44.24	29000	53.08	0.120
Zhang et al.	SW9	5.75	54.39	29000	65.27	0.120	44.24	29000	53.08	0.120
Segura	WP6	6.71	77.00	29000	107.60	0.111	83.90	29000	105.30	0.103
Segura	WP7	12.48	62.84	29000	92.39	0.100	121.25	29000	121.40	0.100
Lu et al.	C1	5.58	43.60	29000	66.98	0.126	43.60	29000	66.98	0.126
Lu et al.	C2	5.00	43.60	29000	66.98	0.126	43.60	29000	66.98	0.126
Lu et al.	C3	5.25	43.60	29000	66.98	0.126	43.60	29000	66.98	0.126
Lu et al.	C4	5.03	43.60	29000	66.98	0.126	43.60	29000	66.98	0.126
Lu et al.	C5	5.13	43.60	29000	66.98	0.126	43.60	29000	66.98	0.126
Lu et al.	C6	5.41	43.60	29000	66.98	0.126	43.60	29000	66.98	0.126
Hube et al.	W5	3.97	68.02	29000	98.05	0.166	64.63	29000	86.88	0.151
Hube et al.	W7	3.97	68.02	29000	98.05	0.166	64.63	29000	86.88	0.151
Hube et al.	W8	3.97	68.02	29000	98.05	0.166	64.63	29000	86.88	0.151
Hube et al.	W9	3.97	68.02	29000	98.05	0.166	64.63	29000	86.88	0.151

Table A.2 Computed demand and measured response quantities for wall data set

Author	Specimen	Loading					Measured Response
		CSAR	Shear Span	ALR	$V_{max}/(A_{cv}f'_c{}^{0.5})$	Δu	FM
		--	--	%	psi	%	--
Dazio et al.	WSH1	13.33	2.28	5.10	2	1.04	BR
Dazio et al.	WSH2	13.33	2.28	5.69	2.25	1.43	BR
Dazio et al.	WSH3	13.33	2.28	5.83	2.92	2.03	BR
Dazio et al.	WSH5	13.33	2.28	12.8	2.81	1.36	BR
Dazio et al.	WSH6	13.33	2.26	10.8	3.49	2.07	CB
Liu	W1	6.07	3.13	7.64	2.31	2.98	CB
Liu	W2	6.07	3.13	3.58	1.67	2.91	BR
Lowes et al.	PW4	20	2	11.7	4.31	1.01	CB
Wallace	RW1	12	3.13	10.2	2.44	2.1	BR
Wallace	RW2	12	3.13	8.99	2.63	2.25	CB
Oh et al.	WR20	7.5	2	8.39	2.71	2.7	CB
Oh et al.	WR10	7.5	2	7.92	2.5	2.82	CB
Shegay	C10	11.25	4.6	9.17	2.12	3.1	CB
Shegay	A10	11.25	4.6	9.17	2.11	3.1	BR/Global
Shegay	A14	11.25	4.6	14.1	2.15	2.5	CB
Shegay	A20	11.25	4.6	20.6	2.45	2.05	CB
Tran.	S38	8	2	7.32	4.54	3.1	CB
Tran	S63	8	2	7.29	6.88	3	CB
Zhang et al.	SW7	7	2.14	24.0	6.01	2	CB
Zhang et al.	SW8	7	2.14	35.0	6.46	1.5	CB/Global
Zhang et al.	SW9	7	2.14	25.0	8.31	2	CB
Segura	WP6	12	3.57	7.46	2.2	3.55	BR
Segura	WP7	10	3.51	7.10	1.63	3.7	CB
Lu et al.	C1	9.33	2	3.59	1.6	2.5	BR
Lu et al.	C2	9.33	4	4.00	0.87	2.5	BR
Lu et al.	C3	9.33	6	3.81	0.54	2.5	BR
Lu et al.	C4	9.33	2	0	0.93	1.5	BR
Lu et al.	C5	9.33	2	7.47	2.28	1.98	BR
Lu et al.	C6	9.33	4	3.70	0.8	2.45	BR
Hube et al.	W5	7	1.9	15.0	6.21	1.45	CB
Hube et al.	W7	7	2.5	15.0	4.62	2.3	CB
Hube et al.	W8	7	2.5	15.0	5.13	2.71	CB
Hube et al.	W9	7	2.5	15.0	4.69	2.68	CB

Appendix B Experimental Data

Table B.1 Computed demand and measured response quantities for wall data set

		Flexural Response					Shear Response				Drift	
Author	ID	ALR	My	Mn	Mb,max	Mb,max/Mn	Vn, ACI	Vb,max	vmax	Vb,max/Vn	Δy	Δu
		%	kip-ft	kip-ft	kip-ft	--	kip	kip	--	--	%	%
Dazio et al.	WSH1	5.1	930	1088	1124	1.03	174	75	2.00	0.43	0.24	1.04
Dazio et al.	WSH2	5.69	960	1060	1201	1.13	153	80	2.25	0.52	0.23	1.43
Dazio et al.	WSH3	5.83	1140	1376	1530	1.11	153	102	2.92	0.67	0.36	2.03
Dazio et al.	WSH5	12.83	1210	1316	1458	1.11	157	97	2.81	0.62	0.2	1.36
Dazio et al.	WSH6	10.79	1530	1651	1956	1.18	163	132	3.49	0.81	0.28	2.07
Liu	W1	7.64	615	712	714	1.00	150	59	2.31	0.39	0.64	2.98
Liu	W2	3.58	650	769	756	0.98	191	62	1.67	0.33	0.55	2.91
Lowes et al.	PW4	11.7	3660	1624	2436	1.50	247	203	4.31	0.82	0.4	1.01
Thomsen et al.	RW1	10.23	330	400	396	0.99	67	32	2.44	0.47	0.48	2.1
Thomsen et al.	RW2	8.99	330	387	443	1.14	68	35	2.63	0.52	0.55	2.25
Oh et al.	WR20	8.39	790	639	857	1.34	130	87	2.71	0.67	0.35	2.7
Oh et al.	WR10	7.92	795	741	814	1.10	151	83	2.50	0.55	0.47	2.82
Shegay et al.	C10	9.17	2561	2818	3409	1.21	311	102	2.12	0.33	--	3.1
Shegay et al.	A10	9.17	2561	2757	3378	1.23	312	101	2.11	0.32	0.35	3.1
Shegay et al.	A14	14.08	3231	3331	3997	1.20	331	118	2.15	0.36	0.46	2.5
Shegay et al.	A20	20.59	3818	3185	4538	1.42	347	136	2.45	0.39	0.31	2.05
Tran et al.	S38	7.32	680	651	864	1.33	108	108	4.54	1.00	0.53	3.1
Tran et al.	S63	7.29	1135	1094	1331	1.22	160	166	6.88	1.04	0.63	3
Zhang et al.	SW7	21.44	191	198	223	1.13	70	45	6.01	0.64	0.4	2
Zhang et al.	SW8	31.26	211	160	249	1.56	75	51	6.46	0.67	0.37	1.5
Zhang et al.	SW9	21.44	283	244	337	1.38	89	68	8.31	0.77	0.56	2
Segura et al.	WP6	7.46	3128	3438	4194	1.22	128	122	2.20	0.95	0.59	4.08
Lu et al.	C1	3.59	259	363	352	0.97	90	39	1.60	0.43	0.55	2.5
Lu et al.	C2	4	255	338	368	1.09	90	20	0.87	0.22	0.52	2.5
Lu et al.	C3	3.81	257	332	350	1.05	90	13	0.54	0.14	0.68	2.5
Lu et al.	C4	0	103	251	194	0.77	85	21	0.93	0.25	0.27	1.5
Lu et al.	C5	7.47	368	411	481	1.17	101	53	2.28	0.53	0.76	2
Lu et al.	C6	3.7	248	343	354	1.03	84	19	0.80	0.23	1	2.5
Hube et al.	W5	14.96	155	127	244	1.92	50	42	6.21	0.85	0.31	1.45
Hube et al.	W7	14.96	127	142	181	1.27	50	32	4.62	0.63	0.36	2.3
Hube et al.	W8	14.96	129	136	202	1.48	50	35	5.13	0.70	0.42	2.71
Hube et al.	W9	14.96	122	121	184	1.51	50	32	4.69	0.64	0.34	2.68

Appendix C Data Structures

Structure Level 1	2	3	4	5		
Variable Name					**Variable type**	**Variable description**
Authors					Cell Array	Representative author of the study
SpecimenID					Cell Array	Specimen ID as classified by author
UniqueID					Cell Array	Unique specimen ID - amalgamation of Author and SpecimenID
WallType					Structure	General wall overview
	Shape				Cell Array	Cross sectional shape of the wall ('Rect' or 'Flanged' or 'Barbell')
	SteelLayout				Cell Array	BE or Dist
Geometry					Structure	Wall geometrical details
	t				Double	Wall web thickness (in)
	h				Double	Clear height of specimen (between foundation block and capping block, if present) (in)
	l				Double	Length of the wall edge to edge (in)
	h_v				Double	Effective specimen height, base moment divided by base shear (in)
	l_be				Double	Length of the boundary element measured as the cumulative center to center distance of the bars in the BE plus cover to the bar centerlines either side (in). For flanged section, this is 0 if there is no BE in the web portion.
	endCover				Double	Clear cover to the confinement reinforcement at end of wall (in)
	sideCover				Double	Clear cover to the confinement reinforcement at face of wall (in)
	t_f				Double	Flange thickness (in)
	b_f				Double	Width of the flange (in)
	AspectRatio				Double	Clear height of wall divided by length of wall (h/l)
	ShearSpan				Double	Shear span ratio. Base moment/base shear/length of wall (h_v/l)
	SlenderRatio				Double	Cross-sectional aspect ratio. Length of wall/thickness of web (l/t)
	BeRatio				Double	Area of both boundary elements (BEs) divided by the gross cross sectional wall area
	WallVolume				Double	thickness x length x clear height (t x l x h) (in^3)
	WallSurfaceArea				Double	(t x h + l x h)x2 for most walls. Calculation for T-section and barbell walls is appropriately adjusted
	Area				Double	Gross cross sectional wall area
	numStory				Double	Number of stories constructed
	Igross				Double	Gross moment of inertia (in^4)
	h_measured				Double	Height at which lateral displacement is measured in the experiment
	l_bef				Double	Length of the boundary element in the flange of the wall (if present), measured as the center to center distance of the bars in the BE plus cover to the bar centerlines either side (in)
	LoadingDirection				Double	Indicates the direction towards which the load is initially loaded in the protocol: + 1: load is applied which puts the 'right' boundary element in compression -1: load is applied which puts the 'left' boundary element in compression The 'right' and 'left' definitions are consistent with the section data entered in the Layers section of the SectionAnalysis part of the database. i.e., for T-sections, +1 puts the flange in compression at start of test.
	BuildingAspectRatio				Double	This is the aspect ratio of the wall in the building design. Often this is larger than the shear span ratio because the shear span ratio is based on an effective height, which is 60-70% of the actual wall design to be used in a building. This parameter is needed for some code comparisons

Structure Level Variable Name	1	2	3	4	5	Variable type	Variable description
Reinf						Structure	Wall reinforcement detailing
	rho_be					Double	Reinforcement ratio in the BE (area of longitudinal reinforcement in the BE divided (l_be*t)
	rho_v					Double	Vertical reinforcement ratio in the web of the wall (area of longitudinal reinforcement in the web divided (l*t -2l_be*t)
	rho_v_all					Double	Vertical reinforcement ratio of the entire cross section (area of all longitudinal reinforcement divided by l*t)
	rho_h					Double	Horizontal reinforcement ratio of the wall in the web (area of horizontal reinforcement divided by spacing*t)
	rho_z					Double	Reinforcement ratio of the confinement legs in the BE (area of BE hoops and ties divided by spacing*l_be)
	rho_h_be					Double	Reinforcement ratio of the horizontal confinement hoops in the BE (area of BE hoops and ties divided by spacing*t)
	NoCH					Double	Number of curtains of longitudinal reinforcement in the horizontal direction
	NoCV					Double	Number of curtains of longitudinal reinforcement in the vertical direction
	s_h					Double	Spacing of horizontal web reinforcement (in)
	s_v					Double	Spacing of the vertical longitudinal reinforcement in the web (in)
	s_hoop					Double	Hoop spacing in the BE (in)
	d_be					Double	Diameter of longitudinal bars in the BE (in)
	d_v					Double	Diameter of longitudinal bars in the web (in)
	d_h					Double	Diameter of the horizontal reinforcement in the web (in)
	d_hoop					Double	Diameter of the hoops in the BE (in)
	rho_vol					Double	Transverse reinforcement volumetric ratio (volume of one layer of hoops/ties in BE divided by (l_be*s_hoop*t)
	Confinement					Structure	Confinement reinforcement detailing of the wall
		UniqueID	cTog			Double	1 or 0 to indicate of wall does (1) or does not (0) have confinement reinforcement in the BE, respectively
			xdir	bars		2D Matrix	2 column matrix with single confinement leg area in first column (in^2) and yield strength in the second column (ksi). The number of rows corresponds to the number of confinement legs in the BE crossing the longitudinal axis of the wall cross section
				b		Double	The length of the boundary element to the outside of the peripheral confinement/transverse reinforcement legs
				s1		Double	Spacing of longitudinal reinforcement in the BE. This is averaged if the number value fluctuates (hoops or cross ties)
				sHoop		Double	Vertical spacing of the confinement hoops/ties
			ydir	bars		2D Matrix	2 column array with single confinement leg area in first column (in^2) and yield strength in the second column (ksi). The number of rows corresponds to the number of confinement legs in the BE crossing the transverse axis of the wall cross section
				b		Double	The length of the boundary element to the outside of the peripheral confinement/transverse reinforcement legs
				s1		Double	Spacing of longitudinal reinforcement in the BE. This is averaged if the number value fluctuates (hoops or cross ties)
				sHoop		Double	Vertical spacing of the confinement hoops
			webcTog			Double	1 or 0 to indicate of wall does or does not have confinement reinforcement in the web, respectively
			web_xdir	bars		2D Matrix	2 column matrix with single confinement leg area in first column (mm^2) and yield strength in the second column (Mpa). The number of rows corresponds to the number of confinement legs in the BE crossing the longitudinal axis of the wall cross section
				s1		Double	Spacing of longitudinal reinforcement in the web. This is averaged if the number value fluctuates (hoops or cross ties)
				sHoop		Double	Vertical spacing of the web confinement reinforcement
			web_ydir	bars		2D Matrix	2 column array with single confinement leg area in first column (mm^2) and yield strength in the second column (Mpa). The number of rows corresponds to the number of confinement legs in the BE crossing the transverse axis of the wall cross section
				s1		Double	Spacing of longitudinal reinforcement in the web. This is averaged if the number value fluctuates (hoops or cross ties)
				sHoop		Double	Vertical spacing of the web confinement reinforcement
			minHookAngle			Double	Number indicating the WORST hook shape in the BE. 1 if the worst shape is a hoop corner or a 180-180 hook. 0.5 if the worst shape has a 90 degree hook. This is used to reduce effectiveness of confinement. See: Shegay, A. V. (2019). Seismic Performance of Reinforced Concrete Walls Designed For Ductility. Ph.D. Thesis. University of Auckland. Welt, T. S. (2015). Detailing for Compression in Reinforced Concrete Wall Boundary Elements: Experiments, Simulations, and Design Recommendations. Ph.D. Thesis, University of Illinois at Urbana-Champaign.
			asymTog			Double	Number to indicate if the cross section of the wall is symmetrical (0) or asymmetrical (1)
	s_hoop_e					Double	Hoop spacing in the BE (in) of the opposite side (in case where wall detailing is assymetrical)
	rho_be_e					Double	Reinforcement ratio in the BE of the opposite side (in case where wall detailing is assymetrical)
	d_be_e					Double	Diameter of longitudinal bars in the BE (in) of the opposite side (in case where wall detailing is assymetrical)
	d_v_e					Double	Diameter of longitudinal bars in the web (in) of the opposite side (in case where wall detailing is assymetrical)
	d_h_e					Double	Diameter of the horizontal reinforcement in the web (in) of the opposite side (in case where wall detailing is assymetrical)
	d_hoop_e					Double	Diameter of the hoops in the BE (in) of the opposite side (in case where wall detailing is assymetrical)
	rho_vol_e					Double	Transverse reinforcement volumetric ratio of the opposite side (in case where wall detailing is assymetrical)

Variable Name	Structure Level 1	2	3	4	5	Variable type	Variable description
Material							
	age					Double	Age of concrete when test was conducted (days)
	fc					Double	Measured concrete compressive strength (psi)
	eps					Double	Strain at peak concrete compressive stress
	Ec					Double	Measured Youngs modulus of concrete (psi)
	fr					Double	Measured rupture stress of concrete (if available) (psi)
	fsp					Double	Measured splitting stress of concrete (if available) (psi) - split cylinder test
	fy_be					Double	Measured yield strength of BE longitudinal reinforcement (ksi)
	fu_be					Double	Measured ultimate strength of BE longitudinal reinforcement (ksi)
	fy_v					Double	Measured yield strength of vertical web longitudinal reinforcement (ksi)
	fu_v					Double	Measured ultimate strength of web vertical longitudinal reinforcement (ksi)
	fy_h					Double	Measured yield strength of horizontal web reinforcement (ksi)
	fu_h					Double	Measured ultimate strength of horizontal web reinforcement (ksi)
	fy_hoop					Double	Measured yield strength of hoop reinforcement (ksi)
	fu_hoop					Double	Measured ultimate strength of hoop reinforcement (ksi)
	eps_ult_be					Double	Strain at ultimate stress of BE longitudinal reinforcement
	eps_ult_v					Double	Strain at ultimate stress of vertical web longitudinal reinforcement
	eps_ult_h					Double	Strain at ultimate stress of horizontal web reinforcement
	eps_max					Double	Strain at rupture of longitudinal BE reinforcement
	fyt_web					Double	Measured yield strength of web confinement reinforcement (ksi)
	fut_web					Double	Measured ultimate strength of web confinement reinforcement (ksi)
	fy_be_e					Double	Measured yield strength of BE longitudinal reinforcement (ksi) in the opposite wall end (if the wall is asymmetrical)
	fu_be_e					Double	Measured ultimate strength of BE longitudinal reinforcement (ksi)in the opposite wall end (if the wall is asymmetrical)
	eps_ult_be_e					Double	Strain at ultimate stress of BE longitudinal reinforcement in the opposite wall end (if the wall is asymmetrical)
	eps_ult_hoop					Double	Strain at ultimate stress of BE hoop reinforcement
Loading						Structure	Information on the loading conditions on the test wall during the experiment
	Mtop_Vtop					Double	Applied moment at top of specimen (at height of shear load application) divided by applied shear at top of specimen
	LoadingType					Cell	Horizontal loading condition of the wall. Eitehr 'Cyclic' or 'monotonic'
	AxialLoad					Double	Axial load magnitude (kips)
	TotalAxialLoad					Structure	
		UniqueID				Double	Axial load plus self weight of the specimen (including capping block), calculated using 0.087lb/in^3 (kips)
	CyclicHistory						
		UniqueID				2D Matrix	Loading protocol of the tests determined from raw data or digitized graphs when available. Structure is a 2D array with positive drift steps in 1st column and negative drift steps in second column, including all cycles.

Appendix D Simulation Data

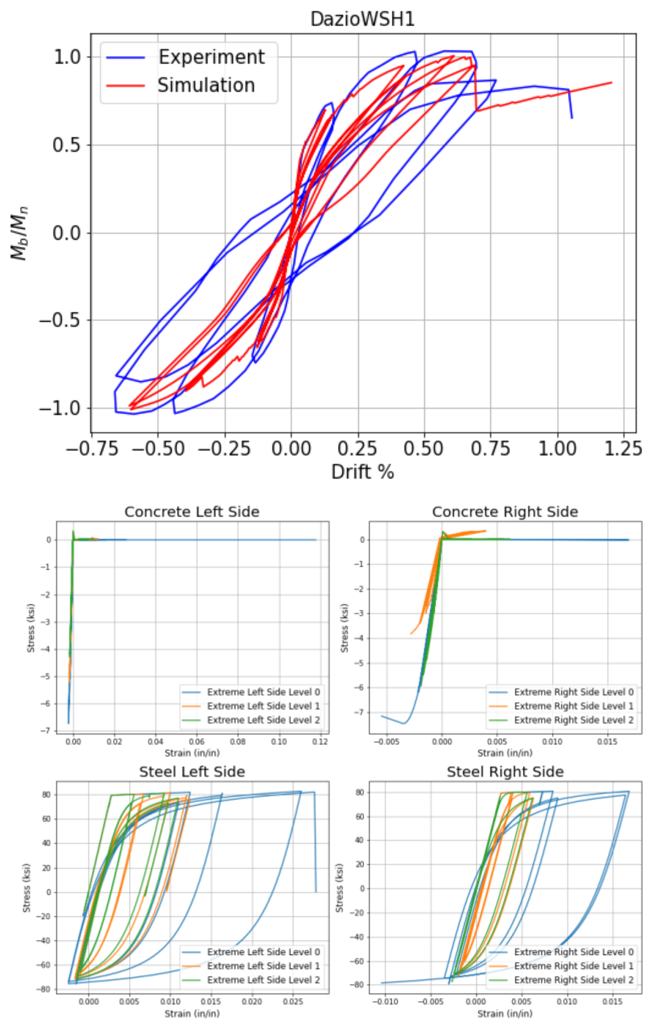

Figure D.1 WSH1 Load-displacement and stress-strain response (BR failure mode in both the laboratory and simulation)

Link to interactive Stress and Strain wall plots:
https://stokljos.github.io/thesis/wsh1_movie.html

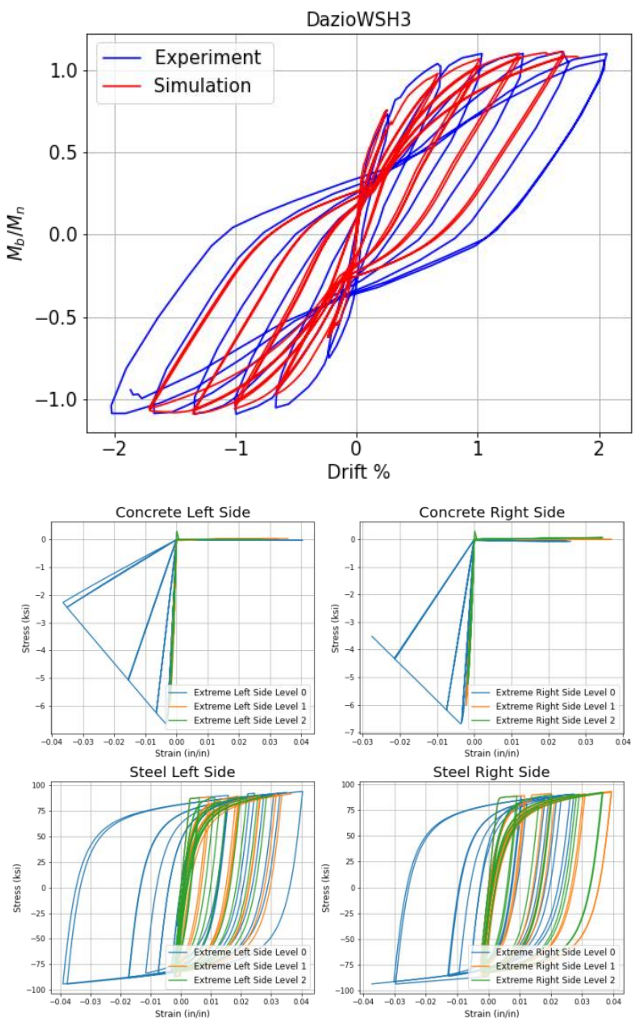

Figure D.2 WSH3 Load-displacement and stress-strain response (BR failure mode in the laboratory; CB failure in the simulation)

Link to interactive Stress and Strain wall plots:
https://stokljos.github.io/thesis/DazioWSH3_221104203416_movie.html
*Note file is too large to preview and needs to be downloaded to be viewed.

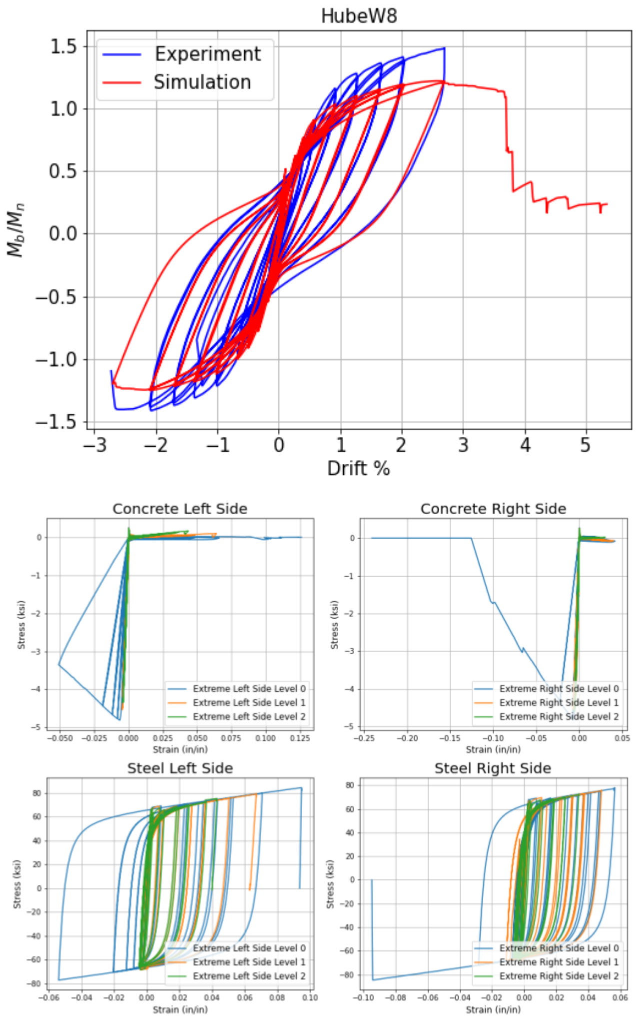

Figure D.3 W8 Load-displacement and stress strain-response (CB failure in the laboratory and simulation)

Link to interactive Stress and Strain wall plots:
https://stokljos.github.io/thesis/HubeW8_221104203424_movie.html

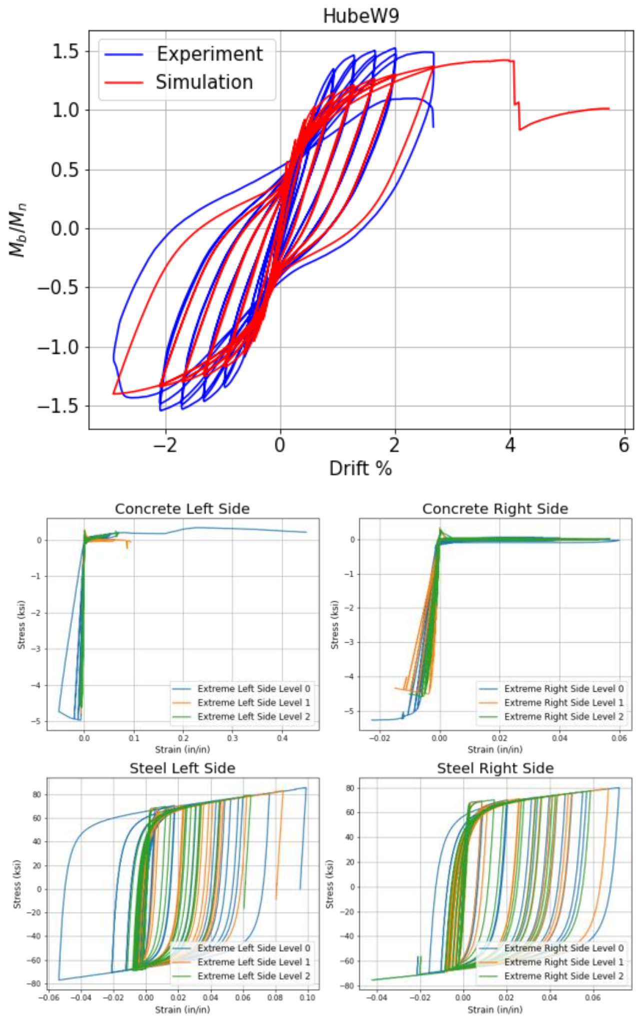

Figure D.4 W9 Load-displacement and stress-strain response (CB failure in the laboratory; BR failure in the simulation)

Link to interactive Stress and Strain wall plots:
https://stokljos.github.io/thesis/HubeW9_230305015202_movie.html

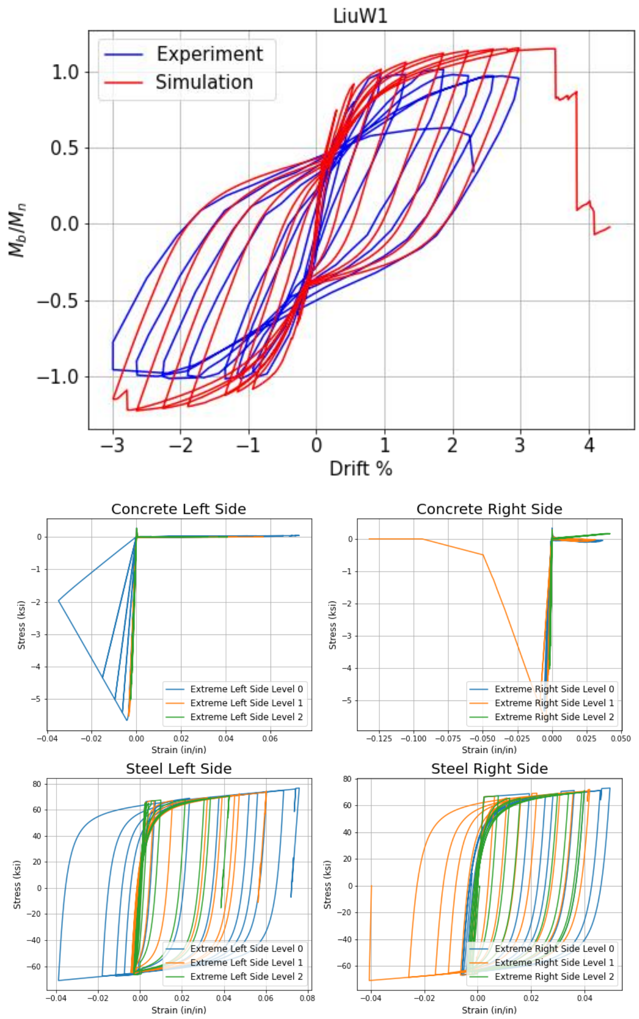

Figure D.5 W1 Load-displacement and stress-strain response (CB failure in the laboratory and simulation)

Link to interactive Stress and Strain wall plots:
https://stokljos.github.io/thesis/LiuW1_221104203417_movie.html

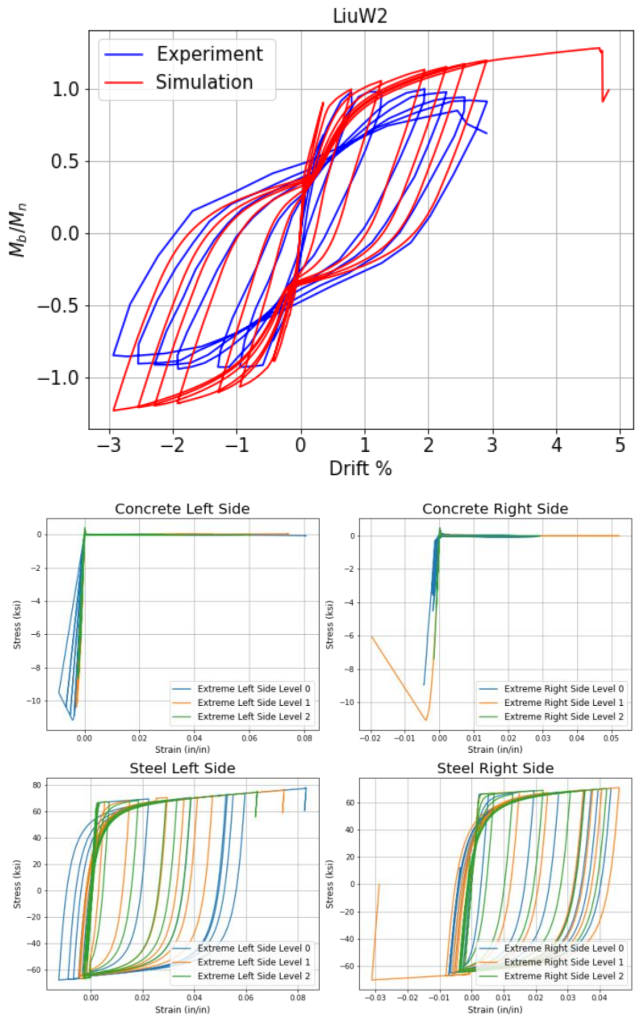

Figure D.6 **W2 Load-displacement and stress-strain response (BR failure in the laboratory; CB failure in the simulation)**

Link to interactive Stress and Strain wall plots:
https://stokljos.github.io/thesis/LiuW2_221104203418_movie.html

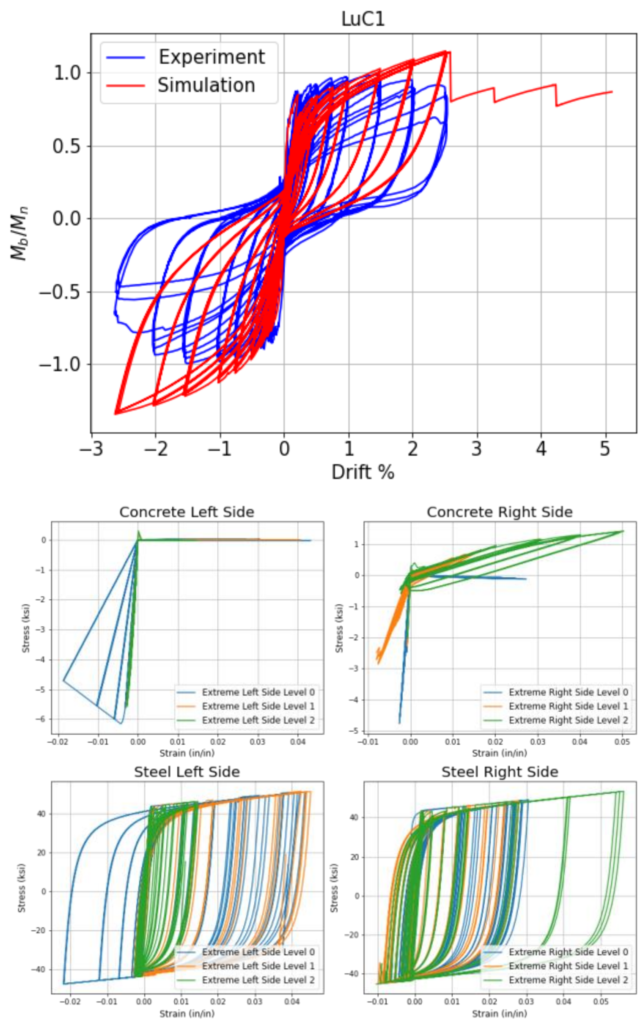

Figure D.7 **C1 Load-displacement and stress-strain response (BR failure in the laboratory and simulation)**

Link to interactive Stress and Strain wall plots:
https://stokljos.github.io/thesis/LuC1_230305015158_movie.html

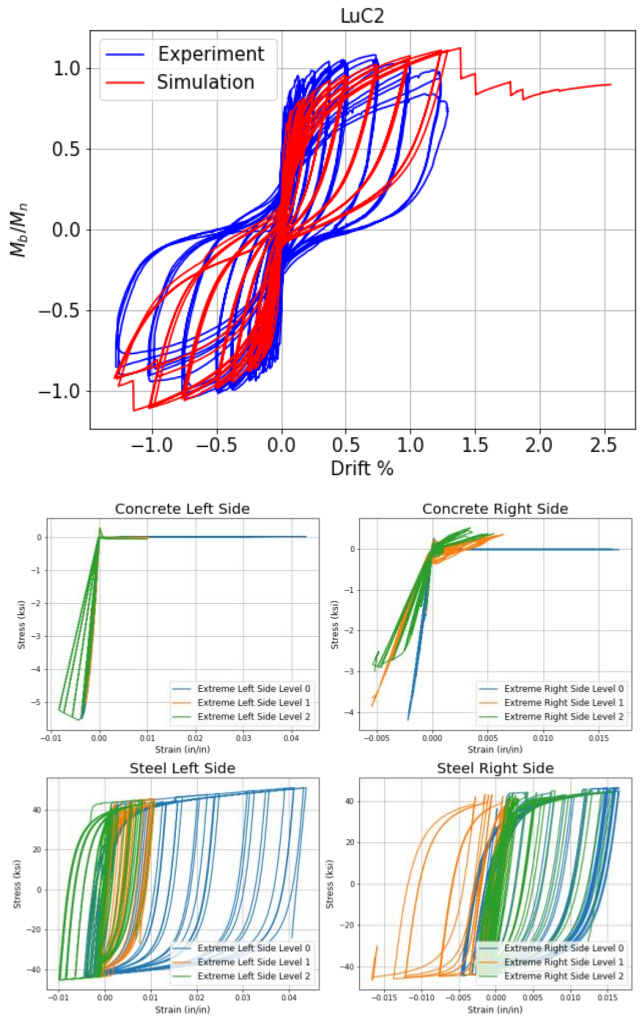

Figure D.2 C2 Load-displacement and stress-strain response (BR failure in the laboratory and simulation)

Link to interactive Stress and Strain wall plots:
https://stokljos.github.io/thesis/LuC2_230305015159_movie.html

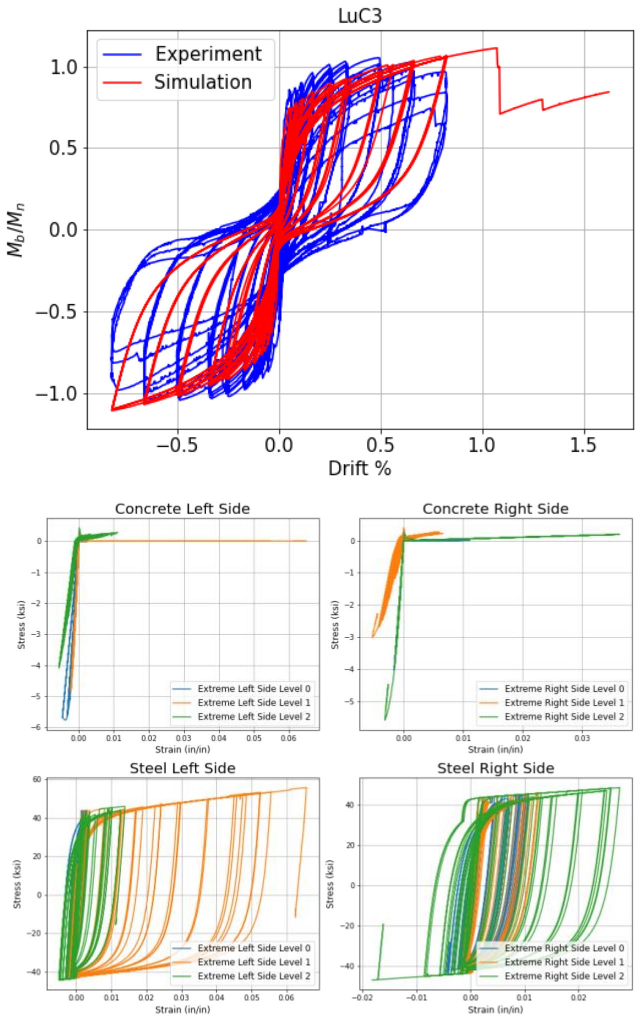

Figure D.9 C3 Load-displacement and stress-strain response (BR failure in the laboratory and simulation)

Link to interactive Stress and Strain wall plots:
https://stokljos.github.io/thesis/LuC3_230305015200_movie.html

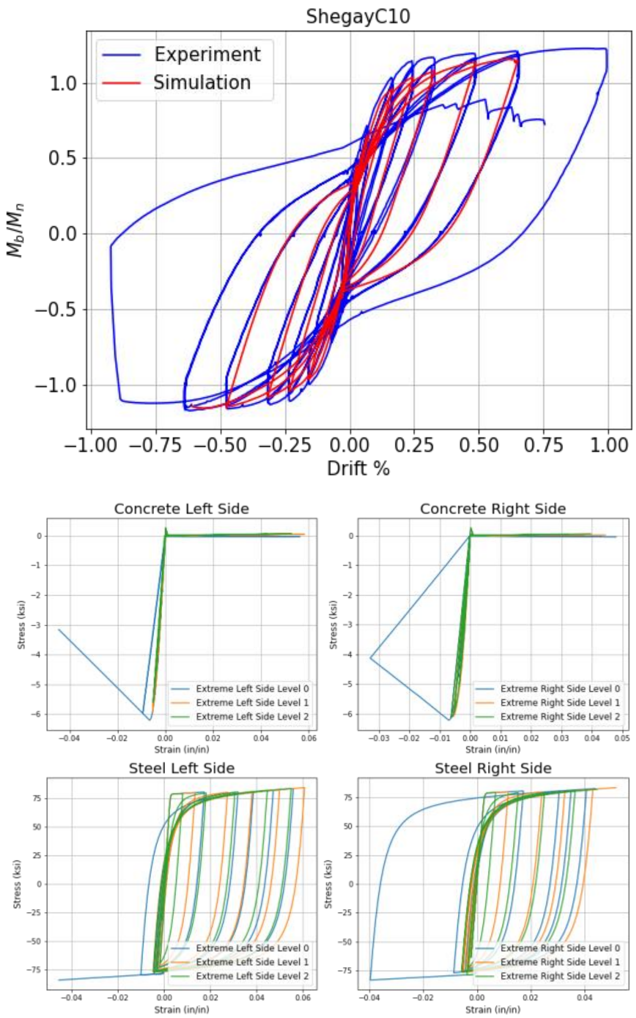

Figure D.10 C10 Load-displacement and stress-strain response (CB failure in the laboratory and simulation)

Link to interactive Stress and Strain wall plots:
https://stokljos.github.io/thesis/ShegayC10_230211125342_movie.html

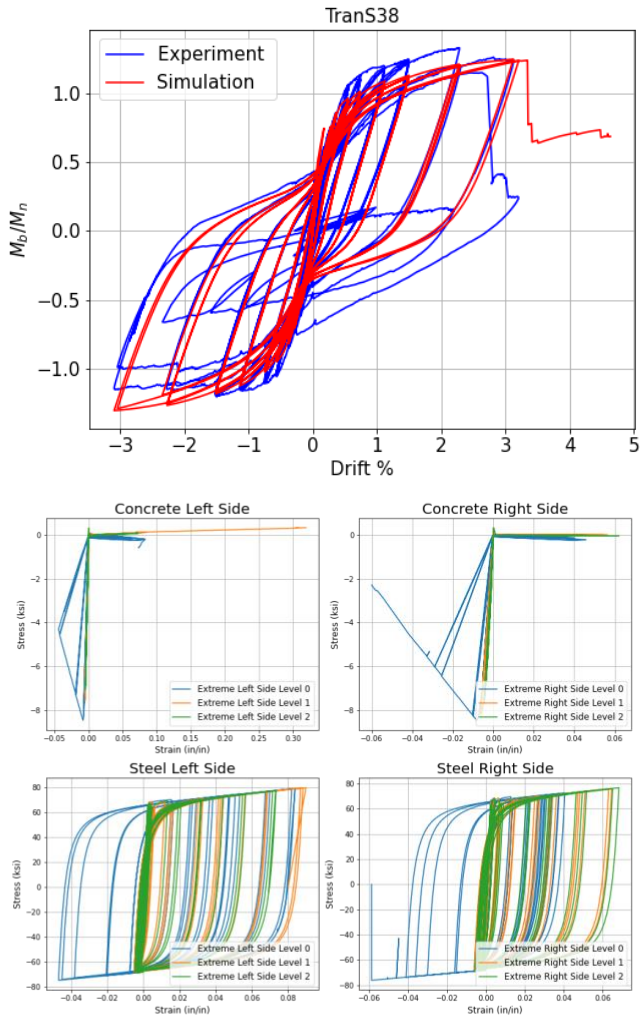

Figure D.11 S38 Load-displacement and stress-strain response (CB failure in the laboratory and simulation)

Link to interactive Stress and Strain wall plots:
https://stokljos.github.io/thesis/TranS38_221104203422_movie.html
*Note file is to large to preview and needs to be downloaded to be viewed.

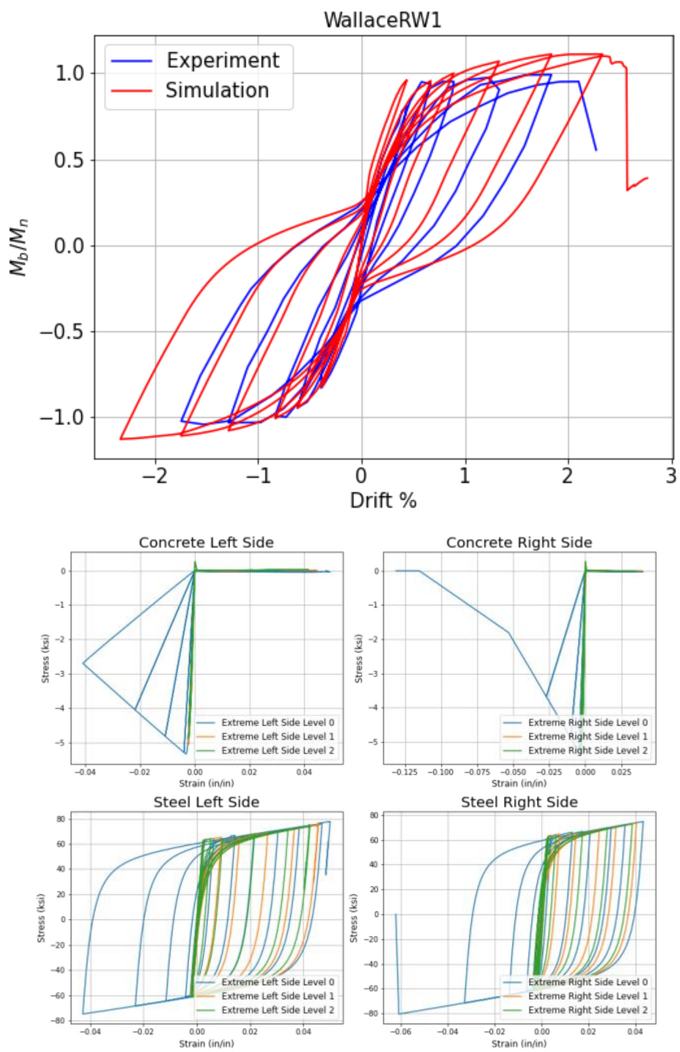

Figure D.12 RW1 Load-displacement and stress-strain response (BR failure in the laboratory; CB failure in the simulation)

Link to interactive Stress and Strain wall plots:
https://stokljos.github.io/thesis/WallaceRW1_221104203419_movie.html

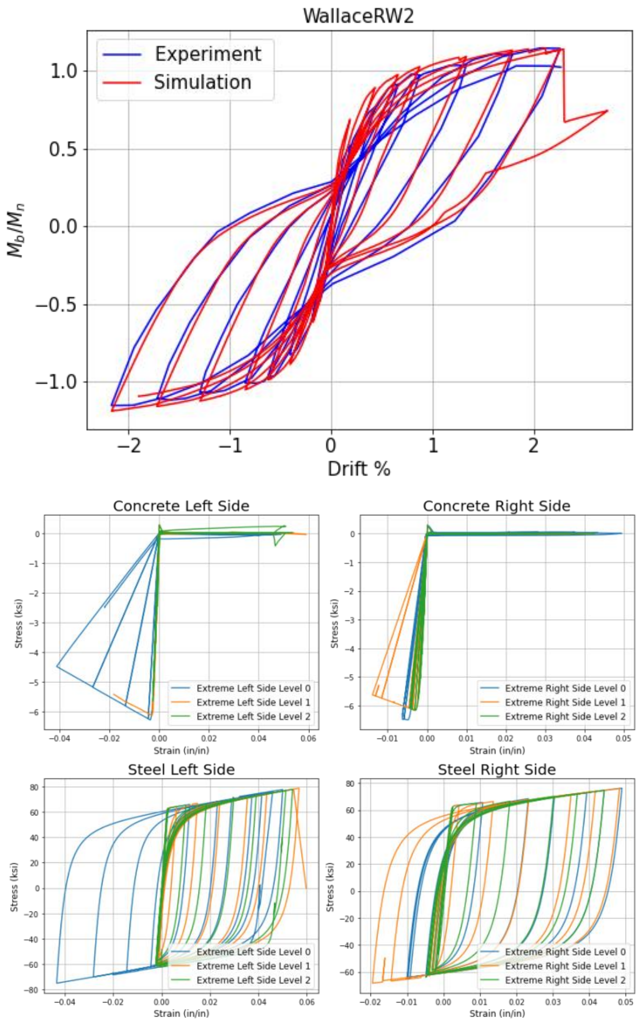

Figure D.3 RW2 Load-displacement and stress-strain response (CB failure in the laboratory; BR failure in the simulation)

Link to interactive Stress and Strain wall plots:
https://stokljos.github.io/thesis/WallaceRW2_230305015041_movie.html
*Note file is to large to preview and needs to be downloaded to be viewed.

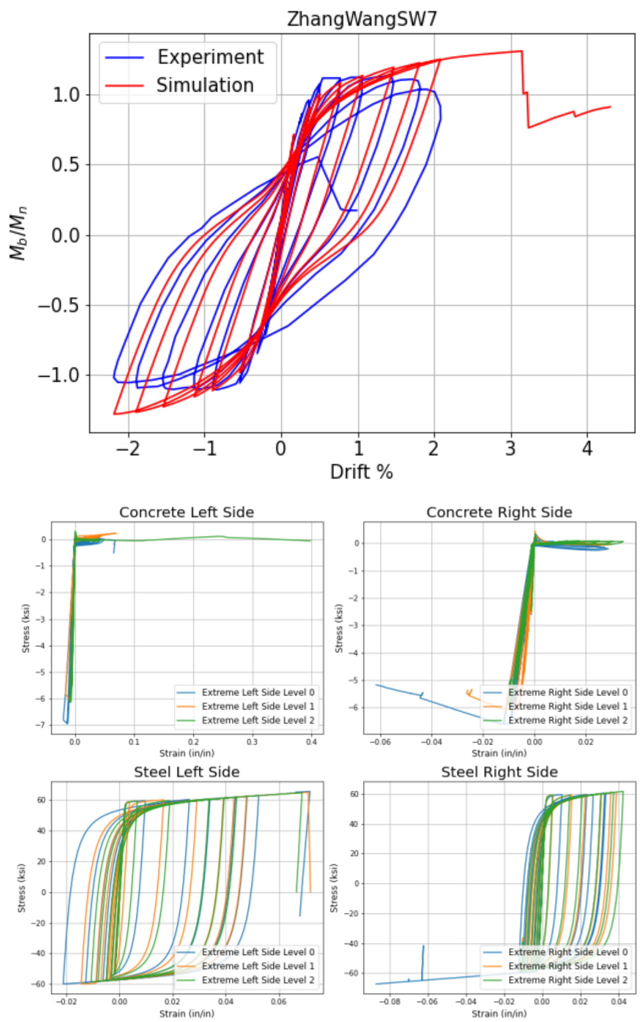

Figure D.14 SW7 Load-displacement and stress-strain response (CB failure in the laboratory; BR failure in the simulation)

Link to interactive Stress and Strain wall plots:
https://stokljos.github.io/thesis/ZhangWangSW7_230211125344_movie.html

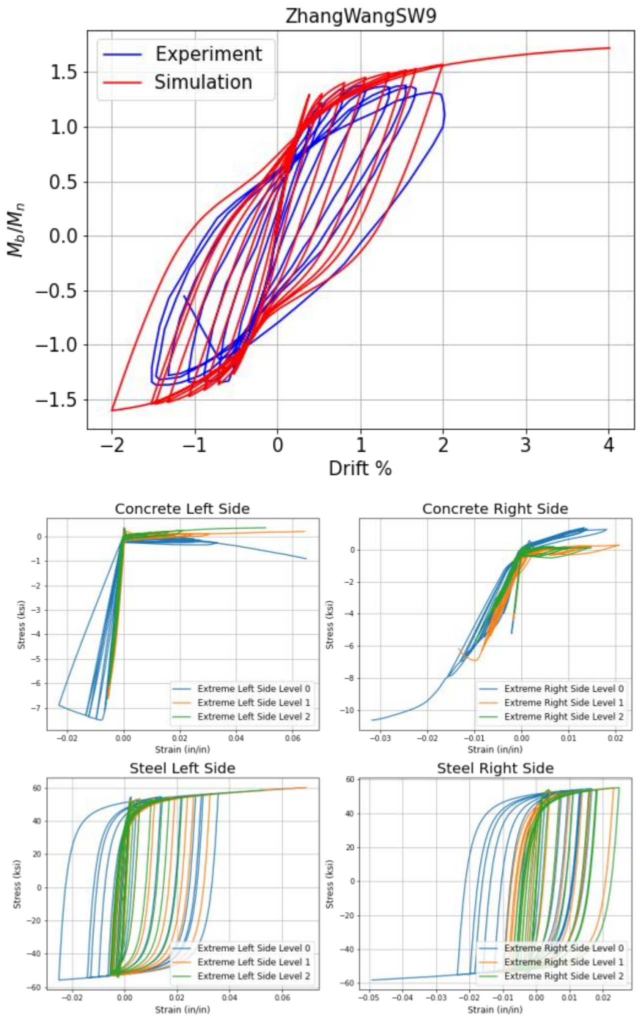

Figure D.15 SW9 Load-displacement and stress-strain response (CB failure in the laboratory; failure not simulated)

Link to interactive Stress and Strain wall plots:
https://stokljos.github.io/thesis/ZhangWangSW9_221104203425_movie.html

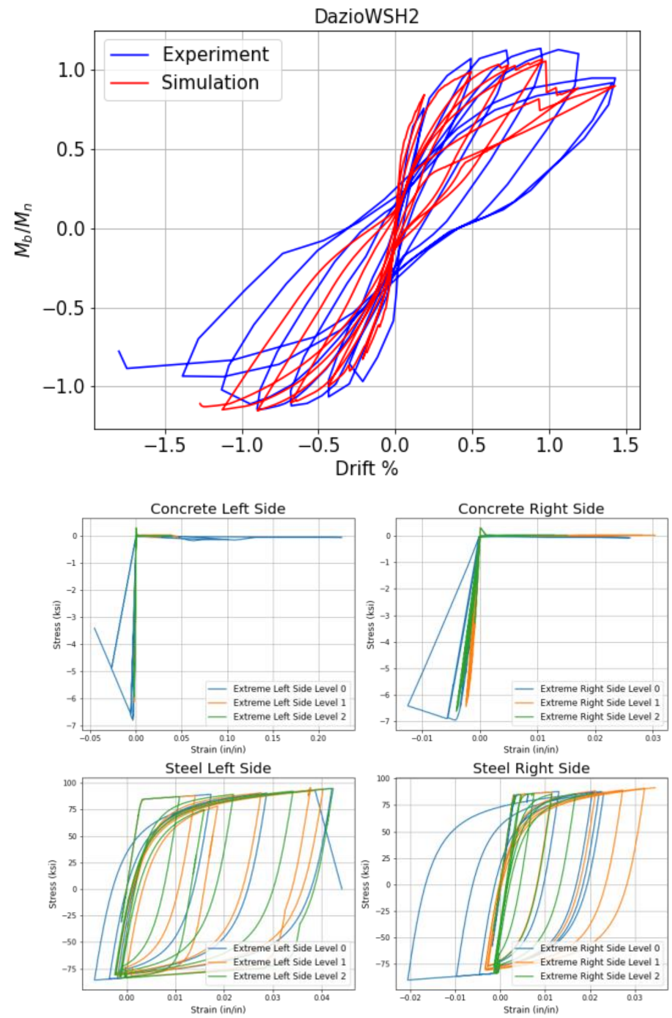

Figure D.16 WSH2 Load-displacement and stress-strain response (BR failure in the laboratory and simulation)

Link to interactive Stress and Strain wall plots:
https://stokljos.github.io/thesis/DazioWSH2_230305015050_movie.html

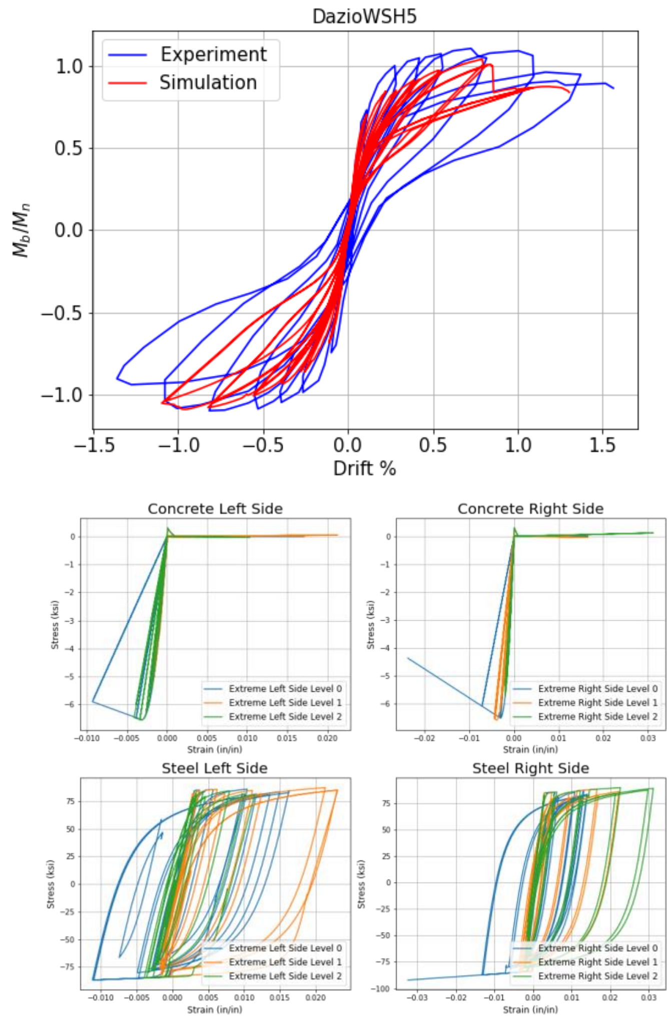

Figure D.17 WSH5 Load-displacement and stress-strain response (BR failure in the laboratory; CB failure in the simulation)

Link to interactive Stress and Strain wall plots:
https://stokljos.github.io/thesis/DazioWSH5_230305015204_movie.html
*Note file is to large to preview and needs to be downloaded to be viewed.

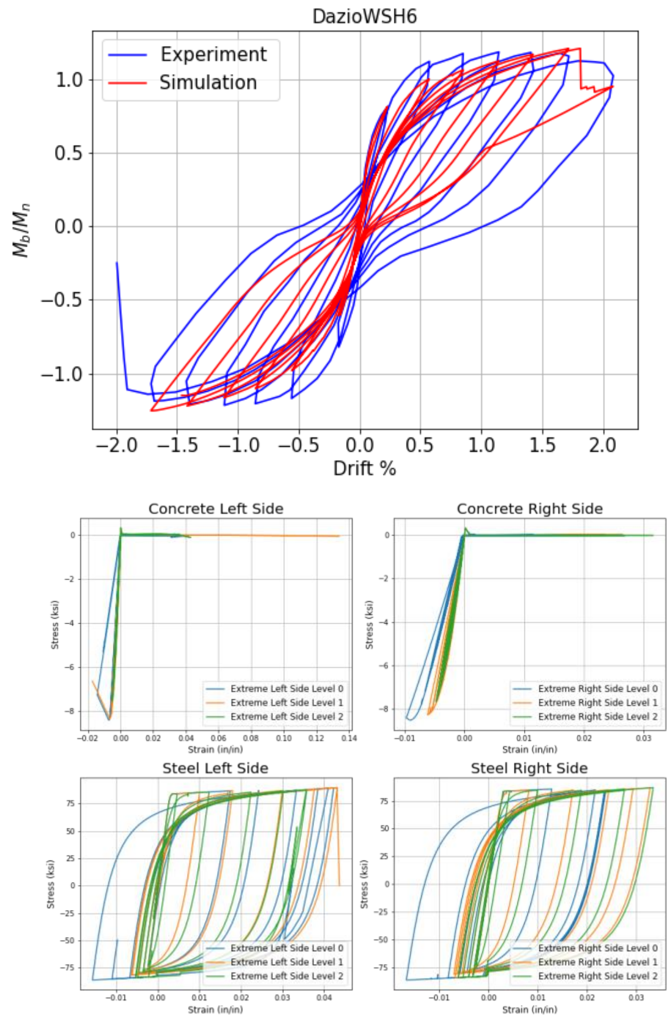

Figure D.18 WSH6 Load-displacement and stress-strain response (CB failure in the laboratory; BR failure in the simulation)

Link to interactive Stress and Strain wall plots:
https://stokljos.github.io/thesis/DazioWSH6_230305015205_movie.html
*Note file is to large to preview and needs to be downloaded to be viewed.

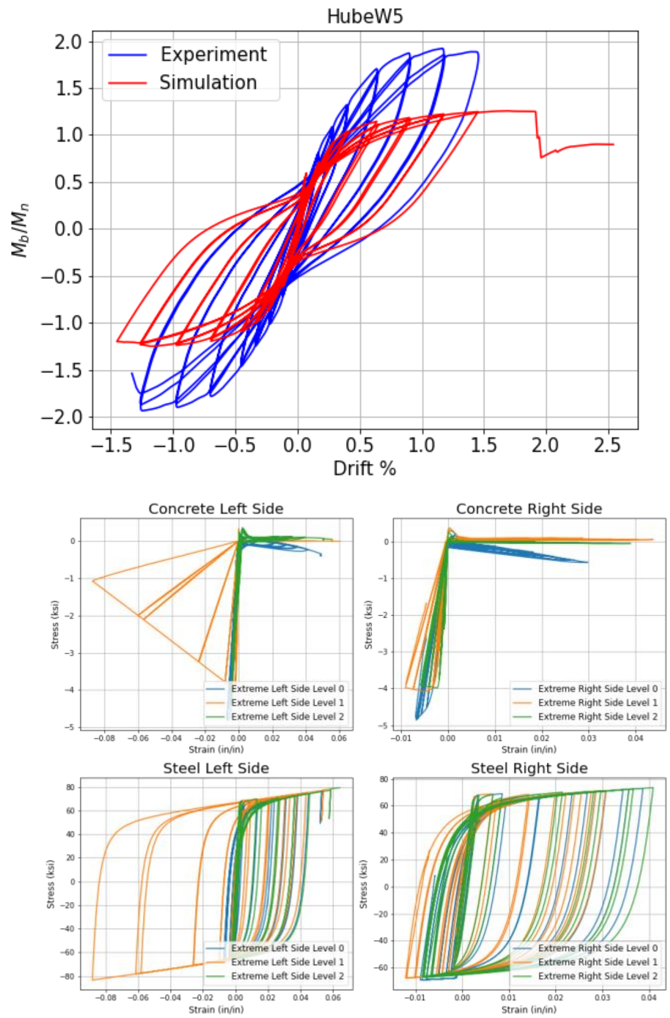

Figure D.19 W5 Load-displacement and stress-strain response (CB failure in the laboratory and simulation)

Link to interactive Stress and Strain wall plots:
https://stokljos.github.io/thesis/HubeW5_230301204159_movie.html

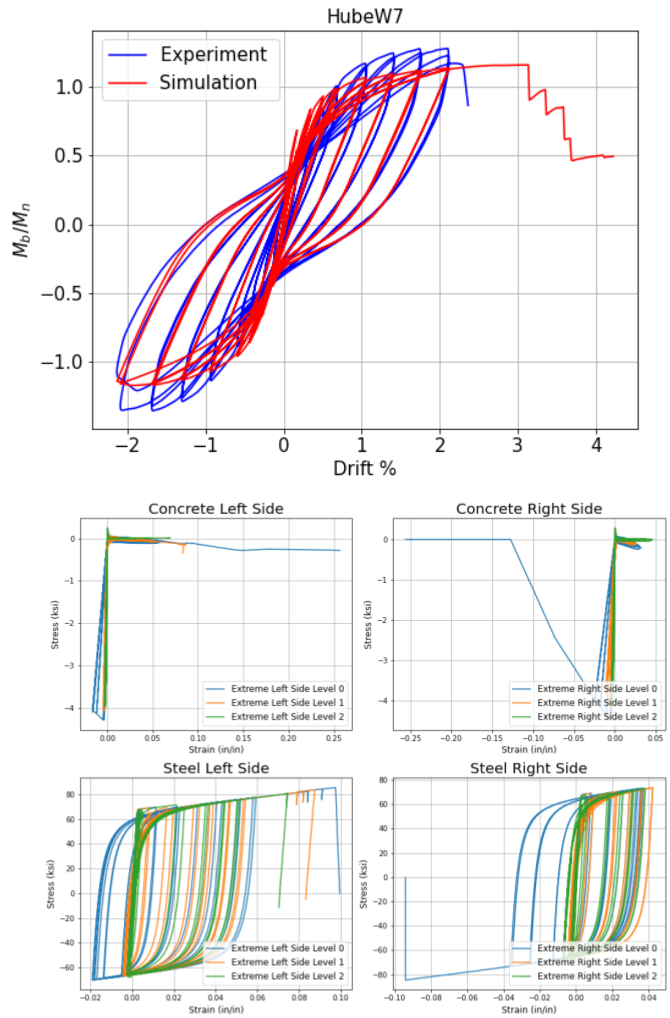

Figure D.20 W7 Load-displacement and stress-strain response (CB failure in the laboratory and simulation)

Link to interactive Stress and Strain wall plots:
https://stokljos.github.io/thesis/HubeW7_230301204200_movie.html

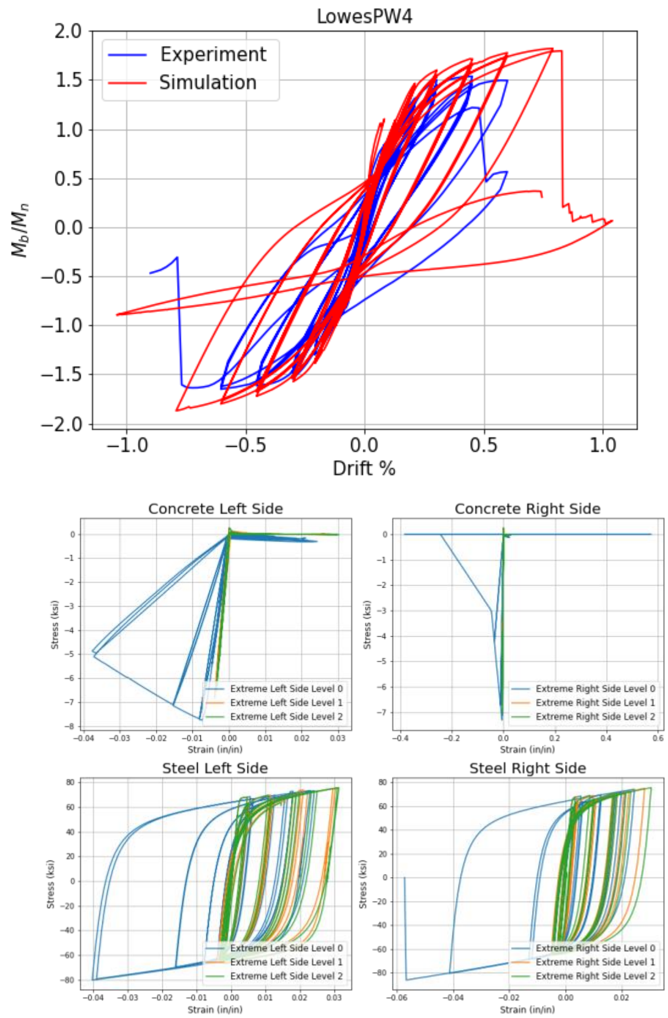

Figure D.21 PW4 Load-displacement and stress-strain response (CB failure in the laboratory and simulation)

Link to interactive Stress and Strain wall plots:
https://stokljos.github.io/thesis/LowesPW4_230304205135_movie.html
*Note file is to large to preview and needs to be downloaded to be viewed.

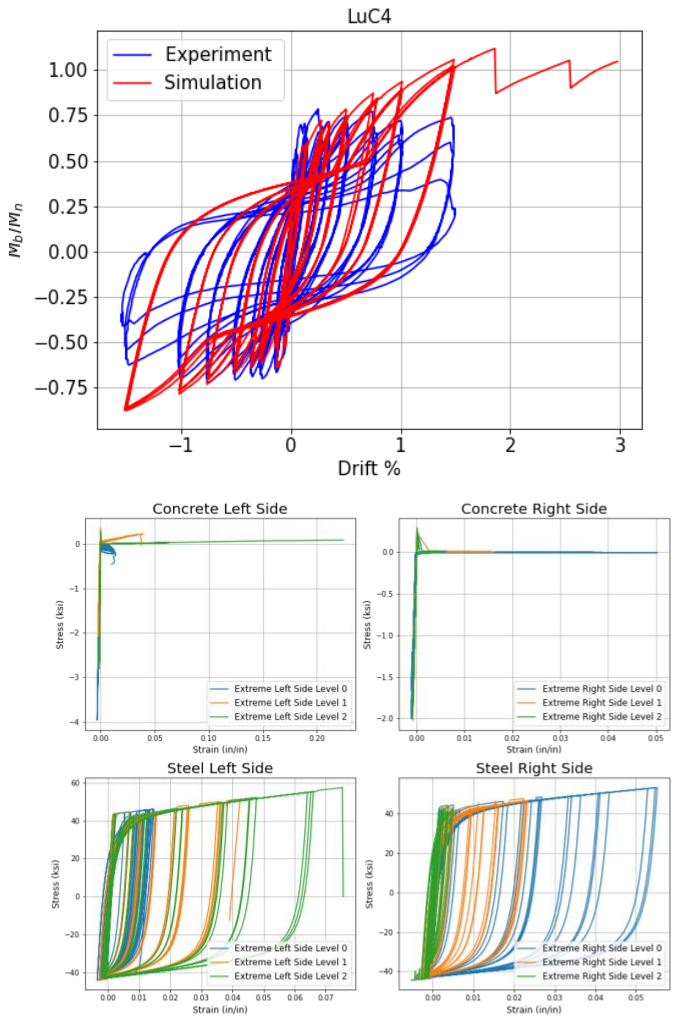

Figure D.22 C4 Load-displacement and stress-strain response (BR failure in the laboratory and simulation)

Link to interactive Stress and Strain wall plots:
https://stokljos.github.io/thesis/LuC4_230305015217_movie.html

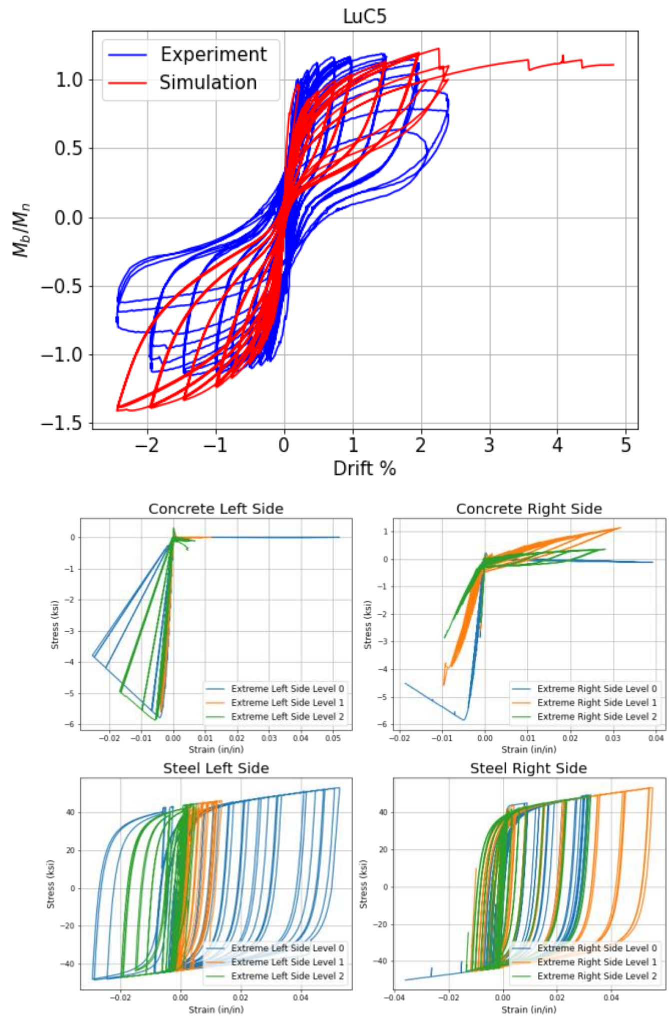

Figure D.23 C5 Load-displacement and stress-strain response (BR failure in the laboratory; CB failure in the simulation)

Link to interactive Stress and Strain wall plots:
https://stokljos.github.io/thesis/LuC5_230305015218_movie.html

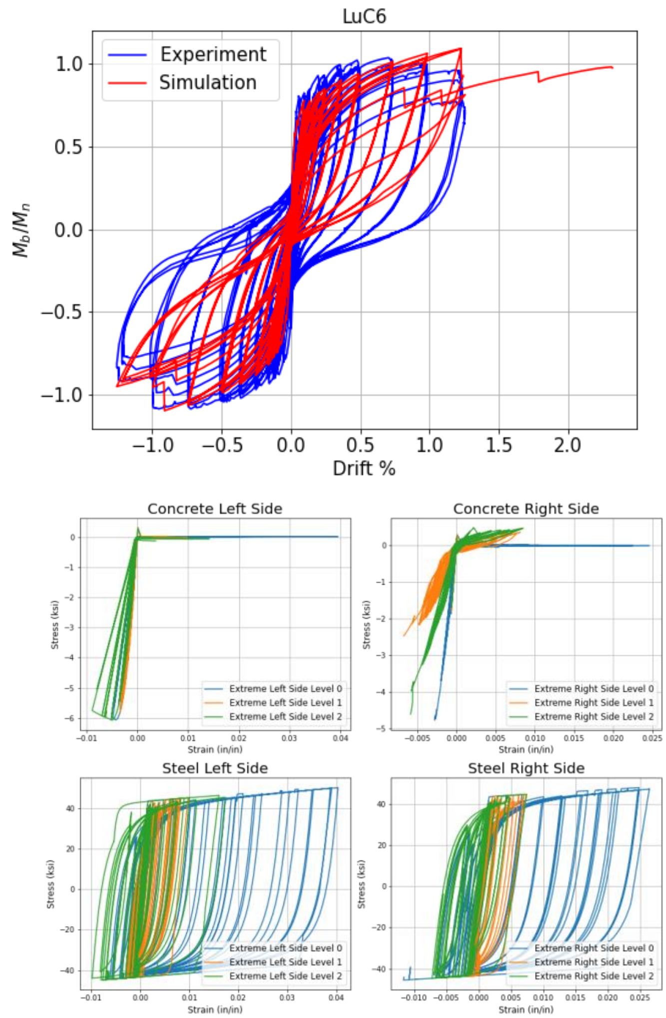

Figure D.26 C6 Load-displacement and stress-strain response (BR failure in the laboratory and simulation)

Link to interactive Stress and Strain wall plots:
https://stokljos.github.io/thesis/LuC6_230305015219_movie.html

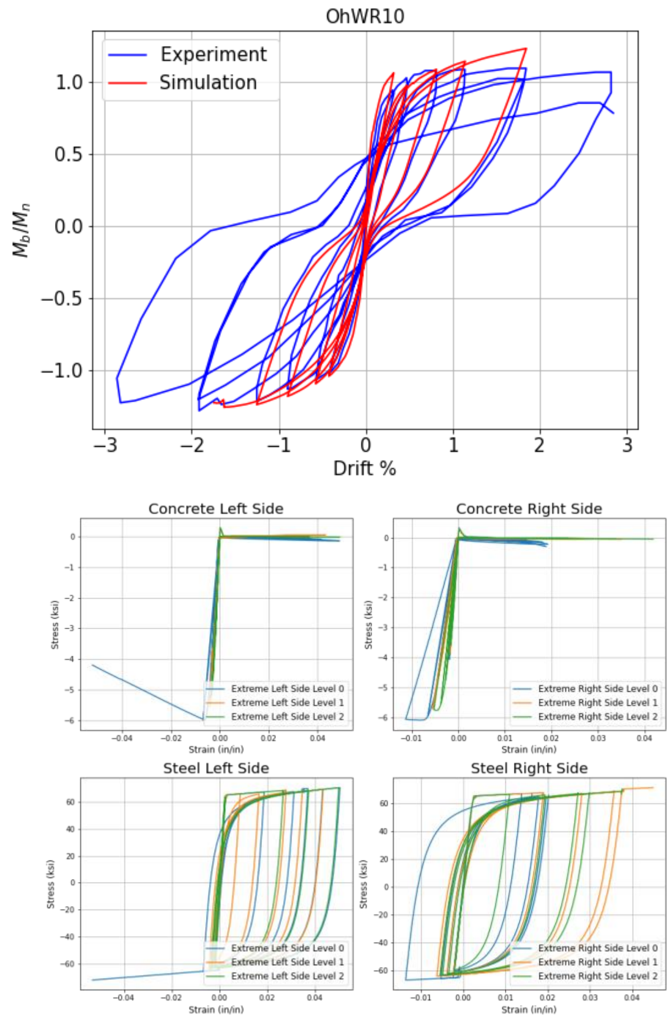

Figure D.27 WR10 Load-displacement and stress-strain response (CB failure in the laboratory and simulation)

Link to interactive Stress and Strain wall plots:
https://stokljos.github.io/thesis/OhWR10_230305015206_movie.html

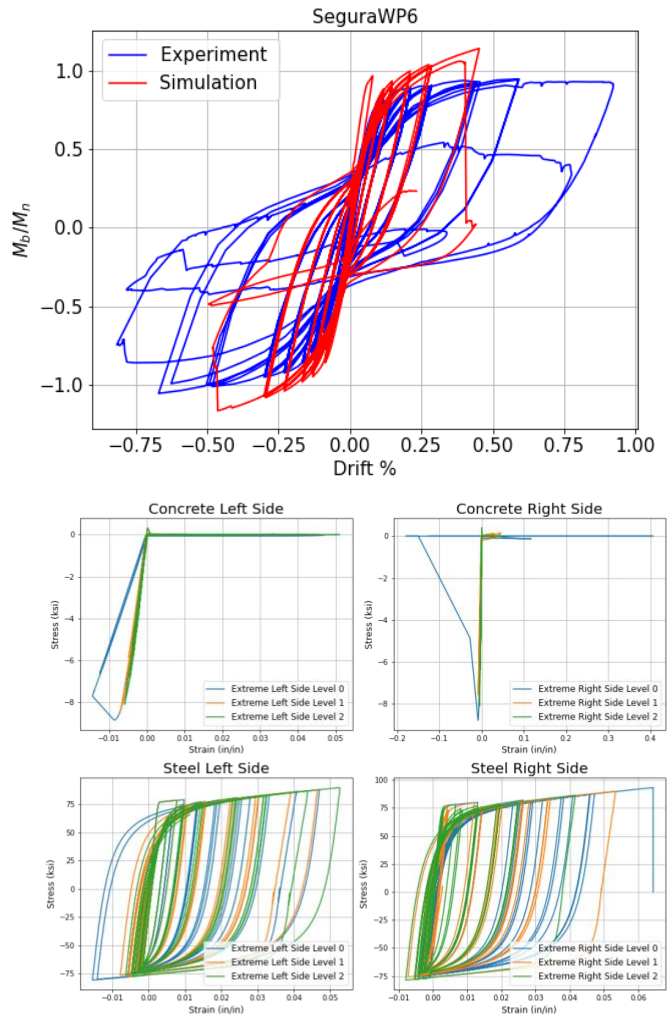

Figure D.28 WP6 Load-displacement and stress-strain response (BR failure in the laboratory and simulation)

Link to interactive Stress and Strain wall plots:
https://stokljos.github.io/thesis/SeguraWP6_230301204151_movie.html

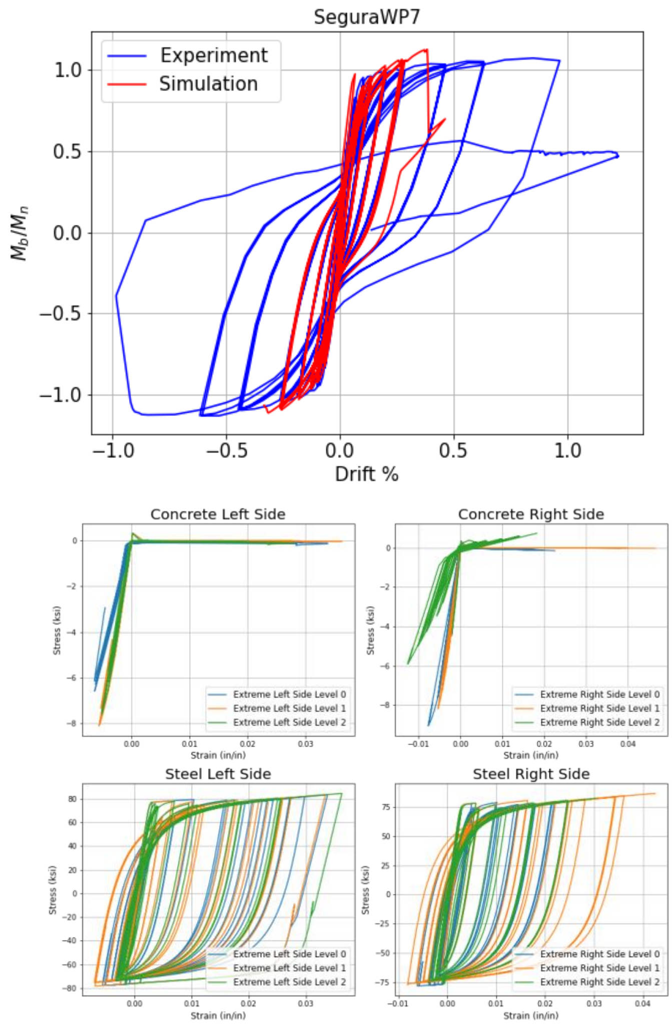

Figure D.29 WP7 Load-displacement and stress-strain response (CB failure in the laboratory and simulation)

Link to interactive Stress and Strain wall plots:
https://stokljos.github.io/thesis/SeguraWP7_230305015217_movie.html
*Note file is to large to preview and needs to be downloaded to be viewed.

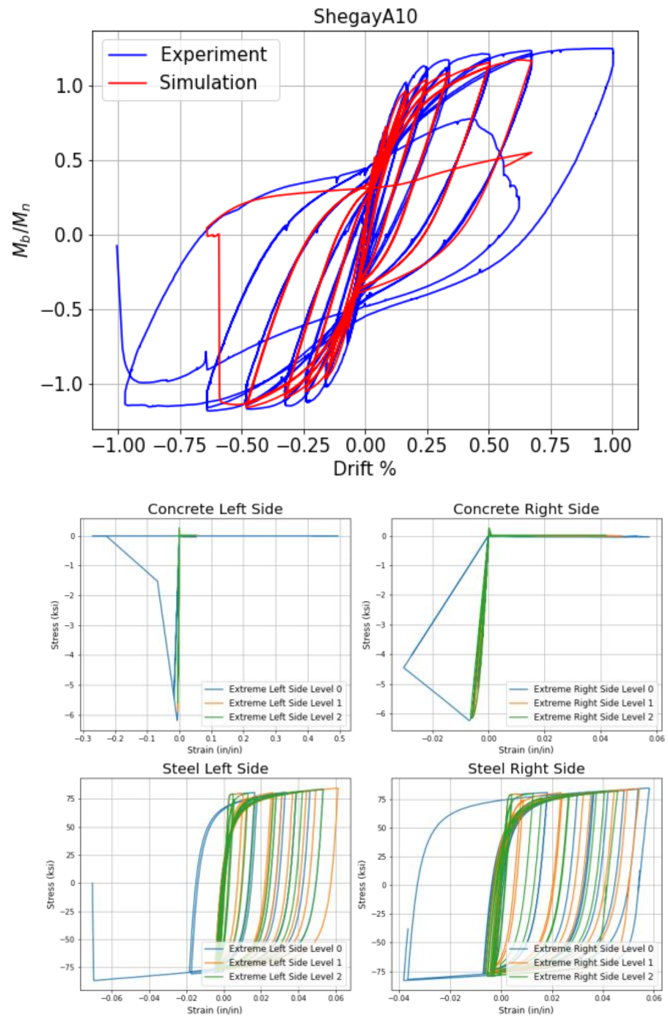

Figure D.30 A10 Load-displacement and stress-strain response (BR failure in the laboratory; CB failure in the simulation)

Link to interactive Stress and Strain wall plots:
https://stokljos.github.io/thesis/ShegayA10_230305015206_movie.html
*Note file is to large to preview and needs to be downloaded to be viewed.

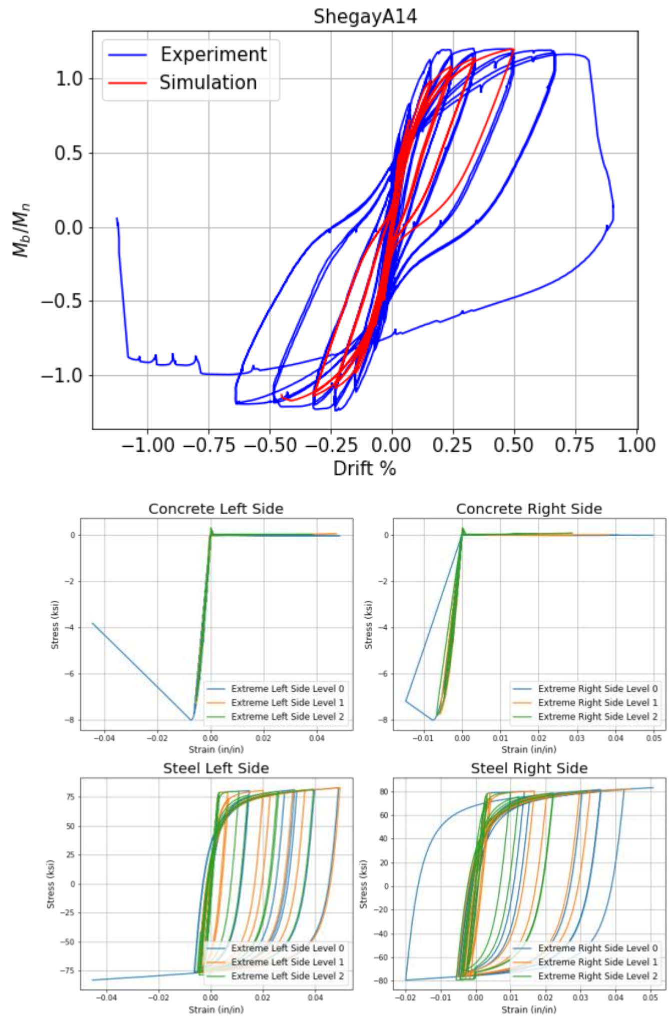

Figure D.31 A14 Load-displacement and stress-strain response (CB failure in the laboratory and simulation)

Link to interactive Stress and Strain wall plots:
https://stokljos.github.io/thesis/ShegayA14_230305015207_movie.html

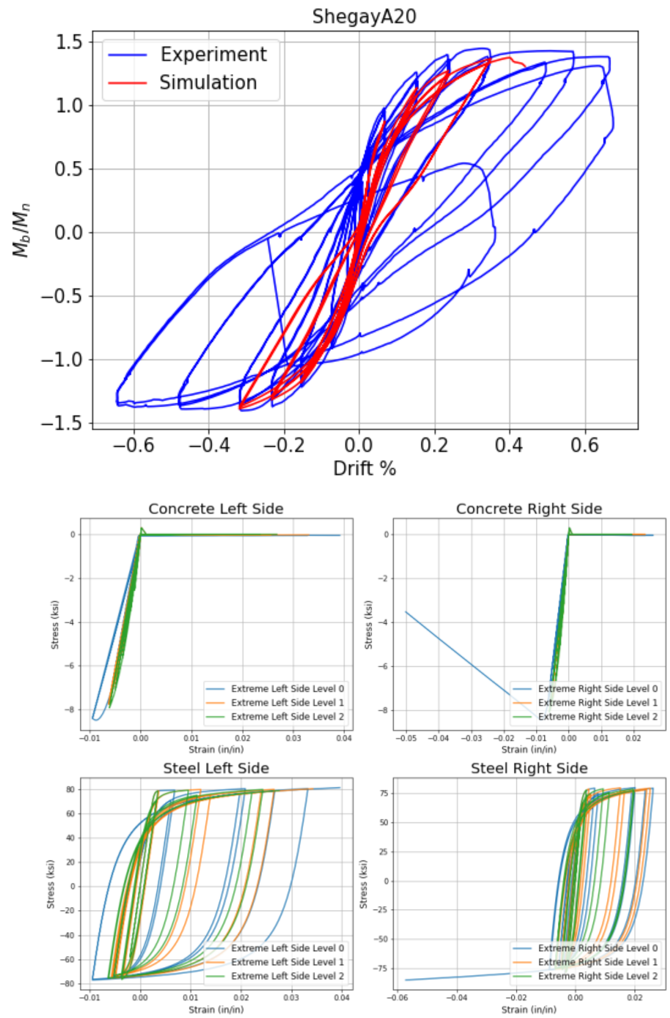

Figure D.32 A20 Load-displacement and stress-strain response (CB failure in the laboratory and simulation)

Link to interactive Stress and Strain wall plots:
https://stokljos.github.io/thesis/ShegayA20_230305015208_movie.html

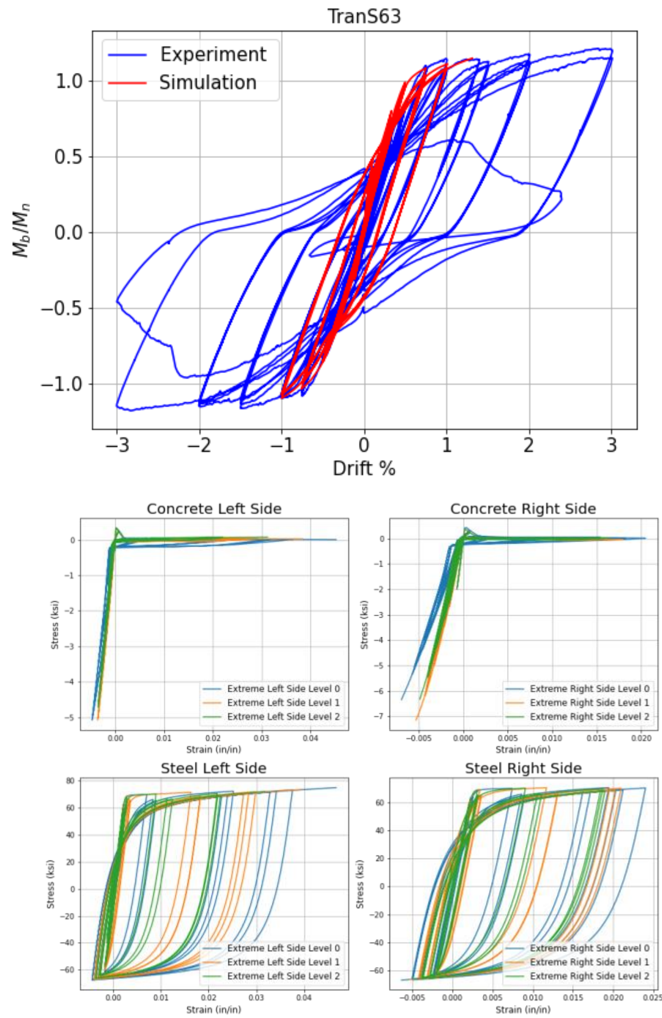

Figure D.33 S63 Load-displacement and stress-strain response (CB failure in the laboratory and simulation)

Link to interactive Stress and Strain wall plots:
https://stokljos.github.io/thesis/TranS63_230305015209_movie.html

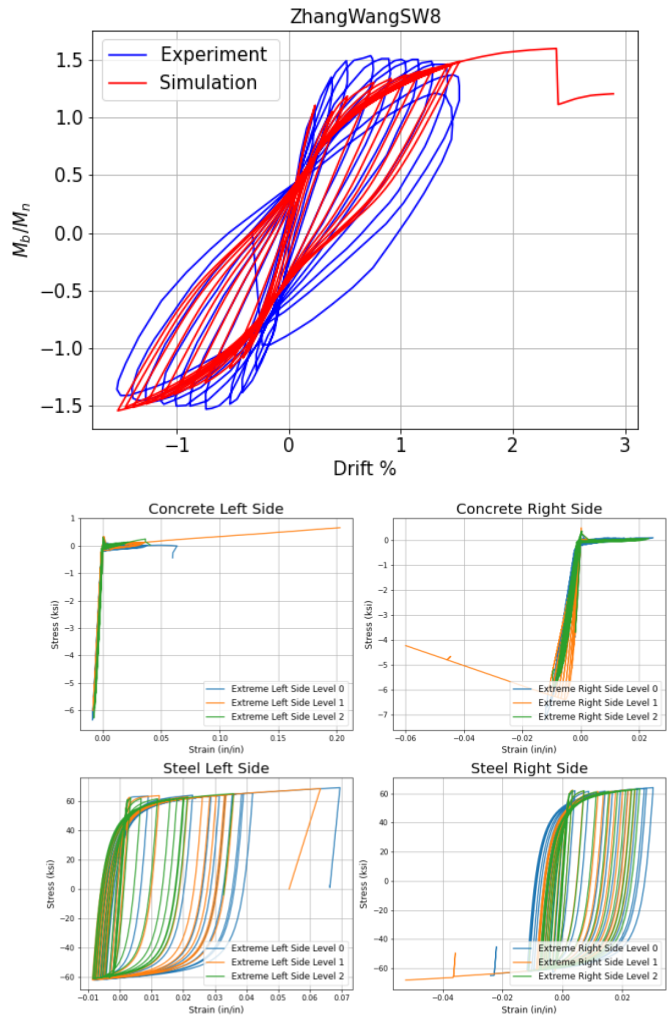

Figure D.34 SW8 Load-displacement and stress-strain response (CB failure in the laboratory; BR failure in the simulation)

Link to interactive Stress and Strain wall plots:
https://stokljos.github.io/thesis/ZhangWangSW8_230301204146_movie.html

The Pacific Earthquake Engineering Research Center (PEER) is a multi-institutional research and education center with headquarters at the University of California, Berkeley. Investigators from over 20 universities, several consulting companies, and researchers at various state and federal government agencies contribute to research programs focused on performance-based earthquake engineering.

These research programs aim to identify and reduce the risks from major earthquakes to life safety and to the economy by including research in a wide variety of disciplines including structural and geotechnical engineering, geology/seismology, lifelines, transportation, architecture, economics, risk management, and public policy.

PEER is supported by federal, state, local, and regional agencies, together with industry partners.

PEER Core Institutions

University of California, Berkeley (Lead Institution)
California Institute of Technology
Oregon State University
Stanford University
University of California, Davis
University of California, Irvine
University of California, Los Angeles
University of California, San Diego
University of Nevada, Reno
University of Southern California
University of Washington

Pacific Earthquake Engineering Research Center
University of California, Berkeley
325 Davis Hall, Mail Code 1792
Berkeley, CA 94720-1792
Tel: 510-642-3437
Email: peer_center@berkeley.edu

ISSN 2770-8314
https://doi.org/10.55461/AMQF4907